

# **A High-Latitude Convective Cloud Feedback**

A dissertation presented

by

Dorian Schuyler Abbot

to

The School of Engineering and Applied Sciences

in partial fulfillment of the requirements  
for the degree of  
Doctor of Philosophy  
in the subject of  
Applied Mathematics

Harvard University  
Cambridge, Massachusetts

August, 2008

© 2008 by Dorian S. Abbot

All rights reserved.

**Dissertation Advisor:** Professor Eli Tziperman

**Author:** Dorian S. Abbot

## **A High-Latitude Convective Cloud Feedback**

### **Abstract**

Available data suggest that during the late Cretaceous and early Paleogene ( $\sim 100$  to  $\sim 35$  million years ago) Earth had an "equable" climate: the equator to pole surface temperature difference and seasonal cycle in high-latitude surface temperature were both much smaller than they are today. The combination of much warmer high latitudes, particularly during winter, and only somewhat warmer tropics has traditionally been difficult to model in global climate models and to explain physically. In this thesis a positive feedback on high-latitude surface temperatures based on the onset of convection and convective clouds is proposed and investigated using a hierarchy of climate models. This feedback mechanism is based on an initial warming leading to destabilization of the high-latitude atmosphere to convection, causing convection, which results in convective clouds and increased atmospheric moisture, both of which trap outgoing longwave radiation and lead to further warming. It is also shown that this convective cloud feedback could be active in a future atmosphere with increased greenhouse gasses, increasing high-latitude climate uncertainty under global warming scenarios.

A variety of climate models are used to understand the convective cloud feedback in this thesis. Simple, analytical models are used in two chapters to understand more complex models and their underlying physics. A zonally-averaged, two-level model of the atmo-

sphere without a seasonal cycle, but containing a hydrological cycle and parameterizations of convection, precipitation, and clouds, and a longwave radiation scheme that explicitly depends on CO<sub>2</sub>, water vapor, and cloud fraction is constructed and used as an initial test of the feedback mechanism. The National Center for Atmospheric Research (NCAR) single column model (SCAM), which contains state-of-the-art atmospheric physics parameterizations, high vertical resolution, a full seasonal cycle, a thermodynamic sea ice model, and a mixed layer ocean is used in two chapters. Finally, it is shown that the feedback is active at high carbon dioxide levels in some of the fully-coupled state-of-the-art ocean-atmosphere global climate models used in the Intergovernmental Panel on Climate Change (IPCC) fourth assessment report.

# Contents

<b>1</b>	<b>Introduction</b>	<b>1</b>
<b>2</b>	<b>A High-Latitude Convective Cloud Feedback and Equable Climates</b>	<b>11</b>
<b>3</b>	<b>Sea Ice, High-Latitude Convection, and Equable Climates</b>	<b>69</b>
<b>4</b>	<b>Winter Arctic Climate Uncertainty Under Global Warming due to a Cloud Radiative Feedback</b>	<b>85</b>
<b>5</b>	<b>Controls on the Activation and Strength of a High-Latitude Convective Cloud Feedback</b>	<b>99</b>
<b>6</b>	<b>Conclusion</b>	<b>127</b>

## **Acknowledgments**

Thanks especially to Eli Tziperman. The spell checker had it right all along, he truly is Professor Superman! Thanks to John Dykema, Ian Eisenman, Kerry Emanuel, Brian Farrell, Jake Gebbie, John Higgins, Matt Huber, Peter Huybers, Zhiming Kuang, Richard Lindzen, Dan Schrag, Jacob Sewall, Howard Stone, and Chris Walker for excellent science talk and guidance.

Thanks to Nicole for taking me all over the world (robbing me of my simplicity?) and making my life most enjoyable! Thanks to Mom, Dad, Greg, grandparents, uncles, aunties, and cousins for letting me be a big nerd all the time! Thanks to my good old buddy Isaac Schapira for some good old times and some bad old times.

Thanks to Sarah Colgan and Susan Wieczorek for helping me get all the right forms to the right people, be at the right airport at the right time, and generally stay out of trouble. Thanks to the EPS department for letting me hang out with them and thanks to my EPS cohort for making things fun.

Thanks to the Department of Defense, which sponsored me with an NDSEG fellowship and to the National Science Foundation, which sponsored me with an NSF graduate research fellowship. Thanks to the McDonnell Foundation and the NSF paleoclimate program for covering publication and travel expenses.

# Chapter 1

## Introduction

Clouds represent the largest source of uncertainty in our understanding of the climate system (Cess and co authors, 1990, 1996; Murphy et al., 2004; Stainforth et al., 2005; Soden and Held, 2006; Bony et al., 2006). This is because of the important role they play in Earth's radiative balance (e.g., Ramanathan et al., 1989; Hartmann et al., 1992) and our relative inability to accurately include them in global climate models (GCMs), the climate models upon which much of our understanding of the climate system is based. It is difficult to simulate clouds in GCMs because these models are so computationally intensive that they can only be run in a reasonable amount of time at horizontal grid resolutions on the order of 100 km, whereas important microphysical cloud processes occur on length scales of micrometers to millimeters (Baker, 1997), i.e., 8-11 orders of magnitude smaller than typical GCM resolutions, and the clouds themselves have length scales on the order of 0.1-1 km. This disparity in resolution has necessitated the use of "cloud parameter-

izations” to simulate clouds in GCMs (e.g., Slingo, 1987; Slingo and Slingo, 1991; Xu and Krueger, 1991; Rasch and Kristjánsson, 1998; Klein and Hartmann, 1993a). These cloud parameterizations, which are often empirically-based, attempt to predict grid-scale cloud characteristics based on other grid-scale model properties, such as relative humidity, vertical velocity, and convective tendency. This situation is in contrast with many other better-understood components of the climate system. For example we can take relative confidence in the baroclinic eddies produced by GCMs, at least in their dry behavior, because eddies result from the well-understood Navier-Stokes equations which, as they have length scales on the order of 1000 km, are well-resolved by GCMs.

Our relative inability to accurately include clouds in GCMs, the most sophisticated available climate models, makes clouds an important component of the climate system on which we can focus in order to attempt to understand the climate system better. If we are able to successfully do so we may be able to improve climate models, which should improve our ability to accurately forecast future climate under increased greenhouse gas concentrations. Moreover, improving our understanding of the physics of clouds could help us explain some of the mysterious, and at times seemingly inexplicable, climates that appear to lurk in Earth’s shrouded history. These ancient climates can be difficult to explain based on the physics we understand from the modern climate and have put into climate models. Insofar as both our relatively poor understanding of the physics of clouds and the significant role clouds play in determining Earth’s radiative balance make them a key contributor to climate uncertainty, clouds may be ideally-suited for a role in helping to

explain some of these paleoclimates.

Among the most mysterious climates of Earth's past are the so-called "Equable Climates" which prevailed during the late Cretaceous and early Paleogene (~100 to ~35 million years ago). During these periods Earth's climate was "equable" in that polar temperatures were much closer to equatorial temperatures than they are today (low equator to pole temperature difference) and high-latitude winter temperatures were much more like summer temperatures than they are today (low seasonality). Various sources of evidence support a low equator to pole temperature difference during equable climates, for example data suggest that during the early Paleogene tropical sea surface temperatures were only 0-10°C warmer than modern (Pearson et al., 2001; Norris et al., 2002; Roche et al., 2006; Tripathi et al., 2003), whereas the mean-annual surface air temperature was 25-40°C warmer than modern in the Arctic (Zachos et al., 1994; Schouten et al., 2002; Sluijs and coauthors, 2006; Moran and coauthors, 2006). Some of the most robust evidence for reduced seasonality during equable climates is that frost-intolerant plants and animals were able to survive in the interior of continents at paleolatitudes of up to 60-70° (Markwick, 1998; Wing and Greenwood, 1993; Greenwood and Wing, 1995), which is notable because evidence for the absence of sustained frosts during winter deep in continental interiors at such high latitudes provides a particularly strong and, given the relatively small increase in equatorial temperatures, difficult-to-explain constraint on climate.

The explanation for equable climates remains elusive. It does not appear that changes in continental configuration play a dominant role in explaining equable climates. The con-

tinental configuration changed drastically between the late Cretaceous and the early Paleogene, yet equable climates prevailed throughout these periods. Additionally, the early Paleogene continental configuration was broadly consistent with that of today, yet the climate has changed dramatically since then. Changes in the Sun's output also do not appear to offer a viable explanation for equable climates, as the solar constant was about 0.5% weaker 100 million years ago than it is today. Changes in greenhouse levels represent a more flexible avenue of explanation, as the carbon dioxide level during equable climates is very uncertain, although it was probably higher than modern and may have been as high as 4000 ppm during the early Paleogene (Pagani et al., 2005; Pearson and Palmer, 2000) and the concentration of methane and other trace gasses is entirely unknown.

When GCMs are run with "best-guess" topographic, bathymetric, and vegetative boundary conditions for periods of Equable Climates, it is difficult for them to simulate warm polar temperatures and reduced equator to pole temperature difference without also producing increases in tropical sea surface temperatures that seem to violate the data (e.g., Sloan and Rea, 1995; Bush and Philander, 1997; Otto-Bliesner and Upchurch, 1997; Upchurch et al., 1998; Huber and Sloan, 2001; Shellito et al., 2003). This is the paradox of equable climates: there seems to be some physical process missing from the GCMs that would explain either the warm poles or the cool tropics. This is a potentially important point because these same GCMs are used to forecast future climate under global warming, so that ensuring they contain all the relevant physics to simulate a warm world has important social, economic, and ecological implications. Recent upward revision of esti-

mates of tropical sea surface temperature during equable climates (see in particular Pearson et al. (2001) and Huber (2008)) has softened this equable climate paradox somewhat, as it makes some of the higher-CO<sub>2</sub> GCM simulations, which produce very warm tropical sea surface temperatures but a high-latitude climate more consistent with the data, more viable (e.g., Sloan and Rea, 1995; Shellito et al., 2003); however, even if GCMs can provide a reasonably accurate simulation of equable climates, understanding exactly how they do so remains an important undertaking because, aside from the intrinsic value of understanding the system, it could help us to determine whether and to what extent such processes could activate in the future under global warming.

Many physical processes have been proposed that might help to produce either warm poles or cool tropics during equable climates. They include mechanisms that increase meridional heat transport by the atmosphere (Lindzen and Farrell, 1980; Norris et al., 2002; Pierrehumbert, 2002; Farrell, 1990) or by the ocean (Hotinski and Toggweiler, 2003; Brass et al., 1982; Emanuel, 2002) and mechanisms that lead to a dramatic increase in polar stratospheric clouds, which can warm the high-latitude surface during winter (Sloan et al., 1992; Sloan and Pollard, 1998; Peters and Sloan, 2000; Kirk-Davidoff et al., 2002; Kirk-Davidoff and Lamarque, 2008). In this thesis, we will propose a positive feedback on high-latitude surface temperatures based on the onset of convection and convective clouds and investigate it using a hierarchy of climate models (Abbot and Tziperman, 2008a,b,c; Abbot et al., 2008a,b). In this proposed feedback, an initial warming, perhaps due to increased greenhouse gas concentration, leads to destabilization of the high-latitude atmo-

sphere to convection, causing convection, which results in convective clouds and increased atmospheric moisture, both of which trap outgoing longwave radiation and lead to further warming. A related suggestion of such a feedback was also briefly made by Sloan et al. (1999) and Huber and Sloan (1999).

In Chapter 2 we propose and introduce the convective-cloud feedback using a simple, zonally-averaged, two-level model of the atmosphere that is forced with annually-averaged solar radiation (no seasonal cycle) and run at various CO<sub>2</sub> concentrations. The model contains simplified parameterizations of convection, precipitation, and clouds, and a longwave radiation scheme that explicitly depends on CO<sub>2</sub>, water vapor, and cloud fraction. We find that at high CO<sub>2</sub> concentrations the convective cloud feedback is activated, causing large warming of the high-latitudes and a dramatic reduction in the equator to pole temperature difference. We view this chapter as an argument for the plausibility of the high-latitude convective-cloud feedback as a mechanism that could greatly warm the high latitudes either during equable climates or in future climate under global warming.

In Chapter 3 we analyze the convective cloud feedback in more detail using the National Center for Atmospheric Research (NCAR) single column model (SCAM), which contains state-of-the-art atmospheric physics parameterizations, high vertical resolution, a full seasonal cycle, a thermodynamic sea ice model, and a mixed layer ocean. As SCAM is a single column and is isolated dynamically from its surroundings, we must prescribe heat transports and horizontal and vertical velocities to it. We run SCAM over the Arctic ocean and find that when the ocean is ice-free at the beginning of winter, turbulent fluxes of

latent and sensible heat from the ocean to the lower atmosphere, as well as radiative cooling of the upper atmosphere, destabilize the atmosphere to convection and thereby activate the convective cloud feedback. The resulting convection produces optically-thick convective clouds that trap outgoing longwave radiation and warm the surface to such a great extent that these clouds are essential for the maintenance of ice-free conditions throughout the winter: without these clouds the ocean becomes covered with sea ice unless the heat transport and CO<sub>2</sub> concentration are increased to very high values. We find that the convective-cloud feedback occurs preferentially during winter because during summer low-level clouds block low-level atmospheric absorption of solar radiation so that atmospheric absorption of solar radiation occurs preferentially in the mid-troposphere and stabilizes the lower atmosphere to convection. As the convective cloud feedback is mostly active during winter, when the incoming solar radiation is small or zero at high latitudes, the cloud albedo is irrelevant and any clouds the mechanism produces must lead to warming.

In Chapter 4 we show that the convective cloud feedback is active in fully-coupled state-of-the-art ocean-atmosphere GCMs used in the 1%/year CO<sub>2</sub> increase to quadrupling scenario of the Intergovernmental Panel on Climate Change (IPCC) fourth assessment report. We also show that the convective cloud feedback dramatically increases the uncertainty in the Arctic winter sea ice forecasts of these models. Additionally, we find that if initiated by global warming, the convective cloud feedback could lead to rapid winter sea ice loss and might also make such loss difficult to reverse.

In Chapter 5 we determine the critical threshold CO<sub>2</sub> concentration at which the con-

vective cloud feedback can become active and the magnitude of the warming caused by the feedback using both a highly idealized model and SCAM. The critical CO<sub>2</sub> is particularly important because it helps to establish the relevance of the feedback for past and future climates. Both models agree that, in general, increased heat flux into the high latitudes at the surface or low altitudes decreases the critical CO<sub>2</sub>. Increases in poleward oceanic heat transport and in solar radiation absorbed during the summer should cause a sharp decrease in the critical CO<sub>2</sub>, but the effect of increases in poleward atmospheric heat transport depends on its vertical distribution. It is furthermore found that (1) if the onset of convection produces more clouds and moisture, the critical CO<sub>2</sub> should decrease and the maximum temperature increase caused by the convective cloud feedback should increase; (2) reducing the depth of convection reduces the critical CO<sub>2</sub> but has little effect on the maximum temperature increase caused by the convective cloud feedback. We discuss how these results should help with interpretation of the strength and onset of the convective cloud feedback as found, for example, in the IPCC coupled ocean-atmosphere models with different cloud and convection schemes of Chapter 4.

Chapter 6 contains the main conclusions of this thesis.

In summary, in this thesis we will propose a convective cloud feedback that could activate under high-latitude warming and produce dramatic further high-latitude warming, particularly during winter. This feedback could help to explain past equable climates and might be important in a future climate under global warming. We will investigate the feedback using a hierarchy of models ranging from simple semianalytical models to the most

sophisticated state-of-the-art global climate models and find that it is a robust aspect of the climate system. We will also use these models and theory to try to determine what factors control whether the feedback was actually active during equable climates and whether it could activate in the future.



# **Chapter 2**

## **A High-Latitude Convective Cloud**

### **Feedback and Equable Climates**

#### **2.1 Introduction**

A plethora of paleoclimatic data exists suggesting that Earth's climate during the late Cretaceous period ( $\sim 100$  to  $\sim 65.5$  Ma) and the early Paleogene period ( $\sim 65.5$  Ma to  $\sim 34$  Ma) was vastly different from Earth's modern climate. Oxygen isotopic ratios in the shells of Foraminifera indicate that during these periods the tropical sea surface temperatures (SSTs) were a few degrees Celsius warmer than they are at present (Pearson et al., 2001; Norris et al., 2002; Roche et al., 2006; Tripathi et al., 2003), whereas deep ocean temperatures were  $8\text{-}12^{\circ}\text{C}$  (Zachos et al., 2001), much higher than their modern value of  $0\text{-}3^{\circ}\text{C}$ . Provided deep ocean water was formed at high latitudes during the late Cretaceous and

early Paleogene, as it is currently, warm deep water temperatures can be interpreted as indicating warm high-latitude SSTs. Direct proxy data of high-latitude SSTs supports this supposition. Foraminiferal Oxygen isotopic ratios suggest SSTs were 10-15°C at about 75° paleolatitude (Zachos et al., 1994), Oxygen isotopic ratios in the shells of mollusks suggest that SSTs in coastal regions of the Arctic ocean were about 10-15°C during the early Paleogene, and the TEX<sub>86</sub> method (Schouten et al., 2002) provides evidence that the summer SST near the North Pole was as high as 23°C during the Paleocene/Eocene thermal maximum (PETM) (~55 Ma) and 15-18°C throughout the early Paleogene (Sluijs and coauthors, 2006; Moran and coauthors, 2006). Other data indicate that warm high-latitude SSTs were accompanied by warm continental temperatures. Examples of such evidence include the existence of fossils of frost intolerant plant and animal species such as crocodilians, palm trees, cycads, and gingers in continental interiors at up to 60-70° paleolatitude (Markwick, 1998; Wing and Greenwood, 1993; Greenwood and Wing, 1995). This implies that there were times when even during winter there were not sustained frosts at high latitudes in continental interiors. Additionally, leaf margin analysis indicates that during the Eocene (~56 to ~34 Ma) the terrestrial surface temperature had an annual mean of about 10°C and a cold month mean of roughly 0°C at a paleolatitude of about 75°, which is warmer than modern by about 20-25°C and 30-40°C, respectively (Greenwood and Wing, 1995). In aggregate, these data represent strong evidence that the climate during the late Cretaceous and early Paleogene was generally warm and remarkably equable, *i.e.*, having a low equator to pole temperature difference (EPTD; The term “equable climate” is also

used by some authors to denote a low seasonal variation in temperature (*e.g.*, Greenwood and Wing, 1995; Huber and Sloan, 1999)).

The causes of equable climates remain elusive. During the early Paleogene the continental configuration was broadly similar to that of today, although there have been major changes since the Cretaceous. The atmospheric CO<sub>2</sub> concentration may have been higher than today, although indirect measurements can only constrain the CO<sub>2</sub> to between 400-4000 ppm during the early Paleogene (Pagani et al., 2005; Pearson and Palmer, 2000). One approach to understanding equable climate dynamics is to analyze the results of sophisticated primitive equation global climate models run with boundary conditions chosen to correspond with those believed to have prevailed during the late Cretaceous or early Paleogene and increased greenhouse gas (GHG) concentrations. Studies using atmospheric general circulation models (GCMs), whether coupled to a mixed-layer ocean (Shellito et al., 2003; Sloan and Rea, 1995; Otto-Bliesner and Upchurch, 1997; Upchurch et al., 1998) or to a full ocean GCM (Huber and Sloan, 2001; Bush and Philander, 1997) have consistently yielded the important result that these models are unable to produce a climate consistent with available proxy data. In particular, the extreme polar warmth and moderate equatorial temperatures that define equable climates have escaped simulation. Shellito et al. (2003), for example, achieved a simulation relatively close to proxy data by running an atmospheric model coupled to a slab ocean at a CO<sub>2</sub> concentration of 2000 ppm. Still, in their simulation, the cold month mean temperatures are as low as -14°C at 70°N, the Arctic annual mean temperature is 1°C, and the tropical temperatures warm by 5°C, all of which may be

at odds with proxy data, although it is possible that biases in these data are responsible for this discrepancy. If the proxy data reflect reality, GCMs do not seem to provide accurate simulations upon extrapolation to vastly different boundary conditions and GHG forcings, even though they do reasonably well at simulating the current climate. As Huber and Sloan (2001) note, there may be some mechanism that “maintains warm poles without warming the tropics” that operated in Nature during periods of equable climate, but is missing from even the most sophisticated climate models.

A multitude of hypotheses have been proposed for the missing mechanism that would explain equable climates. Most focus on a combination of increased GHG concentrations and increased meridional heat transport, either by the atmosphere (Lindzen and Farrell, 1980; Norris et al., 2002; Pierrehumbert, 2002; Farrell, 1990) or by the ocean (Hotinski and Toggweiler, 2003; Brass et al., 1982; Emanuel, 2002). A third class concentrates on feedbacks that could affect the local high-latitude heat balance and leverage increases in the high-latitude temperature under increased GHG concentrations (Sloan et al., 1992; Kirk-Davidoff et al., 2002). We will give the recent hypotheses involving tropical cyclones and ocean heat transport (OHT) (Emanuel, 2002) and polar stratospheric clouds (PSCs) (Sloan et al., 1992; Kirk-Davidoff et al., 2002) special attention below.

Emanuel (2002) argued that increased oceanic mixing by tropical cyclones could drive a stronger oceanic meridional overturning circulation and increase the meridional OHT enough to reduce the EPTD. Korty et al. (2008) showed that increasing the tropical diffusion coefficient in an ocean GCM, even by an order of magnitude, does not significantly

alter the OHT poleward of  $40^\circ$ . However, increasing the tropical diffusion does increase vertical mixing of cool abyssal water with tropical surface water and does increase low latitude OHT. So an increased level of tropical cyclones during equable climates could represent a mechanism to keep tropical surface temperatures low even at greatly increased GHG levels.

Sloan et al. (1992) speculated that more extensive wetlands led to a greatly increased atmospheric methane concentration during the Eocene, which they argued could cause increased levels of winter PSCs. The greenhouse effect of these PSCs could produce marked high-latitude surface warming during winter. By imposing optically thick winter PSCs in a GCM, Sloan and Pollard (1998) and Peters and Sloan (2000) estimated that this effect could produce a maximum winter surface warming of about  $20^\circ\text{C}$  in some local high-latitude areas. Kirk-Davidoff et al. (2002) criticized this work on the grounds that there is no evidence for high methane concentrations throughout the late Cretaceous and early Paleogene. They instead proposed a positive feedback mechanism by which changes in EPTD could be greatly enhanced through a complex pathway leading to changes in polar stratospheric clouds. A crucial aspect of the Kirk-Davidoff et al. (2002) mechanism, that the winter polar stratosphere cool if the EPTD is reduced, results from the linear relationship between stratospheric overturning circulation and the EPTD that they enforce by fiat in their model. However, using an atmospheric GCM (AGCM) modified to provide greatly increased vertical resolution in the stratosphere, Korty and Emanuel (2007) argued that energy carried into the stratosphere by higher wavenumbers prevents significant decreases in

the stratospheric circulation and winter stratospheric temperatures under a large weakening of the EPTD. Although increased levels of PSCs could potentially represent part of the solution to the equable climates problem, it remains unclear whether there is a physically consistent mechanism to explain their presence.

We wish to pursue the idea of a cloud radiative feedback causing high-latitude warming in an equable climate, but focus on convective clouds instead of PSCs. The low altitude stratus clouds that prevail at high latitudes have a large and negative cloud radiative forcing (CRF) (Klein and Hartmann, 1993b; Hartmann et al., 1992; Kyle et al., 1991), while clouds associated with convection have a nearly zero CRF in the tropics (Ramanathan et al., 1989; Harrison et al., 1990) and could potentially have a positive CRF at high latitudes under lower solar insolation. This allows the possibility of a positive feedback on surface temperatures upon the initiation of convection. Specifically, if the extratropical surface temperature were to increase enough to initiate strong convection, the resulting change from low to high clouds and from negative to neutral or positive CRF could further warm the surface, leading to more atmospheric convection and hence to a positive feedback. We propose that this feedback could take part in maintaining warm mid and high latitudes and a low EPTD.

Some AGCM simulations of equable climates show high-latitude convection (see section 2.6) and changes in CRF represent the largest source of uncertainty in GCM climate change predictions (Cess and co authors, 1990, 1996; Soden and Held, 2006). We believe that these factors allow for an exquisite opportunity to use a relatively simple model that can be easily run for a wide range of climate regimes to test the feasibility of a high-latitude

convective cloud feedback as an explanation for the low EPTD of equable climates. We have constructed such a simple model. Given the model's simplicity we emphasize in the strongest terms that our purpose is not a quantitative solution of the equable climate puzzle. All we set out to do is make the case that the positive feedback due to convection and high clouds should be an important part of the discussion of equable climate dynamics.

Our model is zonally-averaged two-level model of the atmosphere in which we attempt to capture the main effects of water vapor and clouds on climate, although we neglect much of the detailed physics. We have made many assumptions, which are of varying validity. Among our more questionable assumptions is the very geometry of our model. We assume that we can provide reasonable analogs to processes such as convection using a model with only two vertical levels and that we can capture the main effects of the complex three-dimensional motion of air caused by baroclinic eddies through simple parameterizations in a zonally-averaged model. We acknowledge that such an approach may be problematic and try to account for some of its more egregious drawbacks. That said, significant progress has been made in climate research using atmospheric models with two vertical layers (*e.g.*, Phillips, 1956; Held and Suarez, 1978; Held, 2000; Holton, 1992) and zonally-averaged models (*e.g.*, Farrell, 1990; Held and Hou, 1980; Budyko, 1969; Sellers, 1969; Yao and Stone, 1987; North, 1975; North et al., 1981; Sokolov and Stone, 1998; Shell and Somerville, 2005; Stone and Yao, 1990, 1987). Furthermore, like similar idealized studies of equable climates before ours (*e.g.*, Farrell, 1990), we force our model with annual-average shortwave (SW) radiation as a first step, in spite of the importance of

seasonality for equable climates. We emphasize that we ask of our model only that it be a source of ideas to be later tested using fuller models and that it offer a semi-quantitative method of evaluating these ideas, not that it provide a realistic simulation of all aspects of climate.

This chapter is laid out as follows. We give a brief description of the model in section 2.2. Section 2.3 contains the results for the model run with 3 and 30 vertical columns ( $30^\circ$  and  $3^\circ$  meridional resolution, respectively). We use an idealized model of an atmospheric column to understand some of our results in section 2.4. We analyze the sensitivity of our results to parameter changes in section 2.5. We discuss the relation of our work to existing and future GCM experiments in section 2.6 and to proxy data for tropical SSTs in section 2.7. We conclude in section 3.5. The appendix (section 2.9) contains a full description of the model.

## 2.2 Model

We offer only a brief overview of the model here. We encourage readers interested in model details to consult the appendix (section 2.9).

The model is two-dimensional, in height and latitude (Fig. 2.1). It uses pressure coordinates in the vertical direction and spherical coordinates in the meridional direction. The meridional extent of the model is one hemisphere. It contains JMAX atmospheric columns, where JMAX is either 3 or 30 in the runs described here. Nearly all model parameters retain their values as the meridional resolution is changed (Tables 2.2 and 2.3). Each column

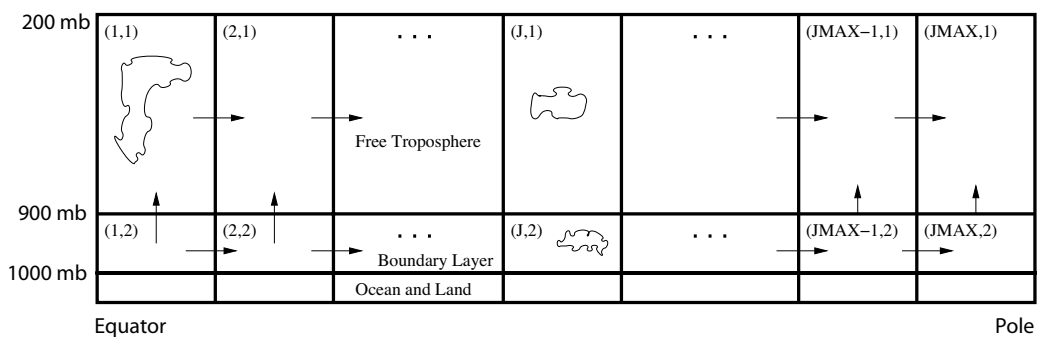


Figure 2.1: A diagram of the atmospheric box model.  $JMAX$  is the total number of columns, which are oriented meridionally. The upper level represents the free troposphere and the lower level represents the boundary layer. The surface consists of land and a mixed layer ocean with a specified ocean heat transport. Arrows represent transport of moisture and DSE by both advection and baroclinic eddies. Arrows point in the direction taken to be positive, not necessarily in the direction of transport when the model is run.

consists of two vertical levels - a boundary layer chosen to be between 900 and 1000 mb, and a free troposphere between 200 and 900 mb. We calculate dry static energy (DSE) and specific humidity ( $q$ ) prognostically in the center of each level. Energy and moisture are conserved in the model. Zonal mean velocities, which are calculated by solving the zonally-averaged nonlinear primitive equations, advect DSE and  $q$ . Parameterized baroclinic eddies diffuse DSE,  $q$ , and zonal momentum with a diffusivity that is dependent on the meridional gradient of boundary layer DSE (Stone, 1972). This parameterization does not allow up-gradient eddy momentum mixing, which may reduce the realism of our simulation. Annual mean shortwave (SW) radiation (North, 1975) drives the model. The longwave (LW) radiation scheme includes an explicit calculation of level emissivities as a function of water vapor, carbon dioxide, and cloud fraction (Sasamori, 1968; Lunkeit et al., 2005). The radiation scheme contains a third level above the center of the upper level to simulate the effects of high clouds.

We parameterize convection as a vertical mixing of DSE and moisture between the two vertical layers, both of which are conserved during this mixing. We calculate convective and stratiform clouds diagnostically as a function of the strength of convective mixing and the relative humidity, respectively (Xu and Krueger, 1991; Slingo and Slingo, 1991). These clouds interact with both LW and SW radiation. Precipitation occurs if the relative humidity in any box exceeds a critical value. The lower surface of the model consists of a mixed layer ocean with a specified OHT and a simple land surface. The land fraction is fixed at 0.3 for all latitudes. Specific heat and moisture are exchanged with the surface

using standard bulk aerodynamic formulae. See Fig. 2.2 for a diagram of processes that occur within a column of the model.

Fig. 2.3 contains results of a “present-climate” model run with 30 columns at a CO<sub>2</sub> of 280 ppm and with the albedo of both land and ocean specified to increase linearly from their standard value at 60° to 0.7 at the pole. This increased high-latitude albedo is a crude approximation of the effect of ice in the modern climate. We do not include the ice albedo parameterization in the runs we present in section 2.3. The model yields reasonable correspondence with modern climatology. We note in particular the similarity between Fig. 2.3i and the observed annual-average CRF (*e.g.*, Kyle et al., 1991, Fig. 2). The model simulates the near cancellation between the large and opposing cloud LW and SW forcings in regions of tropical convection (Ramanathan et al., 1989; Harrison et al., 1990) especially well. The only major qualitative difference between observed and modeled CRF is that the transition from neutral tropical CRF to strongly negative midlatitude CRF is sharper in our model, since the model switches from convective to stratiform clouds sharply. The similarity of modeled and observed CRF is important for this work since the CRF plays a central role in our mechanism. However, due to the model’s simplicity, exact correspondence with modern climatology for all output should be neither expected nor required of it - the model is a conceptual tool. The model could be tuned so that the displayed output more closely approximates modern climatology, but such a tuning would be misleading since there would certainly be other aspects of the model that would not be in agreement with modern climatology. Furthermore, the results we present in section 2.3 are not sensitive to

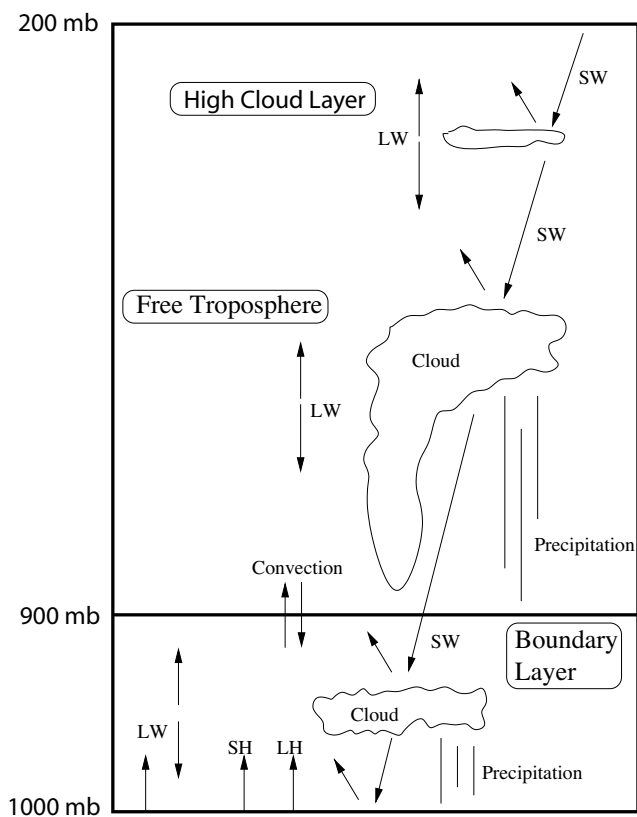


Figure 2.2: A diagram of single column processes in the model. SW stands for shortwave radiation, LW stands for longwave radiation, LH stands for latent heat flux, and SH stands for sensible heat flux.

important parameter choices (section 2.5). Finally, we note that we cannot validate much of our high CO<sub>2</sub> model output because corresponding data from the late Cretaceous and early Paleogene do not exist, *e.g.*, CRF.

## 2.3 Results

### 2.3.1 3 Columns

For illustrative purposes, we first describe our model run with 3 columns. At this resolution the latitude ranges of the columns are 0° – 30°, 30° – 60°, and 60° – 90°. Throughout this section what we refer to as the EPTD is formally the difference between the boundary layer temperature of the 60° – 90° column and the 0° – 30° column.

We propose that the onset of strong convection at mid and high latitudes could lead to changes in cloud and water vapor distribution and consequently atmospheric radiative properties that could result in a positive feedback on surface temperature. Central to our arguments are the high albedo of low altitude clouds and the greenhouse effect of high-altitude clouds (appendices A(2.9.5) and A(2.9.7)), which allow the CRF to change from strongly negative to slightly positive when convection switches on in a column and high clouds are created there. Since an increase in CRF results in surface warming, this leads to a positive feedback on surface temperature as convection is enabled, which helps to sustain mid- and high-latitude convection and a lower EPTD.

This convective cloud feedback allows two distinct climate modes when the model is

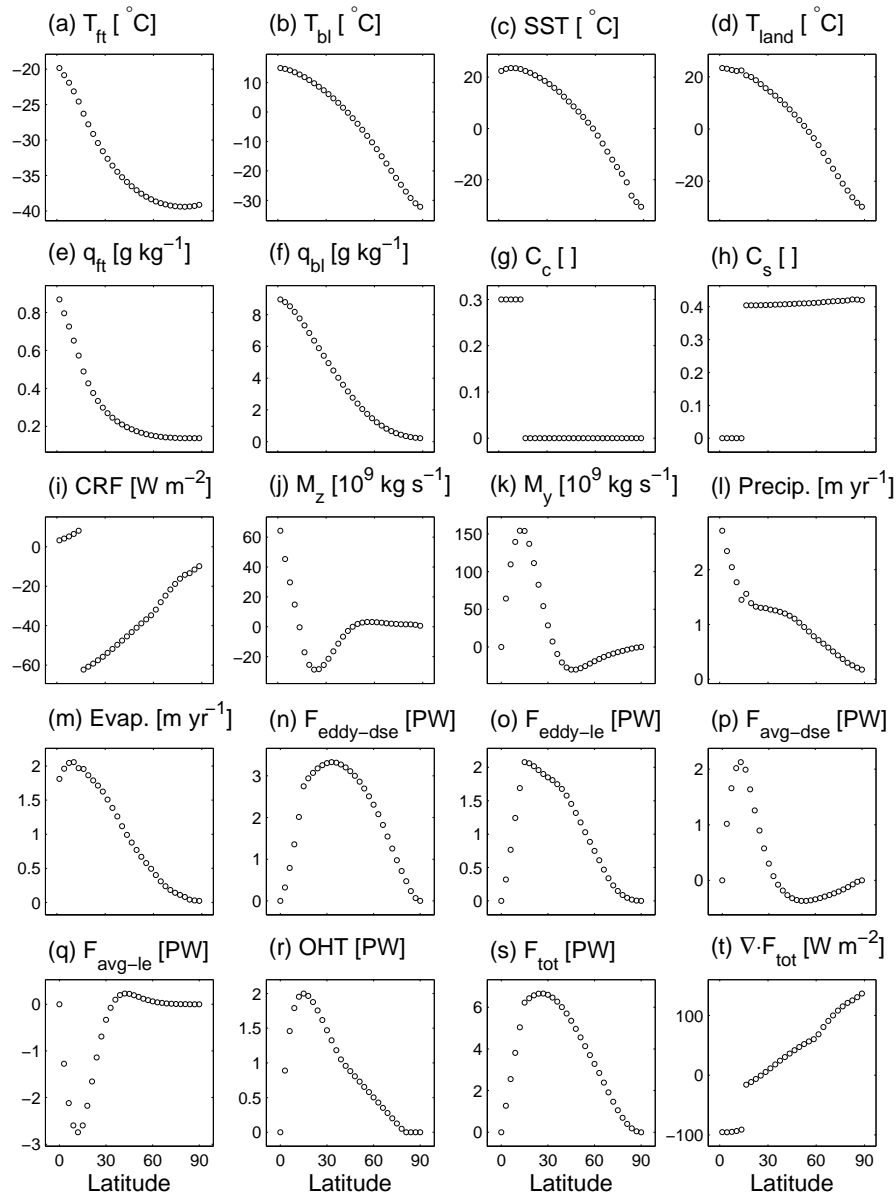


Figure 2.3: Steady-state model output as a function of latitude when the model is run with 30 columns ( $3^\circ$  latitude meridional resolution), a  $\text{CO}_2$  of 280 ppm, and the albedo of both land and ocean increasing linearly from their standard value at  $60^\circ$  to 0.7 at the pole. (a)  $T_{ft}$ , free tropospheric temperature, (b)  $T_{bl}$ , boundary layer temperature, (c) SST, sea surface temperature, (d)  $T_{land}$ , land temperature, (e)  $q_{ft}$ , free tropospheric specific humidity, (f)  $q_{bl}$ , boundary layer specific humidity, (g)  $C_c$ , convective cloud fraction, (h)  $C_s$ , boundary layer stratiform cloud fraction, (i) CRF, cloud radiative forcing, (j)  $M_z$ , vertical mass flux, (k)  $M_y$ , meridional mass flux in the upper layer, (l) Precip., precipitation, (m) Evap., total evaporation from land and ocean surface, (n)  $F_{eddy-dse}$ , meridional flux of dry static energy by eddies, (o)  $F_{eddy-le}$ , meridional flux of latent energy by eddies, (p)  $F_{avg-dse}$ , meridional flux of dry static energy by average circulation, (q)  $F_{avg-le}$ , meridional flux of latent energy by average circulation, (r) OHT, ocean heat transport, (1 PW =  $10^{15}$  W), (s)  $F_{tot}$ , total (atmosphere+ocean) meridional heat flux, (t)  $\nabla \cdot F_{tot}$ , convergence of the total meridional heat flux.

run with 3 columns. In the first mode, which is the only one present at low CO<sub>2</sub> and which we will henceforth refer to as MODE1, only the southern column convects and the EPTD is relatively high. Other climate characteristics are generally similar to those of the modern climate. In MODE2, which is the only mode present at high CO<sub>2</sub>, convection occurs in the northern as well as in the southern column and a reduced EPTD results. The alteration of northern CRF caused by northern convection in MODE2 allows the column to stay continually destabilized and convecting. Strong convection does not occur in the middle column in either mode because there is subsidence there (section 2.9.6).

Some of the differences between MODE1 and MODE2 can be seen in Fig. 2.4, which shows some model output as a function of CO<sub>2</sub>. To generate Fig. 2.4 we first calculated the MODE1 and MODE2 solutions by running the model to steady state under atmospheric CO<sub>2</sub> concentrations of 200 ppm and 6000 ppm, respectively. We then initialized the model with the MODE1 solution and ran the model to steady state at atmospheric CO<sub>2</sub> concentrations ranging from 200 ppm to 6000 ppm (circles in Fig. 2.4). Next, we initialized the model with the MODE2 solution and ran the model to steady state for the same CO<sub>2</sub> range (x's in Fig. 2.4). The figure shows that at 1500 ppm and below only MODE1 is stable<sup>1</sup>, at 1600 ppm to 4900 both MODE1 and MODE2 are stable<sup>2</sup>, and at 5000 ppm and above only MODE2 is stable. When the CO<sub>2</sub> is slowly increased and then decreased, the model

---

<sup>1</sup>Here we use “stable” in the dynamical systems sense, *i.e.*, an equilibrium state is stable if a system returns to it after small perturbations away from it. We will subsequently use “stable” in association with atmospheric column stability as well, *i.e.*, a column is convectively stable if convection is not occurring in that column. To avoid confusion we will qualify stability in the convective sense with some reference to convection.

<sup>2</sup>*N.B.*, MODE2 is not stable even at CO<sub>2</sub>=10 000 ppm when the surface albedo is increased to account for ice at high latitudes, as in section 2.2.

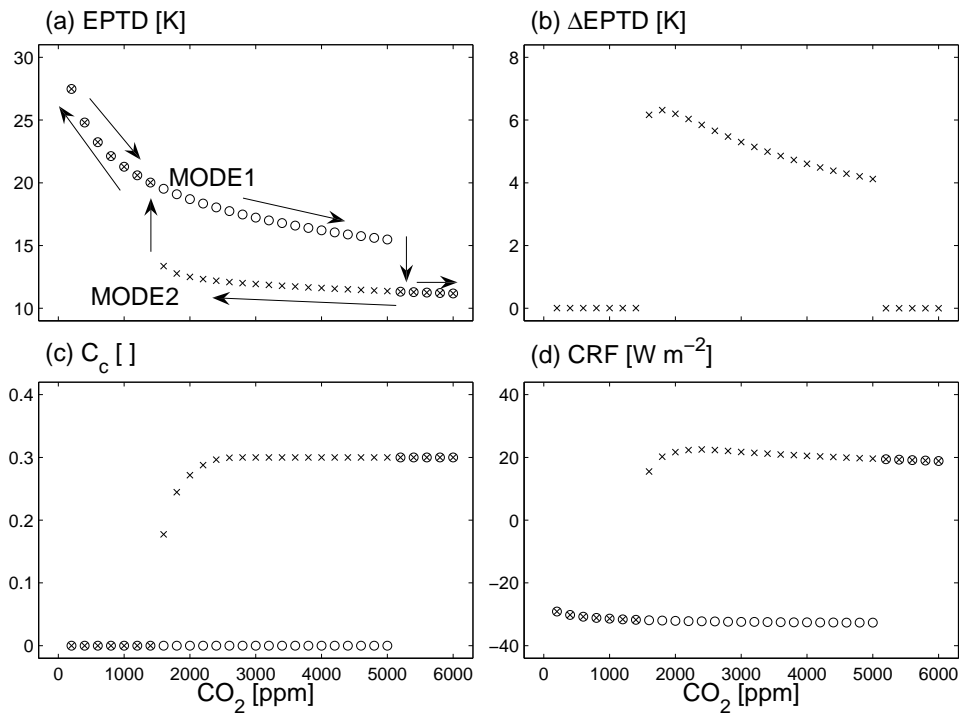


Figure 2.4: Selected steady-state model output for the 3 column model at different atmospheric CO<sub>2</sub> concentrations. At each CO<sub>2</sub> level the model is initialized from both MODE1 (circles) and MODE2 (x's). The variables plotted are (a) equator to pole temperature difference (EPTD), (b) difference in EPTD between the MODE1 solution and the MODE2 solution, (c) convective cloud fraction in the 60° – 90° column, and (d) cloud radiative forcing (CRF) in the 60° – 90° column. MODE1 and MODE2 are labeled in (a). Arrows in (a) indicate the path the model would take if the CO<sub>2</sub> were slowly increased then decreased.

follows a hysteresis cycle.

Fig. 2.4a shows the difference between the boundary layer temperature in the equatorial column and the polar column, *i.e.*, the 3 column EPTD. The EPTD decreases as CO<sub>2</sub> increases mostly because the moist lapse rate feedback (see section 2.4) in the 0°-30° column reduces increases in surface temperature with CO<sub>2</sub> in that column relative to the 60°-90° column, which at low CO<sub>2</sub> is not constrained to the moist adiabatic lapse rate since it is not convecting. When both modes exist, the EPTD is lower in MODE2 by up to 6.5°C (Fig. 2.4b) because of a change in local heat balance in the poleward column. In MODE1 the 60°-90° column is stable to convection and has no convective clouds, while in MODE2 it is convecting and has convective clouds (Fig. 2.4c). The increase in CRF (Fig. 2.4d) caused by this difference in cloud type causes the reduction of the EPTD in MODE2 relative to MODE1, despite a decrease in meridional heat transport in MODE2 (Table 2.1). The increase in CRF is caused by both an increase in absorbed SW and a reduction in OLR. The convective clouds reduce the OLR because they emit from a higher altitude and therefore a colder temperature. Their presence also reduces the EPTD, and therefore the atmospheric meridional heat transport, further reducing the OLR in the polar box. The increase in absorbed SW as the convective clouds form is due to a reduction of the total cloud albedo by about 0.05 as the convective clouds form (Table 2.2). This is a reasonable decrease in cloud albedo for a region changing from low clouds to thick convective high clouds (Fig. 19, Hartmann et al., 1992). If, as Abbot and Tziperman (2008b) find, the convective cloud feedback is most active in the winter when incoming SW is lowest, then

Table 2.1: Temperature and heat balance for the 60°-90° column when the model is run with 3 columns at  $CO_2 = 2000$  ppm. Results for both MODE1 and MODE2 are displayed. The EPTD is  $T_{bl}^1 - T_{bl}^3$ , where  $T_{bl}^1$  denotes the boundary layer temperature in the 0°-30° column and  $T_{bl}^3$  denotes the boundary layer temperature in the 60°-90° column.  $F_{eddy-dse}$ ,  $F_{eddy-le}$ ,  $F_{avg-dse}$  and  $F_{avg-le}$  are the convergences of meridional transport of dry static energy by eddies, latent energy by eddies, dry static energy by average circulation, and latent energy by average circulation, respectively, into the 60°-90° column.  $F_{tot-atm}$  and  $OHT$  are the total convergence of meridional transport of heat by the atmosphere and ocean, respectively, into the 60°-90° column.  $F_{tot-atm}$  is the sum of  $F_{eddy-dse}$ ,  $F_{eddy-le}$ ,  $F_{avg-dse}$ , and  $F_{avg-le}$ .  $SW$  and  $OLR$  are the absorbed shortwave and outgoing longwave radiation for the 60°-90° column. Since the model has reached steady state,  $F_{tot-atm}$ ,  $OHT$ ,  $SW$ , and  $OLR$  sum to zero. For the surface area poleward of 60°,  $1 \text{ W m}^{-2} = 3.4 \times 10^{13} \text{ W} = 0.034 \text{ PW}$ .

Diagnostic	Unit	MODE1	MODE2
<i>EPTD</i>	° C	+18.7	+12.5
$T_{bl}^3$	° C	+4.5	+12.5
$F_{eddy-dse}$	$\text{W m}^{-2}$	+41.4	+17.4
$F_{eddy-le}$	$\text{W m}^{-2}$	+30.2	+13.7
$F_{avg-dse}$	$\text{W m}^{-2}$	-2.2	-4.5
$F_{avg-le}$	$\text{W m}^{-2}$	+15.4	+16.9
$F_{tot-atm}$	$\text{W m}^{-2}$	+84.9	+43.5
<i>OHT</i>	$\text{W m}^{-2}$	+14.7	+14.7
<i>SW</i>	$\text{W m}^{-2}$	+148.1	+159.2
<i>OLR</i>	$\text{W m}^{-2}$	-247.6	-217.6

we may be overestimating the SW CRF in the convective regime and underestimating the warming potential of the convective cloud feedback. However, given that we do not include a seasonal cycle in this model, we feel it is appropriate to err on the side of caution.

We used parameters that lead to a present-day-like climatology at present-day forcings, as described in section 2.2, to generate Fig. 2.4 (Table 2.2). Reasonable variation of model parameters may lead to a change in the position of the bifurcation points that demarcate the three regions of model behavior (MODE1 only, both modes, and MODE2 only), but the basic results are robust - there are two climatic states, one of which has a large EPTD and does not have strong convection in the poleward column (MODE1) and one of which has a low EPTD and does have strong convection in the poleward column (MODE2); the former

state is stable at low CO<sub>2</sub> levels, the latter is stable at high CO<sub>2</sub> levels, and both are stable at intermediate CO<sub>2</sub> levels.

The convective cloud feedback can be triggered and multiple climate states exist when parameters other than CO<sub>2</sub> are varied. All that is necessary for the mechanism to function is for the high-latitude boundary layer temperature to be increased enough to initiate convection there, at which point the positive feedback leads to much greater boundary layer temperatures. For example, this can be done by increasing the specified OHT across 60° (not shown).

We now proceed to the 30 column model, for which the meridional resolution is 3°. The results of the 30 column model confirm those discussed above and add some important perspective on the robustness of different aspects of the proposed mechanism. We have retained the 3 column model results for several reasons. First, this model shows the simplest set of physics which can reproduce the proposed convective cloud feedback. In particular, it shows that detailed momentum dynamics, which are very poorly represented in the 3 column model, are not an essential element. Second, the 3 column model results show stronger hysteresis than the higher resolution model presented in the next section. Similarly strong hysteresis is also seen in the 30 column model in some parameter regimes we explored. The hysteresis and multiple equilibria will likely be further or even completely muted by the addition of a third dimension and the resulting synoptic scale motions, as well as by the addition of a seasonal cycle. However, it is important to realize that the proposed convective cloud feedback results in such multiple equilibria in the absence of additional

physics as this enriches our understanding of the proposed feedback. Specifically the existence of multiple equilibria implies that the convective cloud feedback mechanism involves both an instability mechanism and important nonlinear effects. It also implies the existence of an unstable (in the dynamical system sense) steady convective-equilibrium state between the two stable ones, which would be interesting to explore in future studies. Furthermore, when sea ice is added to the dynamics, the multiple equilibria due to the proposed feedback become even stronger and more robust, as demonstrated by Abbot and Tziperman (2008b) using a single column atmospheric model. It is therefore useful to explore the three column multiple equilibria dynamics without sea ice for comparison as done above. The three column model serves to demonstrate these points, while the higher resolution model demonstrates the perhaps less surprising result that the multiple equilibria are not expected to be robust in the presence of additional more realistic physics.

### **2.3.2 30 Columns**

We ran the 30 column model at various CO<sub>2</sub> concentrations in the following three ways:

1. Case I: With clouds fixed at the values they take when the model is run to steady state with CO<sub>2</sub>=280 ppm (circles in Figs. 2.5 and 2.6). High-latitude ice albedo is not included.
2. Case II: With interactive clouds initialized from the values they take when the model is run to steady state with CO<sub>2</sub>=280 ppm (diamonds in Fig. 2.5). This is a MODE1-like initialization.

3. Case III: With interactive clouds initialized from the values they take when the model is run to steady state with all atmospheric emissivities set to one (x's in Figs. 2.5 and 2.6). This is a MODE2-like initialization.

Fig. 2.5 shows selected model output as a function of CO<sub>2</sub> in each case. The model solutions in Case II and Case III are similar and exhibit a greatly reduced EPTD at CO<sub>2</sub> levels above about 400 ppm<sup>3</sup> (Fig. 2.5a). As with the 3 column model, this reduction in EPTD is due to the convective cloud feedback (Fig. 2.5c,d). The similarity of the solutions in Case II and Case III means that the 30 column analog of MODE1 is nearly equivalent to the 30 column analog of MODE2. Because of this, the appropriate measure of the strength of the convective cloud feedback in the 30 column model is the difference between the EPTD in Case I, when we fix the clouds and keep the feedback inactive, and Case III, when the feedback is fully active ( $\Delta EPTD$ , Fig. 2.5b). Fig. 2.5b shows that the convective cloud feedback leads to a reduction in the EPTD of 8-10°C for CO<sub>2</sub> values ranging from 400 ppm to 5000 ppm.

Fig. 2.6 displays the main 30 column model variables as a function of latitude for Case I and Case III with CO<sub>2</sub>=2000 ppm. The similarity between the model climate with CO<sub>2</sub>=280 ppm (Fig. 2.3) and in Case I at CO<sub>2</sub>=2000 ppm, when the cloud feedback is disabled, (circles, Fig. 2.6) emphasizes the magnitude of the effect the convective cloud feedback has on climate in Case III. The most striking features of the Case III climate are a reduced EPTD and an increased global mean boundary layer temperature relative to

---

<sup>3</sup>N.B., the convective cloud feedback does not activate at midlatitudes in the 30 column model until CO<sub>2</sub>=600-700 ppm when the surface albedo is increased to account for ice at high latitudes, as in section 2.2.

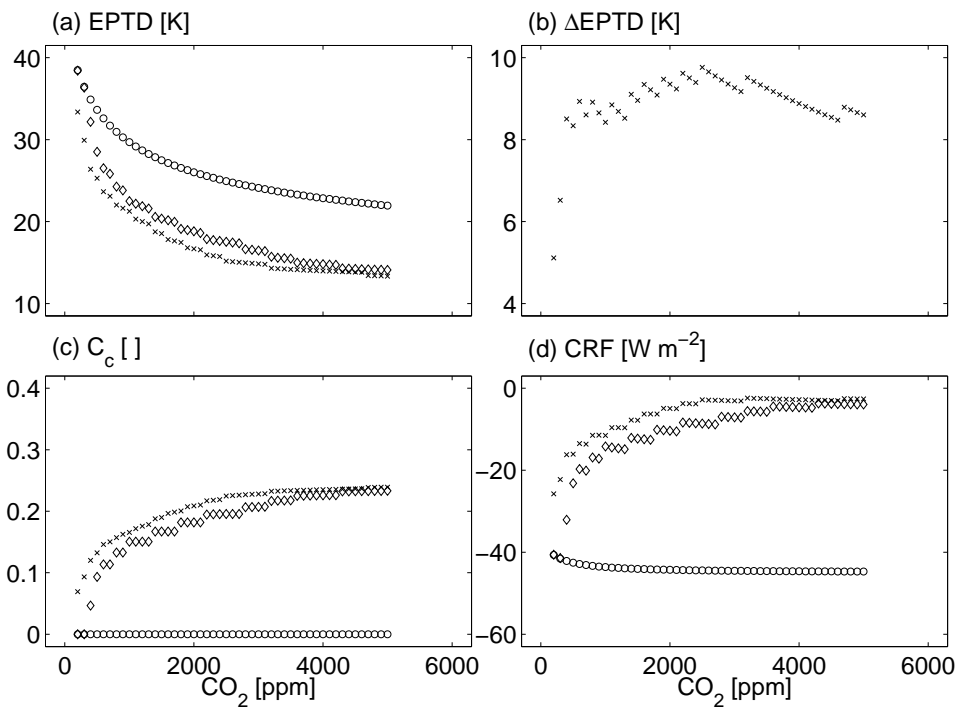


Figure 2.5: Selected steady-state model output for the 30 column model at different atmospheric CO<sub>2</sub> concentrations. At each CO<sub>2</sub> level the model is run with clouds fixed at the values they take when CO<sub>2</sub>=280 ppm (CASE I, circles), with interactive clouds initialized from their values when CO<sub>2</sub>=280 ppm (CASE II, diamonds), and with interactive clouds initialized from their values with all emissivities set to one (CASE III, x's). The variables plotted are (a) equator to pole temperature difference (EPTD), (b) difference in EPTD between the fixed cloud solution (circles in other panels) and the interactive cloud solution (x's in other panels), (c) 30° – 90° convective cloud fraction, and (d) 30° – 90° cloud radiative forcing (CRF).

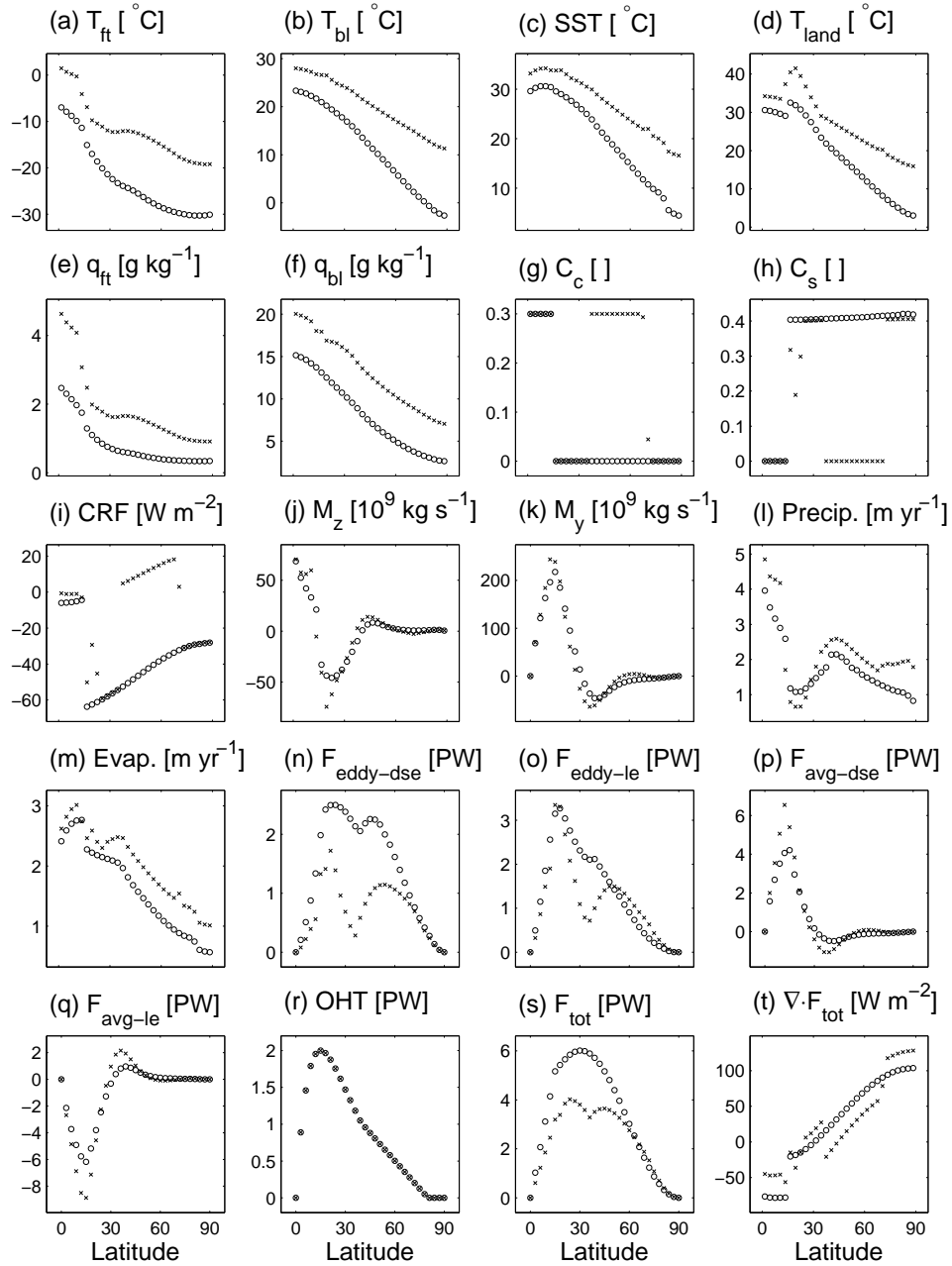


Figure 2.6: Steady-state model output as a function of latitude when the model is run with 30 columns ( $3^{\circ}$  latitude meridional resolution) and at a  $\text{CO}_2$  concentration of 2000 ppm. Output is displayed for the model run both with clouds fixed at the values they take when  $\text{CO}_2=280$  ppm (CASE I, circles) and with interactive clouds initialized from their values with all emissivities set to one (CASE III, x's). Panels are as in Fig. 2.3. The OHT is specified to be equal in both runs.

Case I (Fig. 2.6b), both caused by a dramatic change from stratus to convective clouds (Fig. 2.6g,h) and from negative to slightly positive cloud radiative forcing (Fig. 2.6i) in the extratropics. Mean circulation is roughly the same in both cases (Fig. 2.6j,k) and meridional heat transport is broadly reduced (Fig. 2.6s), although small high-latitude increases in the convergence of meridional heat transport are important (Fig. 2.6t).

In Case III strong extratropical convection extends from  $36^{\circ}$  to  $69^{\circ}$  (Fig. 2.6g), however the increase in boundary layer temperature over Case I extends all the way to the pole (Fig. 2.6b). As far poleward as strong convection extends, the convective cloud feedback can act directly to increase the boundary layer temperature by altering local energy balance, as described using the three column model of section 2.3.1. The 30 column model adds the important result that warming is communicated to the highest latitudes, those poleward of strong convection, by atmospheric heat transport (Fig. 2.6t). Due to the reduction in meridional temperature gradient the convergence of DSE transported by eddies is decreased in Case III, but the increase in temperature causes an increase in convergence of latent energy transported by both eddies and average circulation that more than offsets this.

There are a few important new lessons to be learned from the 30 column model. First, the 30 column model confirms the importance of the convective cloud feedback in increasing high-latitude temperature. Second, the convective cloud feedback activates at a lower  $\text{CO}_2$  in the 30 column model because the extratropics begin to convect gradually as  $\text{CO}_2$  is increased, rather than all at once. Third, the higher resolution indicates how the warming of the pole may have occurred in moderately equable climates, specifically convection might

develop in the mid-latitudes, and the atmosphere might transport latent heat to the highest latitudes. This may allow polar temperatures to increase even at  $\text{CO}_2$  concentrations for which convection is not active at the poles. Fourth, the 30 column model indicates that the hysteresis seen in the 3 column model may not be robust. Although multiple steady states with and without convection still occur at intermediate  $\text{CO}_2$  concentrations with interactive clouds (Cases II and III, Fig. 2.5), the difference between them is small and might be masked by atmospheric weather variability, were we to include such variability in this model.

Finally we note again that our model output should not be quantitatively compared to GCMs or proxy evidence. For example, the fact that more warming occurs in the northern midlatitudes in our model than in the AGCM of Shellito et al. (2003) when both are run at a  $\text{CO}_2$  concentration of 2000 ppm is more likely the result of limitations of our model, such as an unrealistically low land fraction at these latitudes, than positive attributes. We emphasize that our objective is not to quantitatively compare our solution with the proxy record, but rather to isolate and describe a potentially important feedback in a simple model.

## **2.4 Understanding the Onset of High-Latitude Convection at High $\text{CO}_2$**

Here we construct a highly idealized model of an atmospheric column and use it to heuristically explain the onset of the convective cloud feedback at high  $\text{CO}_2$ . Specifically, we

show that if the column is stable to convection, increasing the CO<sub>2</sub> decreases the moist stability and eventually leads to convection. We supply a constant horizontal atmospheric heat transport to the idealized atmospheric column, so we neglect any dynamical feedbacks.

The idealized model contains three levels: a surface (temperature  $T_s$ , emissivity  $\epsilon_s=1$ ), a boundary layer ( $T_2, \epsilon_2$ ), and a free troposphere ( $T_1, \epsilon_1$ ). We assume that the surface emissivity is one and do not account for atmospheric SW absorption. We assume a fixed atmospheric heat transport ( $F_a$ ) into the free tropospheric layer. A turbulent flux ( $F_t$ ) transports heat from the surface to the boundary layer and a convective flux ( $F_c$ ) transports heat from the boundary layer to the free troposphere. Heat balance for the surface, boundary layer, and free troposphere, respectively, leads to the following diagnostic equations

$$S(1 - \alpha) + \epsilon_2 \sigma T_2^4 + \epsilon_1 (1 - \epsilon_2) \sigma T_1^4 - \sigma T_s^4 - F_t = 0,$$

$$F_t + \epsilon_2 \sigma T_s^4 + \epsilon_2 \epsilon_1 \sigma T_1^4 - 2\epsilon_2 \sigma T_2^4 - F_c = 0,$$

$$F_a + F_c + \epsilon_1 (1 - \epsilon_2) \sigma T_s^4 + \epsilon_1 \epsilon_2 \sigma T_2^4 - 2\epsilon_1 \sigma T_1^4 = 0,$$

where  $S$  is the top of the atmosphere SW,  $\alpha$  is the total albedo and  $\sigma$  is the Stefan-Boltzmann constant. We choose  $F_t$  to enforce a constant temperature difference ( $\Delta T$ ) between the surface and the boundary layer,

$$T_s = T_2 + \Delta T.$$

Let the moist static energy in the boundary layer (defined in section 2.9.6) be  $MSE_2$  and the saturation moist static energy in the free tropospheric layer be  $MSE_1^*$ . We choose  $F_c$  to

enforce the moist stability criticality ( $MSE_2 \leq MSE_1^*$ ), so  $F_c=0$  if  $MSE_2 < MSE_1^*$  and  $F_c$  only becomes non-zero to prevent  $MSE_2$  from exceeding  $MSE_1^*$ . To calculate  $MSE_2$  and  $MSE_1^*$ , we assume a constant boundary layer relative humidity ( $RH_2$ ) and constant layer heights ( $z_1$  and  $z_2$ ).

We model changes in  $CO_2$  by changing both  $\epsilon_1$  and  $\epsilon_2$  by the same amount (let  $\epsilon = \epsilon_1 = \epsilon_2$ ). Results are qualitatively similar regardless of how we increase  $\epsilon_1$  and  $\epsilon_2$ . At low  $\epsilon$ ,  $MSE_2 < MSE_1^*$ , the model does not convect, and in the upper layer there is a balance between  $F_a$  and LW radiation terms. Increases in the optical depth of the atmosphere ( $\epsilon$ ) lead to larger changes in  $T_2$  than  $T_1$  (Fig. 2.7a,b, see also Weaver and Ramanathan, 1995). The resulting increase in  $MSE_2 - MSE_1^*$  (Fig. 2.7c,d) is leveraged by boundary layer moisture increasing more than free tropospheric saturation moisture because  $T_2 > T_1$  (Fig. 2.7e,f) and because of the Clausius-Clapeyron equation. This continual destabilization of the column with respect to convection eventually causes the column to convect, at  $\epsilon \approx 0.85$  in Fig. 2.7, which causes a kink in the plots in Fig. 2.7 and a major change in model behavior. Once the column is convecting  $MSE_2$  is constrained to equal  $MSE_1^*$ , so both must increase at the same rate as  $\epsilon$  is increased. Since  $T_2 > T_1$  the moisture term in  $MSE_2$  (Fig. 2.7f) increases faster than the saturation moisture term in  $MSE_1^*$  (Fig. 2.7e). Consequently the free tropospheric temperature  $T_1$  increases more than the boundary layer temperature  $T_2$  and the lapse rate decreases (Fig. 2.7b) as  $\epsilon$  increases (this is known as the moist lapse rate feedback).

This simple model elucidates the physics leading to the onset of mid- and high-latitude

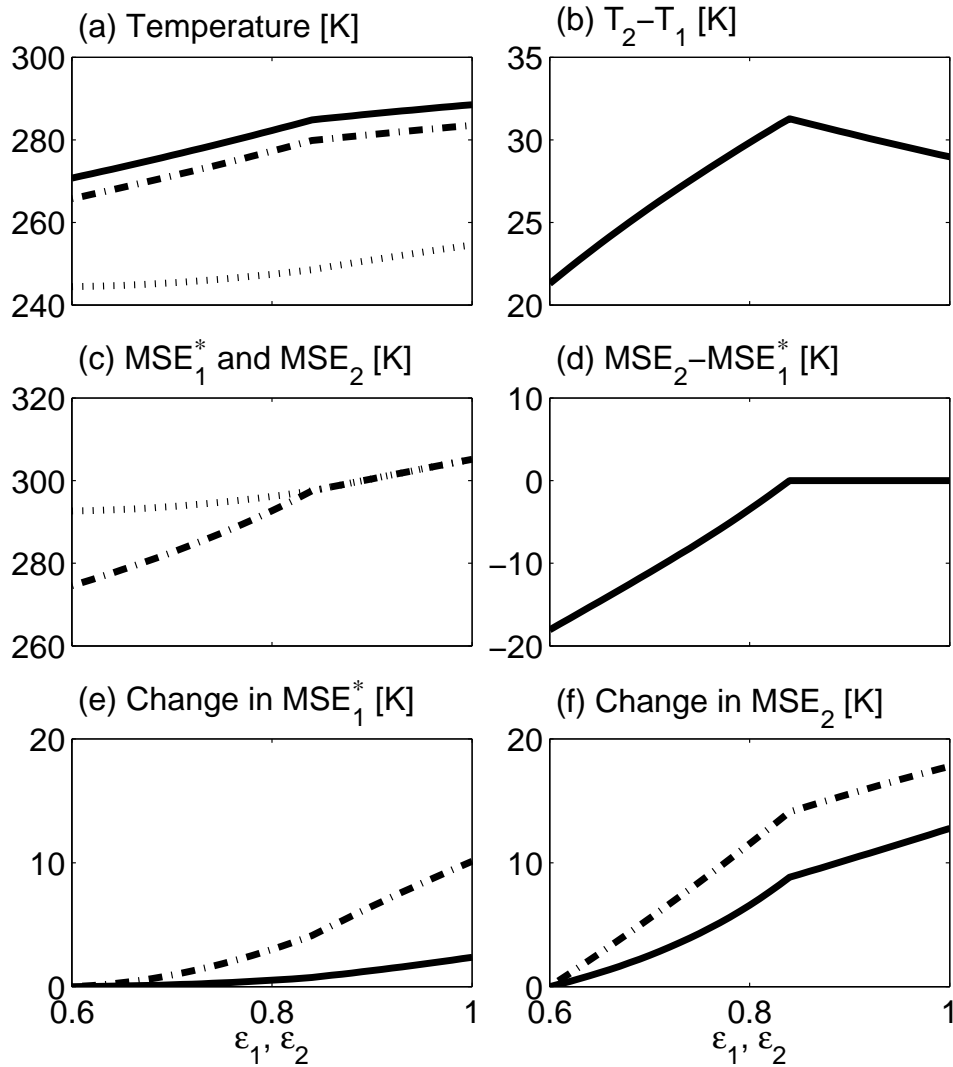


Figure 2.7: Equilibrium results for a two level atmospheric column idealized model (section 2.4) as a function of the specified level emissivities ( $\epsilon_1$  and  $\epsilon_2$ ), where  $\epsilon_1$  and  $\epsilon_2$  are varied together.  $S=250 \text{ W m}^{-2}$ ,  $\alpha=0.2$ ,  $F_a=80 \text{ W m}^{-2}$ ,  $\Delta T=5 \text{ K}$ ,  $z_1=4.8 \text{ km}$ ,  $z_2=410 \text{ m}$ ,  $RH_2=0.85$  (section 2.4). These parameter choices are a rough approximation of modern conditions at  $60^\circ$ .  $z_1$  and  $z_2$  correspond to pressures of 950 mb and 550 mb, respectively, if a scale height of 8 km is assumed. Panels are as follows: (a) surface temperature (solid line), boundary layer temperature (dash-dotted line) and free tropospheric temperature (dotted line), (b) boundary layer temperature minus free tropospheric temperature, *i.e.*, the temperature lapse rate, (c) boundary layer moist static energy (dash-dotted line) and free tropospheric saturation moist static energy (dotted line), (d) boundary layer moist static energy minus free tropospheric saturation moist static energy, (e) change (from lowest value of  $\epsilon_1$  and  $\epsilon_2$ ) in temperature (dash-dotted line) and moisture (solid line) contributions to free tropospheric saturation moist static energy, and (f) change in temperature (dash-dotted line) and moisture (solid line) contributions to boundary layer moist static energy.

convection in our more detailed models. As  $\text{CO}_2$  increases in an atmospheric column that is stable to convection, the boundary layer temperature increases at least as much as the free tropospheric temperature. Because the boundary layer is warmer, the Clausius-Clapeyron relation dictates that the moisture content increases more there than in the free troposphere. The resulting decrease in the convective stability ( $MSE_1^* - MSE_2$ ) destabilizes the air column and eventually leads to convection.

## 2.5 Sensitivity Tests

To build confidence in the results of section 2.3, we investigate the effects of varying important cloud and convection parameters over large ranges in the 30 column model. We establish the limits of the parameter range in which our results apply and find that our results are robust to large perturbations of important model parameters.

We quantify the effect of the convective cloud feedback for a set of parameters as the difference between the EPTD in Case I and the EPTD in Case III with  $\text{CO}_2=2000$  ppm ( $\Delta EPTD_{2000}$ ). Although this  $\text{CO}_2$  choice is arbitrary, it allows uniform comparison.

The convective cloud feedback involves both a reduction in the downwelling SW reflected by clouds and an increase in the upwelling LW trapped by clouds, which combine to lead to an increase in the CRF, as convective clouds form (Table 2.1). When a parameter is altered that plays a role in setting the change in CRF as convection switches on, it affects  $\Delta EPTD_{2000}$ . For example increases (decreases) in the albedo of high clouds and upper level clouds, both of which are caused by convection in this model, decrease (increase)

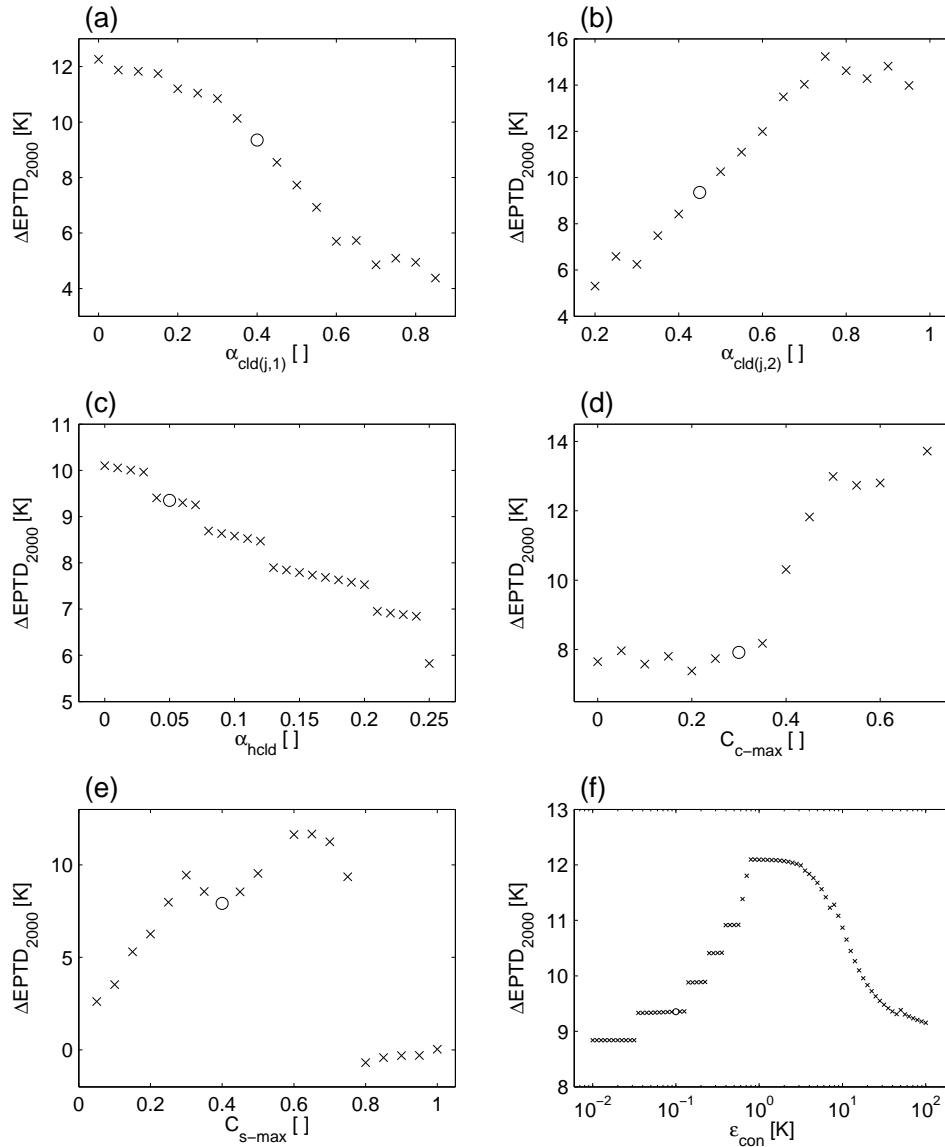


Figure 2.8: Sensitivity analysis: The difference between the EPTD in Case I and the EPTD in Case III with  $\text{CO}_2=2000$  ppm ( $\Delta EPTD_{2000}$ ) plotted as important model parameters are varied in the 30 column model. When a parameter is varied, all other parameters retain their values given in Table 2.2. Circles represent standard parameter choices (Table 2.2). The varied parameters are as follows: (a) Upper level cloud albedo. The model does not converge to a physical solution in CASE III for  $\alpha_{cld(j,1)} \geq 0.9$ . (b) Lower level cloud albedo. The model does not converge to a physical solution in CASE III for  $\alpha_{cld(j,2)} \leq 0.15$ . (c) High cloud albedo. (d) Maximum convective cloud fraction. The model does not converge to a physical solution in CASE III for  $C_{c-max}=0.65$  and for  $C_{c-max} \geq 0.75$ . (e) Maximum stratiform cloud fraction. The model does not converge to a physical solution in CASE III for  $C_{s-max}=0.0$  and for  $C_{s-max}=0.55$ . (f) Thickness of the convective switch.

$\Delta EPTD_{2000}$  (Fig. 4.5a,c), while changes in the lower level cloud albedo have the opposite effect (Fig. 4.5b). Increasing (decreasing) the maximum convective cloud fraction is more complex because doing so simultaneously increases the upper level emissivity and albedo, however the former effect dominates over the latter in determining  $\Delta EPTD_{2000}$  (Fig. 4.5d). Since low clouds produce only a small LW forcing, changing the maximum stratiform cloud fraction has a similar effect on  $\Delta EPTD_{2000}$  as changing the low cloud albedo (Fig. 4.5e). In these experiments, the convective cloud feedback is only eliminated at  $\text{CO}_2 = 2000$  ppm ( $\Delta EPTD_{2000} = 0$ ) when the low cloud albedo or cloud fraction is increased so much that the feedback is only active at  $\text{CO}_2 > 2000$  ppm.

Remarkably, the convective cloud feedback remains strong as we vary  $\epsilon_{con}$ , the parameter controlling the scale of the convective switch, over four orders of magnitude (Fig. 4.5f). The convective cloud feedback mechanism functions even when  $\epsilon_{con}$  is so large that convection and convective clouds are nearly linear in convective stability, instead of switch-like. For  $\epsilon_{con} \lesssim 1^\circ\text{C}$ , increasing (decreasing)  $\epsilon_{con}$  allows successively more columns to convect in CASE III, producing step-like increases (decreases) in  $\Delta EPTD_{2000}$ . For  $\epsilon_{con} \gtrsim 1^\circ\text{C}$ , increasing (decreasing)  $\epsilon_{con}$  causes convecting columns to convect less strongly, and so decreases (increases)  $\Delta EPTD_{2000}$ .

Here we have shown that our results are robust to large changes in important cloud and convection parameters. While developing the model we performed another set of sensitivity experiments in which we increased and decreased nearly all model parameters by 25% and found that our preliminary results were robust to these changes.

## 2.6 Discussion: The convective cloud feedback and GCMs

It seems that the proposed convective cloud feedback mechanism is sufficiently simple and robust that it should also be seen in at least some GCM simulations of equable climate. If a model has significant deep convective activity it should produce high clouds and associated positive CRF, as well as some LW warming due to enhanced water vapor content. Indeed, there is AGCM evidence (Huber and Sloan, 1999) that winter convection might occur over high-latitude oceans if SSTs are kept high enough to eliminate sea ice. The above paper only briefly mentions that such high latitude convection is present, but does not discuss its role in producing high clouds and the effect of a radiative feedback on interactive surface temperatures.

We cannot conclusively determine whether other equable climate GCM simulations see such high latitude convection, and if not why, but we offer some speculations here. The difficulty with discussing some of the published GCM runs is that they have not analyzed convection and radiation feedbacks as proposed here in most cases, so the available information is limited. It is quite possible that some of these runs did show at least some parts of our proposed high latitude convective cloud feedback. We hope that the present chapter raises the awareness to this feedback so that it can be examined in future GCM studies.

Korty and Emanuel (2007) found moist lapse rates year-round throughout the extra-tropics when they fix surface meridional temperature gradients to be low in an AGCM, providing indirect evidence of high latitude convective activity. Furthermore, Abbot and Tziperman (2008b) used the NCAR single column model with state-of-the-art atmospheric

physics and a mixed layer ocean to show that when there is no sea ice at high latitudes, high clouds and water vapor caused by winter convection exert a strong positive radiative forcing on the surface that could keep winter sea ice from forming.

Shellito et al. (2003) ran an AGCM coupled to a slab ocean at a CO<sub>2</sub> concentration of 2000 ppm, and obtained warm high latitude temperatures relatively close to the proxy data. The largest warming they see is during winter in the nearly ice-free Arctic, which they attribute to the sea ice albedo feedback. Given that shortwave radiation is reduced or zero during winter in the Arctic, the sea ice insulating feedback and the convective cloud feedback proposed here may represent more plausible causes of this warming. Their annual-mean Arctic precipitation increases by some 0.5 mm/day when the CO<sub>2</sub> concentration is increased from 500 ppm to 2000 ppm, in a manner quantitatively consistent with the triggering of atmospheric convection (Abbot and Tziperman, 2008b). However, they briefly indicate increased large-scale precipitation at high latitudes rather than convective precipitation, although the results shown in the paper do not enable us to judge conclusively the existence of our proposed feedback in their run.

That GCM simulations of equable climate may not all find high latitude convection, could be due to several factors. The first, relevant to GCMs with an active sea ice component, is based on the finding of Abbot and Tziperman (2008b) of enhanced multiple equilibria due to the interaction of proposed convection cloud feedback and sea ice in a full-physics single column model. If this is indicative of the behavior of 3D GCMs, it is possible that the GCMs only see the ice equilibria, but have not explored the parameter

regime sufficiently to see the no-ice equilibria due to the computational cost of running these models. A second factor, relevant also to atmosphere-only GCMs, is the possibility that the CO<sub>2</sub> concentration, which is highly uncertain during periods of equable climate, was not high enough in these runs. The precise CO<sub>2</sub> concentration at which the Arctic, for example, becomes sea ice free, deep atmospheric convection initiates and our feedback is triggered, may vary between different GCMs. This critical CO<sub>2</sub> value may depend on the ocean meridional heat transport and on convection, cloud, sea ice thermodynamics and sea ice albedo parameterizations, all of which have sufficient uncertainty to collectively result in a different switching point of this feedback. Given the logarithmic dependence of the radiative forcing of CO<sub>2</sub> and the uncertainty in the true climate sensitivity to CO<sub>2</sub>, one may need to try significantly higher values. Note that Shellito et al. (2003) see significant warming nearly consistent with proxy observations only at 2000 ppm with their ocean-slab AGCM runs, while some other runs only used a CO<sub>2</sub> of about 560 ppm (Huber and Sloan, 1999). A third factor explaining the absence of the proposed feedback is relevant to coupled ocean-atmosphere GCMs. Even if the atmospheric component of a coupled GCM shows convection at high CO<sub>2</sub> values with a prescribed SST or even with a mixed layer ocean, it is possible that the coupled model could drift into a different regime with no high latitude convection. Such a drift might occur due to inconsistencies between the meridional heat transport carried by the ocean model and the implied ocean heat transport expected by the atmosphere in atmosphere-only simulations. Climate drift forced the use of flux corrected models for many years in the context of present-day climate studies, and this may still be

an issue for equable climate simulations.

Because our model, like many of those used in previous theoretical studies of equable climates (*e.g.*, Kirk-Davidoff et al., 2002; Farrell, 1990), is zonally averaged, the atmospheric state is the same over both ocean and land. This means that when convection occurs, it occurs over both land and ocean. However, cooling and drying at the surface should inhibit land convection during winter. This calls into question the capacity of our proposed convective cloud feedback to produce continental interior winter temperatures high enough to be consistent with proxy data. However, modern observations (Korty and Schneider, 2007; Harrison et al., 1990) and a single column modeling study (Abbot and Tziperman, 2008b) suggest that over ocean the convective cloud feedback should be most active during winter. We speculate that moisture and cirrus clouds produced by strong convection over the ocean during winter could be advected over continents, where the resulting LW forcing could increase surface temperatures. This LW forcing would result directly from the clouds and water vapor advected over land, and from clouds formed as the water vapor condensed over land.

The high cirrus cloud lifetime of a few days may suffice to create a non-negligible radiative effect over the continents. Atmospheric eddies tend to destroy cirrus clouds and dry the atmosphere. This drying occurs due to the repeated upward and downward motions of air parcels induced by the passing eddies, causing condensation and precipitation. The eddy drying process should be less effective in an equable climate where the meridional temperature gradient is smaller and therefore the eddy activity weaker. As a result the

advection of water vapor and cloud water into continental interiors may be more efficient during equable climates.

We can think of three reasons for why such a process has not shown up in GCM simulations which seem to often suffer from too cold continental interior temperatures. First, many of the atmospheric models used in the past for equable climate simulations used diagnostic cloud water parameterizations rather than including horizontal cloud water advection explicitly. Second, the relatively low vertical resolution used by many climate GCMs can significantly bias the calculated vertical motions due to eddy activity (K. Emanuel, personal communication), and possibly amplify the drying effect of eddies. Both effects may significantly reduce the effect of advected water vapor and clouds on continental interiors in GCM simulations. This suggests the need to use models of higher vertical resolution, prognostic cloud water, and perhaps even prognostic cloud fraction parameterization (Anderson et al., 2004; Tiedtke, 1993) for equable climate simulations. Third, even AGCMs that produce a sufficiently warm high latitude temperatures under high CO<sub>2</sub>, tend to produce a too high EPTD (Shellito et al., 2003). As a result, the eddy field may not weaken sufficiently in these simulations, and the eddy drying effect may inhibit the advection of clouds and moisture over the continents. These suggestions are all highly speculative, and we readily admit that our proposed mechanism, like many other equable climate mechanisms offered before, may not explain the warm continental interiors.

We conclude this section by noting that some elements of the convective feedback have been observed in AGCMs (Korty and Emanuel, 2007; Schneider and Walker, 2006; Huber

and Sloan, 1999) and in a sophisticated, but isolated, single column atmospheric model (Abbot and Tziperman, 2008b). However, the full convective cloud feedback has not yet been observed in a coupled GCM. Although the specific reasons for this discrepancy remain unclear, potential causes are many. In particular, it is possible that the proposed feedback is active in at least some equable climate runs, but that it has not been explicitly documented and analyzed. We feel that such previous and new GCM simulations need to be reexamined in view of the proposed mechanism and that this may contribute to our understanding of the convective cloud feedback mechanism and GCM simulations of equable climates in general.

## 2.7 Further Discussion: Tropical SSTs

An important piece of the equable climate puzzle is the consistent paleoclimatic evidence that tropical SSTs from the late Cretaceous and early Paleogene were not as high relative to modern climate as were polar surface temperatures. In our model (Case III), tropical SSTs are 31-32°C at CO<sub>2</sub>=500 ppm (not shown) and 33-34°C at CO<sub>2</sub>=2000 ppm (Fig. 2.6c) and the model produces tropical SSTs of 22.5-24°C for CO<sub>2</sub>=280 ppm (Fig. 2.3c) and 24.5-26°C for CO<sub>2</sub>=370 ppm (not shown). This corresponds to a warming of tropical SSTs, from “modern” to “equable,” of 5-11.5°C. Estimates of ancient tropical SSTs using the  $\delta^{18}\text{O}$  of oxygen in the shells of planktonic Foraminifera have recently been revised upward because of the failure of previous studies to properly account for diagenetic effects on the Foraminifera and surface seawater  $\delta^{18}\text{O}$  gradients. Modern estimates based on  $\delta^{18}\text{O}$  mea-

measurements are that during the late Cretaceous and early Paleogene, tropical SSTs were “at least 28-32°C” (Pearson et al., 2001), 33-34°C (Norris et al., 2002), and 32-33°C (Roche et al., 2006). In addition Foraminiferal Mg/Ca ratios may support tropical SSTs of up to 34°C, although this result depends on which Mg/Ca history is assumed (Tripathi et al., 2003). Since current tropical SSTs are in the range of 24-30°C (Peixoto and Oort, 1992), tropical SSTs may have been 0-10 degrees warmer during equable climates. So the increase in tropical SSTs in our model as the CO<sub>2</sub> is increased and the convective cloud feedback activates in the extratropics is consistent with the higher end of corresponding data. We believe that this consistency is reasonable given the simplicity of our model.

## 2.8 Conclusion

We have demonstrated the importance of a high-latitude convective cloud feedback in determining the equator to pole temperature difference (EPTD) in a simple model. This feedback is due to a combination of high surface temperatures favoring strong convection and the radiative properties of clouds present during strong convection favoring high surface temperatures. Low clouds have a negative cloud radiative forcing (CRF), while high clouds have a neutral or positive CRF, so if the boundary layer temperature can be increased enough to initiate convection and generate high clouds, the above positive feedback can be activated. The feedback we describe involves convective clouds, which are mostly tropospheric, and is different from those involving PSCs (Kirk-Davidoff et al., 2002; Sloan et al., 1992). However, recent observational evidence implying moistening of the strato-

sphere by extratropical convection could represent a possible connection between the two ideas (Hanisco et al., 2007; Dessler and Sherwood, 2004).

At low CO<sub>2</sub> concentrations the model climate operates similarly to the observed climate, while at higher CO<sub>2</sub> the model displays convection at high latitudes and a drastically reduced EPTD. At intermediate CO<sub>2</sub> concentrations the positive feedback leads to multiple equilibria and allows hysteresis as the CO<sub>2</sub> is varied, but these results may not be robust given the simplicity of our model. The convection at northern latitudes is strong and tropical-like, and a distinction should be drawn between it and the convection in the midlatitudes of the modern observed climate that is associated with the storm track. It is important to note that the reduction of the EPTD is due to a rearrangement of local heat balance at high latitudes, rather than an increase in meridional heat transport, which, in fact, decreases in our model's low EPTD solution.

We wish to propose a possible connection between the physics of our high CO<sub>2</sub> solution and equable climates, such as those present during the late Cretaceous period (~100 to ~65.5 Ma) and the early Paleogene period (~65.5 Ma to ~34 Ma). The results from our model indicate that the existence of strong convection at mid and high latitudes may have contributed to the low EPTD during these warm periods. We find it encouraging that in our model the convective cloud feedback leads to a reduced EPTD for CO<sub>2</sub> > 600 ppm, well within the range of CO<sub>2</sub> estimates for periods of equable climates (Pagani et al., 2005; Pearson and Palmer, 2000).

Although we have made many approximations in our simple model, we believe we have

effectively used it to subject our idea to a rudimentary plausibility test. Furthermore, we think that our model could represent a useful motivation and complement to future coupled GCM runs, as envisioned by Held (2005). Overall, we hope that this chapter adds the proposed feedback based on high latitude convection and the resulting high cloud radiative forcing to the vocabulary of equable climate research.

## **2.9 Appendix: Detailed model description**

This section contains a full description of the model. We outline the dry static energy and moisture equations in section 2.9.1 and the calculation of velocities from the primitive equations in section 2.9.2. We describe the model's grid and the calculation of advective terms in section 2.9.3 and the eddy parameterization in section 2.9.4. Section 2.9.5 contains the radiation scheme. We explain the convection and precipitation schemes in section 2.9.6 and our cloud parameterization in section 2.9.7. We describe ocean and land surface properties and fluxes of sensible and latent heat from the surface in section 2.9.8.

### **2.9.1 Dry static energy and Moisture equations**

Dry static energy is defined as the sum of the gravitational potential energy and the internal energy

$$DSE = \phi + C_p T.$$

Table 2.2: Standard model parameters for both the 3 and 30 column models.

Parameter	Unit	Value	Parameter	Unit	Value
$dt$	s	10	$frac_{land}$	-	0.3
$\alpha_{cld(j,1)}$	-	0.40	$\alpha_{cld(j,2)}$	-	0.50
$\alpha_{hcl d}$	-	0.05	$C_{c-max}$	-	0.30
$M_{min}$	-	0.01	$C_{s-max}$	-	0.40
$\alpha_{land}$	-	0.20	$\alpha_{ocn}$	-	0.10
$r$	$s^{-1}$	$2.0 \times 10^{-6}$	$\tilde{v}$	$m^2 s^{-1}$	$1.0 \times 10^8$
$K_{DSE}$	$m s^{-1} J^{-1}$	$0.8 \times 10^9$	$K_q$	$m s^{-1} J^{-1}$	$4.0 \times 10^9$
$\tau_{precip}$	s	250	$C_{sh-land}$	-	$2.0 \times 10^{-3}$
$C_{sh-ocn}$	-	$1.0 \times 10^{-3}$	$C_{lh-land}$	-	$2.0 \times 10^{-3}$
$C_{lh-ocn}$	-	$1.0 \times 10^{-3}$	$ \mathbf{v} $	$m s^{-1}$	6.0
$k_{con-max}$	$s^{-1}$	$1.0 \times 10^{-5}$	$\epsilon_{con}$	K	0.1
$RH_{crit(j,1)}$	-	0.6	$RH_{crit(j,2)}$	-	0.8
$\epsilon_{r0}$	-	2.5	$C_{land}$	$J m^{-3} K^{-1}$	$2.0 \times 10^6$
$D_{land}$	m	1.0	$C_{ocn}$	$J kg^{-1} K^{-1}$	$4.19 \times 10^3$
$D_{ocn}$	m	1.0	$\rho_{ocn}$	$kg m^{-3}$	$1.0 \times 10^3$
$M_{squash}$	$kg s^{-1}$	7.0	$f_{evap}$	-	0.5
$OHT_0$	W	$2.0 \times 10^{15}$	$\theta_0$	degrees	15.0
$\theta_{lin}$	degrees	40.0	$\theta_{zero}$	degrees	80.0

We solve the following equations for DSE and  $q$ , the specific humidity,

$$\begin{aligned} \frac{\partial DSE}{\partial t} = & \left( \frac{\partial DSE}{\partial t} \right)_{adv.} + \left( \frac{\partial DSE}{\partial t} \right)_{eddy} + \\ & \left( \frac{\partial DSE}{\partial t} \right)_{rad.} + \left( \frac{\partial DSE}{\partial t} \right)_{sens.} + \\ & \left( \frac{\partial DSE}{\partial t} \right)_{conv.} + \left( \frac{\partial DSE}{\partial t} \right)_{precip.} + \\ & \left( \frac{\partial DSE}{\partial t} \right)_{re-evap.}, \end{aligned} \quad (2.1)$$

$$\begin{aligned} \frac{\partial q}{\partial t} = & \left( \frac{\partial q}{\partial t} \right)_{adv.} + \left( \frac{\partial q}{\partial t} \right)_{eddy} + \\ & \left( \frac{\partial q}{\partial t} \right)_{evap.} + \left( \frac{\partial q}{\partial t} \right)_{conv.} + \\ & \left( \frac{\partial q}{\partial t} \right)_{precip.} + \left( \frac{\partial q}{\partial t} \right)_{re-evap.}. \end{aligned} \quad (2.2)$$

We describe the calculation of advective (adv.) and eddy terms in appendices 2.9.3 and 2.9.4, the radiation term in section 2.9.5, sensible heat (sens.) and surface evaporation (evap.) terms in section 2.9.8, and convection (conv.), precipitation (precip.), and re-evaporation (re-evap.) terms in section 2.9.6.

## 2.9.2 Velocity Scheme

We solve the zonally-averaged spherical primitive equations in pressure coordinates.

$$\begin{aligned} \frac{\partial u}{\partial t} = & -\frac{1}{a \cos(\theta)} \frac{\partial}{\partial \theta} (uv \cos(\theta)) + uv \tan(\theta)/a \\ & - \frac{\partial}{\partial p} (\omega u) + 2\Omega \sin(\theta)v \\ & + \left( \frac{\partial u}{\partial t} \right)_{eddy} - r\delta_{k2}u, \end{aligned} \quad (2.3)$$

$$\begin{aligned} \frac{\partial v}{\partial t} = & -2\Omega \sin(\theta)u - \frac{1}{a} \frac{\partial \phi}{\partial \theta} \\ & - r\delta_{k2}v + \tilde{v} \frac{1}{a^2} \frac{\partial^2 v}{\partial \theta^2}, \end{aligned} \quad (2.4)$$

$$\phi_p = -\alpha, \quad (2.5)$$

$$0 = \frac{1}{a \cos(\theta)} \frac{\partial}{\partial \theta} (v \cos(\theta)) + \omega_p, \quad (2.6)$$

$$p\alpha = RT. \quad (2.7)$$

Here  $t$  is time,  $\theta$  is the latitude,  $p$  is the pressure,  $u$  is the zonal velocity,  $v$  is the meridional velocity,  $\omega = \frac{dP}{dt}$  is the pressure velocity,  $\phi$  is the geopotential,  $\alpha = \frac{1}{\rho}$  is the specific volume,  $R$  is the ideal gas law constant,  $\Omega$  is Earth's rotation rate,  $T$  is temperature, and  $\delta_{ij}$  is the Kronecker delta ( $k$  refers to vertical level, see below). The terms with  $r$  in Eqs. (2.3) and

(2.4) represent friction in the boundary layer. Hydrostaticity is assumed in Eq. (2.5). We will discuss the parameterization of the eddy term in Eq. (2.5) in section 2.9.4. We neglect advective terms from the material derivative in Eq. (2.4) because they do not enter the dominant balance. The term involving  $\tilde{v}$  in Eq. (2.4) is for numerical smoothing. All quantities in Eqs. (2.3)-(2.7) are zonally-averaged. This scheme yields a Hadley cell of reasonable magnitude and a Ferrell cell with an amplitude that is somewhat too small (Figs. 2.3j and 2.3k). The simulation of the Ferrell cell in our model may suffer from the fact that eddies cannot mix momentum up-gradient in our model, as they do in Nature.

### 2.9.3 Grid and Advective Terms

We use an Arakawa C-type grid, so  $DSE$ ,  $q$  and  $u$  are defined on box centers while  $v$  and  $\omega$  are defined at box edges (Fig. 2.9). We label model boxes with two indices -  $j$  and  $k$ .  $j$  gives the meridional position and ranges from 1 in the most equatorward column to  $JMAX$  in the most poleward column.  $k$  denotes vertical level and takes the value 1 in the free troposphere and 2 in the boundary layer. We split Eqs. (2.3) and (2.4) into their barotropic and baroclinic components and integrate the barotropic and baroclinic zonal and meridional velocities to steady state using a leapfrog scheme with a Robert filter in time. We calculate pressure velocity and geopotential diagnostically using Eqs. (2.5) and (2.6).

We calculate the advection and eddy tendencies for each grid box by multiplying fluxes

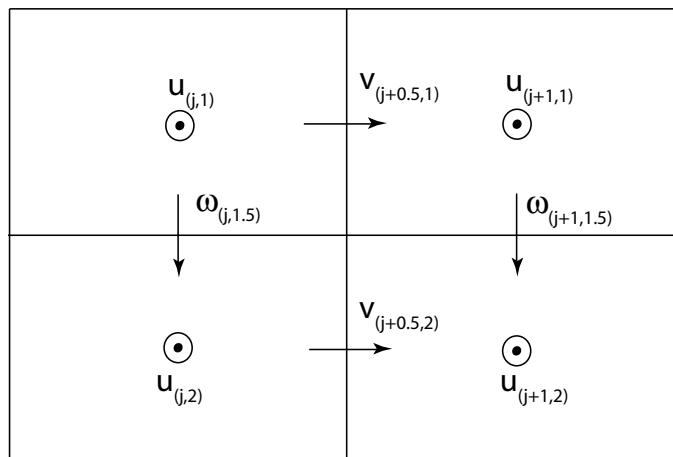


Figure 2.9: A diagram of the Arakawa c-type grid used for velocity variables in the model. Arrows point in the positive direction for each velocity variable. The positive direction for zonal velocities is out of the page. Dry static energy and specific humidity are at box centers with zonal velocity.

across box interfaces ( $\{F\}$ ) by cross-sectional areas and dividing by the box volume

$$\left(\frac{\partial X}{\partial t}\right)_{adv. \text{ or eddy}} = \frac{F_1 \cos(\theta_1) - F_2 \cos(\theta_2)}{R(\sin(\theta_2) - \sin(\theta_1))} + \frac{F_t - F_b}{p_b - p_t}, \quad (2.8)$$

where  $X$  is  $DSE$ ,  $q$ , or  $u$ . The subscripts 1 and 2 stand for the equatorward and poleward sides of the box, respectively, and the subscripts  $t$  and  $b$  stand for the top and bottom of the box, respectively. We calculate the fluxes ( $\{F\}$ ) using an upwind scheme for advection and Eqs. (2.9-2.11) for eddies.

#### 2.9.4 Baroclinic Eddy Parameterization

We simplistically parameterize the meridional transport of DSE, moisture and zonal momentum by baroclinic eddies as a diffusion process with a diffusion coefficient that is dependent on the boundary layer DSE gradient and the vertical level (Stone, 1972). We assume that vertical transport by eddies acts mainly to redistribute DSE and moisture within the free troposphere and neglect transport between the boundary layer and the free troposphere. We also do not include the effect of static stability on eddies. The meridional eddy

transport of  $DSE$ ,  $q$ , and  $u$  are given by

$$\overline{v'DSE'} = -K_{DSE}D_k \frac{\partial DSE}{\partial \theta}, \quad (2.9)$$

$$\overline{v'q'} = -K_q D_k \frac{\partial q}{\partial \theta}, \quad (2.10)$$

$$\overline{v'u'} = -K_u D_k \frac{\partial u}{\partial \theta}. \quad (2.11)$$

We choose the parameters  $K_{DSE}$  and  $K_q$  so that maximum eddy DSE and LE transports for the present-day model simulation are roughly consistent with Trenberth and Stepaniak (2003) and  $K_u$  so that the model produces a reasonable circulation (section 2.9.2).  $D_k$  is the diffusion coefficient, given by

$$D_k = C_k \left| \frac{\partial DSE_2}{\partial \theta} \right|.$$

We include  $C_k$ , the vertical dependence of the diffusion coefficient, because GCM results indicate that friction present in the boundary layer reduces baroclinic eddy transport there (Branscome et al., 1989; Stone and Yao, 1990). Following Nakamura et al. (1994), we parameterize this effect by multiplying transports by a factor of  $1 - e^{-z/\Delta z}$  where  $\Delta z \approx 450$  m, which yields  $C_1 \approx 1$  and  $C_2 \approx 0.5$  upon vertical averaging.

## 2.9.5 Radiation

We use the parameterization of North (1975) and Nakamura et al. (1994) for the meridional distribution of the mean annual SW radiation impinging on the top of the atmosphere

$$Q(\theta) = \frac{Q_0}{4} \left[ 1 + \frac{Q_2}{2} (3 \sin^2(\theta) - 1) \right],$$

where  $Q_0=1365 \text{ W m}^{-2}$  and  $Q_2=-0.482$ . This formula approximates the zonal and annual mean SW radiative flux to within 2%. We do not include seasonal and diurnal variations in SW radiation.

We assume random overlap of the cloud layers for the calculation of SW radiation reaching the surface

$$F_{sw}^{\downarrow} = Q(\theta)(1 - \alpha_{sfc})(1 - f_c^1 \alpha_{cld}^1) \\ (1 - f_c^2 \alpha_{cld}^2)(1 - f_c^{high} \alpha_{cld}^{high}). \quad (2.12)$$

Here  $\alpha_{sfc}$  is the surface albedo, which takes different values over land and ocean.  $f_c^i$  and  $f_c^{high}$  are the cloud fractions and  $\alpha_{cld}^i$  and  $\alpha_{cld}^{high}$  are the cloud albedos. The *high* subscript refers to the third cloud layer, which is above the center of the free tropospheric layer, and which we will describe below. We neglect the scattering of SW radiation by the atmosphere. We assume boundary layer clouds have higher albedos than free tropospheric clouds (Table 2.2) (Baker, 1997; Arking, 1991; Hartmann et al., 1992). We neglect the dependence of cloud albedo on solar zenith angle (Cess, 1976; Lian and Cess, 1977) and

many other potentially important cloud albedo effects.

The LW radiation scheme consists of a three-layer model. The bottom two layers correspond to the model mid-box levels and have emissivities calculated as a function of water vapor and carbon dioxide mixing ratios and cloud fraction (Sasamori, 1968; Lunkeit et al., 2005). We assume that the highest cloud layer, which contains only high convective clouds, is in radiative equilibrium.

The effective path length of a gas in the atmosphere is defined as (Sasamori, 1968)

$$u = \frac{1}{g} \int_{P_1}^{P_2} \hat{q} \times \frac{P}{P_s} dP,$$

where  $\hat{q}$  is the mixing ratio by mass of the species, *e.g.*, CO<sub>2</sub> or water vapor, and  $P_1$  and  $P_2$  are the pressure limits of the layer being considered. We assume the mixing ratio is constant within each box. This is a better approximation for CO<sub>2</sub> than for water vapor, which decays rapidly with height, but we feel that even for water vapor assuming a constant mixing ratio is sufficient for the arguments we make using this model. Assuming constant mixing ratio, the relation for the effective path length can be integrated to yield

$$u = \frac{\hat{q}}{2gP_s} (P_2^2 - P_1^2),$$

which gives the effective path length in kg m<sup>-2</sup>.

We convert the water vapor path length to gm cm<sup>-2</sup> and the carbon dioxide path length to cm at STP (273.15 K and 10<sup>5</sup> Pa) and use the following formulae to calculate emissivities

(Sasamori, 1968)

$$\epsilon_{H_2O} = A_1 \log_{10}(u_{H_2O} + B_1) + C_1, \quad (2.13)$$

$$\epsilon_{CO_2} = A_2 \log_{10}(u_{CO_2}) + B_2. \quad (2.14)$$

See Table 2.3 for values of the constants.

We use the transmissivity of water vapor near the 15 micron region to account for the overlap between water vapor and carbon dioxide absorption (Sasamori, 1968)

$$\tau_{H_2O} = 1.33 - 0.832(u_{H_2O} + 0.0286)^{0.260},$$

so that the clear-sky emissivity is given by (Sasamori, 1968)

$$\epsilon_{clear} = \epsilon_{H_2O} + \epsilon_{CO_2} \times \tau_{H_2O}. \quad (2.15)$$

We take the transmissivity of a layer to be the product of the clear-sky and cloud transmissivities, yielding (Lunkeit et al., 2005)

$$\epsilon = \epsilon_{clear} + f_c \epsilon_c - f_c \epsilon_c \epsilon_{clear}. \quad (2.16)$$

Here  $f_c$  is the cloud fraction and  $\epsilon_c$  is the emissivity of clouds, which we set to one for all cloud types.

We calculate cloud radiative forcing using the following formulae

$$CRF_{lw} = OLR_{clear} - OLR, \quad (2.17)$$

$$CRF_{sw} = (F_{sw}^{\downarrow}) - (F_{sw}^{\downarrow})_{clear}, \quad (2.18)$$

$$CRF = CRF_{lw} + CRF_{sw}. \quad (2.19)$$

Here  $OLR$  is the upward longwave radiation at the top of the atmosphere,  $F_{sw}^{\downarrow}$  is defined in Eq. 2.12, and the *clear* subscript refers to the value of the quantity when the atmosphere is cloud-free. Since we do not include the absorption of shortwave radiation by the atmosphere,  $CRF_{sw}$  is the same whether it is calculated at the surface or at the top of the atmosphere. We first run the model to steady state and calculate  $OLR$  and  $F_{sw}^{\downarrow}$ . We then calculate  $OLR_{clear}$  by running the longwave radiation code using the steady-state temperatures and with all cloud emissivities set to zero. We calculate  $(F_{sw}^{\downarrow})_{clear}$  by setting all cloud albedos to zero.

The positive longwave radiative forcing of high clouds is due to the fact that they radiate at low temperatures. Cirrus and other types of clouds associated with strong convection often occur at or above the tropopause. Our highest model layer is centered at 550 mb, so the warming effect of high clouds is drastically reduced. To get a realistic LW forcing from high clouds we add a layer above the center of the free troposphere model layer made up entirely of convective clouds (section 2.9.7). We assume that this layer is in radiative equilibrium and it only exists in the radiation scheme. It has an emissivity of  $\epsilon_{high} = f_c^{high} \epsilon_c$ ,

where  $f_c^{high}$  is the cloud fraction in this layer, so its emissivity is zero when there is no convection (Eq. (2.25)). With this modification the cloud radiative forcing in the model is reasonable when the model is run at  $CO_2=280$  ppm and with polar ice (Fig. 2.3). We also tried assuming an altitude of the high clouds and then calculating their temperature from the upper box temperature using the moist adiabatic lapse rate. We found that the high-cloud temperatures thus produced are similar to the high-cloud temperatures produced by assuming radiative equilibrium, both at low and high  $CO_2$ . Our method has the advantage that we do not need to specify the altitude of the high clouds.

When we ran the model using the formulae from Sasamori (1968), the global mean surface temperature increased by only  $0.6^\circ C$  with 3 columns and  $0.8^\circ C$  with 30 columns in response to a doubling of atmospheric carbon dioxide from 280 ppm to 560 ppm. These values, which are commonly referred to as the equilibrium climate sensitivity (Cubasch et al., 2001), are consistent with Ohring and Adler (1978), who obtained a value of  $0.5^\circ C$  with ice held constant in a zonally-averaged two-level model with an embedded higher resolution radiation model with a LW scheme based on Sasamori (1968). We modified the Sasamori (1968) coefficients (Table 2.3) so that the equilibrium climate sensitivity is  $2.5^\circ C$  for the 3 column model and  $3.8^\circ C$  for the 30 column model, consistent with the range of  $2.0^\circ C$ - $5.1^\circ C$  given by the Intergovernmental Panel on Climate Change Third Assessment Report (Cubasch et al., 2001). The sensitivity is larger in the 30 column model because when  $CO_2=280$  ppm strong convection only occurs in the 30 column model between  $0^\circ - 15^\circ$ , whereas the entire column spanning  $0^\circ - 30^\circ$  convects in the 3 column model, allowing

Table 2.3: Comparing values of parameters in the LW radiation scheme in this chapter to those in Sasamori (1968).  $B_2=-0.1$  for the 30 column model and  $-0.18$  for the 3 column model.

Parameter	This Chapter	Sasamori (1968)
$A_1$	0.50	0.2400
$B_1$	0.77	0.6220
$C_1$	0.01	0.0100
$A_2$	0.20	0.5460
$B_2$	-0.1,-0.18	0.0581

the moist lapse rate feedback to operate over a much larger area in the 3 column model.

When we held the water vapor constant for the LW scheme, but allowed it to increase elsewhere in the model, the climate sensitivity was  $1.6^\circ\text{C}$  with 3 columns and  $2.1^\circ\text{C}$  with 30 columns, so that the water vapor feedback accounts for one third to one half of the total climate sensitivity, which is roughly consistent with the results of more complex models (Cubasch et al., 2001; Colman, 2003). In all the runs described in this paragraph we held the surface albedo at a constant value of 0.7 poleward of  $60^\circ$  (section 2.2), so there was no surface albedo feedback. The cloud feedback was negligible because the clouds only change from their MODE1 configuration under larger GHG forcings.

## 2.9.6 Convection and Precipitation

The moist static energy is defined as (Emanuel, 1994)

$$MSE = DSE + L_v r.$$

Here  $L_v$  is the latent heat of water and  $r$  is the water vapor mixing ratio. The saturation MSE is calculated using the saturation mixing ratio instead of the actual mixing ratio.

We parameterize convection as a vertical mixing of DSE and  $q$  that activates when the boundary layer moist static energy exceeds the free tropospheric saturation moist static energy (Raymond, 1995). We accomplish this parameterized convection using a tanh-smoothed switch, so that the convective mixing coefficient is given by the following relation

$$k_{con} = k_{con-min} + \frac{1}{2}(k_{con-max} - k_{con-min}) \times \left( 1 + \tanh \left( \frac{MSE_2 - MSE_1^*}{C_{pd}\epsilon_{con}} \right) \right), \quad (2.20)$$

where  $k_{con-min}$  is the vertical mixing coefficient in a stable atmosphere,  $k_{con-max}$  is the vertical mixing coefficient for an unstable atmosphere, and  $\epsilon_{con}$  sets the scale of  $MSE_2 - MSE_1^*$  over which convection turns on. DSE and water vapor are conserved during this mixing. We neglect the vertical mixing of momentum by convection.

Due to low vertical resolution, subsidence does not inhibit convection in our model as effectively as it does in the atmosphere. We therefore shut convection off when the descent mass flux exceeds  $M_{squash}$ . We experimented with slightly more sophisticated parameterizations, such as assuming that the descending air followed a dry adiabat and the ascending air followed a saturation moist adiabat and calculating the stability by comparing the two temperatures at some intermediate pressure and found little difference in the results.

We assume that precipitation occurs within a box when the relative humidity exceeds a

critical relative humidity,  $RH_{crit}$ . When this is the case, the precipitative tendencies are

$$\begin{aligned}\frac{\partial q}{\partial t} &= \frac{q_{crit} - q}{\tau_{precip}}, \\ \frac{\partial DSE}{\partial t} &= -L_v \frac{\partial q}{\partial t}.\end{aligned}$$

Here  $q_{crit}$  is the specific humidity corresponding to the critical relative humidity and  $\tau_{precip}$  is a precipitation timescale. A fraction,  $\epsilon_r$ , of precipitation produced by convection in the upper level is re-evaporated into the lower level as it falls through it

$$\epsilon_r = \epsilon_{r0}(1 - RH).$$

A realistic value of  $\epsilon_r$  is roughly 0.1, but in our model we choose  $\epsilon_{r0}=2.5$  so that  $\epsilon_r$  is sometimes as high as 0.75. This compensates for the tendency of the model to excessively dry the boundary layer of convecting regions, which may result from our treatment of convection with a mixing parameterization, which may not be appropriate in many circumstances. Consequently we consider the re-evaporation parameterization to be part of the convection scheme itself rather than to represent physical process of re-evaporation.

## 2.9.7 Cloud Parameterization

We diagnostically calculate convective clouds as a function of convective mass flux and stratiform clouds as a function of relative humidity (Xu and Krueger, 1991).

We interpret the normalized convective mixing coefficient, which is defined as

$$M = \frac{k_{con} - k_{con-min}}{k_{con-max} - k_{con-min}}, \quad (2.21)$$

as the two-level analog of convective mass flux. Since  $k_{con}$  is a switch-like function (Eq. (2.20)),  $M$  is as well. We parameterize the convective cloud fraction as

$$C_c = C_{c-max} \left( \frac{\log(M/M_{min})}{\log(M_{min})} \right)^2. \quad (2.22)$$

Where  $C_c$  is the convective cloud fraction and  $C_c=0$  if  $M < M_{min}$ . We imagine modeled convective clouds as including anvil clouds spread from the site of convection.

We parameterize the stratiform cloud fraction using relative humidity

$$C_s = C_{s-max} \left( \frac{RH' - RH_0}{RH_2^* - RH_0} \right)^2, \quad (2.23)$$

with  $C_s = 0$  for  $RH' < RH_0$ . Following Slingo and Slingo (1991), we reduce the relative humidity upon which stratiform clouds are calculated in regions in which there is convective cloud activity

$$RH' = RH(1 - C_c). \quad (2.24)$$

This adjustment is based on the assumption that the air is saturated in convective clouds.

We calculate the total cloud fraction in each layer as

$$f_c^{high} = C_c, \quad (2.25)$$

$$f_c^1 = C_c + C_s^1, \quad (2.26)$$

$$f_c^2 = C_s^2. \quad (2.27)$$

Here  $f_c^{high}$  is the cloud fraction in the upper cloud level (section 2.9.5),  $f_c^1$  is the free tropospheric cloud fraction, and  $f_c^2$  is the boundary layer cloud fraction.  $C_s^k$  are the stratiform cloud fractions in the boundary layer and free troposphere, which we calculate based on the relative humidity there.

## 2.9.8 Surface Temperatures and Exchanges

We use bulk aerodynamic formulae to calculate surface sensible heat and evaporative fluxes (Peixoto and Oort, 1992)

$$F_{sh} = \rho C_p C_{sh} |\mathbf{v}| (\theta_s - \theta_2),$$

$$E = \rho C_{lh} |\mathbf{v}| (q_s^* - q_2).$$

The latent heat flux is the product of the evaporative flux and the latent heat of vaporization ( $F_{lh} = L_v E$ ).  $q_s^*$  is the saturation specific humidity based on the surface temperature.  $|\mathbf{v}|$  is the air speed near the surface, which we take to be a constant.  $C_{sh}$  and  $C_{lh}$  take different values over land and ocean (Table 2.2). Over land we reduce the evaporative flux

by multiplication by the fraction  $f_{evap}$ , which we set to a constant. We assume the land has no capacity to store water and we do not allow land evaporation to exceed instantaneous land precipitation.

We calculate land and sea surface temperatures prognostically. Land surface heat balance can be written

$$C_{land}D_{land}\frac{\partial T_{land}}{\partial t} = F_{sw-land}^{\downarrow} + \epsilon_{land}F_{lw}^{\downarrow} - \epsilon_{land}\sigma T_{land}^4 - F_{sh-land}^{\uparrow} - F_{lh-land}^{\uparrow}, \quad (2.28)$$

where  $T_{land}$  is the land surface temperature,  $C_{land}$  is the land volume heat capacity and  $D_{land}$  is the depth of soil that exchanges heat with the atmosphere.  $F_{sw-land}^{\downarrow}$  is given by Eq. (2.12) using the land albedo.  $\epsilon_{land}$  is the land emissivity, which we set to one, and  $F_{lw}^{\downarrow}$  is the downward LW flux of radiation due to re-emission by the atmosphere.

The ocean consists of a mixed layer of vertically uniform temperature with specified meridional ocean heat transport. Heat balance in this mixed layer can be written

$$C_{ocn}D_{ocn}\rho_{ocn}\frac{\partial SST}{\partial t} = \frac{OHT_{in} - OHT_{out}}{A_{ocn}} + F_{sw-ocn}^{\downarrow} + \epsilon_{ocn}F_{lw}^{\downarrow} - \epsilon_{ocn}\sigma(SST)^4 - F_{sh-ocn}^{\uparrow} - F_{lh-ocn}^{\uparrow}. \quad (2.29)$$

Most of Eq. (2.29) is analogous to Eq. (2.28). We set  $\epsilon_{ocn}$  to one. We use the mass heat capacity of water for  $C_{ocn}$ . To decrease the time the model takes to reach steady state, we

set the depth of the mixed layer,  $D_{ocn}$ , to 1 m. The model produced identical steady-state results when we set  $D_{ocn}$  to 50 m in test runs.  $OHT_{in}$  and  $OHT_{out}$  are the energy per unit time transported by the ocean into and out of the column being considered.

We specify the OHT so that it roughly fits the present-day profile as inferred from satellite radiative data and atmospheric reanalysis data given in Trenberth and Caron (2001). The model OHT as a function of latitude ( $\theta$ ) takes the form

$$OHT = \begin{cases} \left(\frac{OHT_0}{e}\right) \left(\frac{\theta}{\theta_{decay}}\right) e^{-\frac{\theta}{\theta_{decay}}} & \text{for } \theta < \theta_{lin}, \\ OHT_{lin} \left(\frac{\theta_{zero}-\theta}{\theta_{zero}-\theta_{lin}}\right) & \text{for } \theta_{lin} \leq \theta < \theta_{zero}, \\ 0 & \text{for } \theta_{zero} \leq \theta. \end{cases} \quad (2.30)$$

The linear portion of this function brings the  $OHT$  to zero without causing excessive heat convergence in a poleward box. Inter hemispheric  $OHT$  is not included so the model's heat budget is closed.  $OHT_0$  is the maximum  $OHT$  and  $\theta_{decay}$  gives both the location of this maximum and the decay scale at higher latitudes.  $\theta_{lin}$  and  $\theta_{zero}$  are the latitudes at which the  $OHT$  becomes linear and zero, respectively.  $OHT_{lin}$  is the  $OHT$  at  $\theta_{lin}$  based on the lower latitude formula

$$OHT_{lin} = \left(\frac{OHT_0}{e}\right) \left(\frac{\theta_{lin}}{\theta_{decay}}\right) e^{-\frac{\theta_{lin}}{\theta_{decay}}}.$$

See Table 2.2 for  $OHT$  parameter choices in the standard run and Fig. 2.3r for a plot of the resulting OHT for the 30 column model.

# Chapter 3

## Sea Ice, High-Latitude Convection, and Equable Climates

### 3.1 Introduction

Paleoclimatic data suggest that during the late Cretaceous period ( $\sim 100$  to  $\sim 65.5$  Ma) and the early Paleogene period ( $\sim 65.5$  Ma to  $\sim 34$  Ma) the global-mean temperature was higher than its modern value and the equator to pole temperature difference and the amplitude of the high-latitude seasonal cycle were both much smaller than they are today, particularly in continental interiors, which has led to the characterization of climates during these periods as “equable” (*e.g.*, Greenwood and Wing, 1995). Researchers have as yet been unable to reproduce equable climates in coupled ocean-atmosphere global climate models (GCMs) by simply changing boundary conditions and increasing greenhouse gas levels (Huber and

Sloan, 2001; Bush and Philander, 1997). Relative to existing data, either the polar regions are too cold or the tropical regions are too warm in these simulations.

It is possible that the resolution of unknown biases in paleoclimatic data will bring them into agreement with GCM results. Proceeding under the assumption that the data faithfully represent paleoclimate, many ideas have been proposed to explain the discrepancy between models and data, including the extension of the Hadley circulation to high latitudes (Farrell, 1990), mixing of the ocean caused by tropical cyclones (Emanuel, 2002; Korty et al., 2008), and polar stratospheric clouds (Sloan et al., 1992; Kirk-Davidoff et al., 2002). Alternatively, Abbot and Tziperman (2008a) used a simple zonally-averaged model forced by equinoctial shortwave (SW) radiation to argue that the advent of convection and convective clouds, which are mostly tropospheric rather than stratospheric, at high latitudes could represent a positive feedback on high-latitude surface temperature. More complex atmospheric models lend some support to the idea of increased high-latitude convection during equable climates when they are forced with a high mean surface temperature and a low meridional surface temperature gradient (Huber and Sloan, 1999; Korty and Emanuel, 2007).

Observations of winter cloud radiative forcing (CRF) in the modern climate suggest that sea ice may play an important role in the high-latitude convective cloud feedback mechanism that Abbot and Tziperman (2008a) proposed. CRF is strongly positive over subpolar oceans without sea ice and near zero over subpolar and polar oceans with sea ice (Fig. 3.1). The clouds causing this positive CRF may be associated with large-scale dynamics, convection, or other processes, although the sharp jumps in CRF at sea ice/open

ocean boundaries may represent evidence that the positive CRF is mainly due to a local process, such as convection.

We will use the single-column version of the NCAR CAM GCM (SCAM, Hack et al., 2004), which has state-of-the-art atmospheric physics parameterizations, high vertical resolution, a full seasonal cycle, a thermodynamic sea ice model, and a mixed layer ocean, to argue that winter convection may indeed be the driver of positive winter CRF over ice-free high-latitude oceans and that sea ice prevents such convection so that the removal of winter sea ice could be an essential prerequisite for the high-latitude convective cloud feedback. We will further show that the surface warming effects caused by winter convection, specifically the increase in the LW optical depth of the atmosphere due to thick convective clouds and increased water vapor concentration, can be essential for the maintenance of an ice-free state on which the winter convection itself depends. The removal of sea ice from high-latitude oceans would lead to greatly increased annual-mean temperatures, a drastically reduced seasonal cycle, and generally equable conditions.

In order to provide a concrete and limiting example, we focus our study on the Arctic ocean. We model the ocean with a mixed layer with a constant depth of 50 m and force SCAM with present-day seasonally and diurnally varying  $79.5^{\circ}\text{N}$  SW radiation. It is unusual to make inferences about high-latitude climate using a single-column model, however we take into account departures from radiative-convective equilibrium by specifying convergences of ocean heat transport (OHT) and atmospheric heat transport (AHT). We sample a large range of OHT and AHT, as their values during equable climates are uncer-

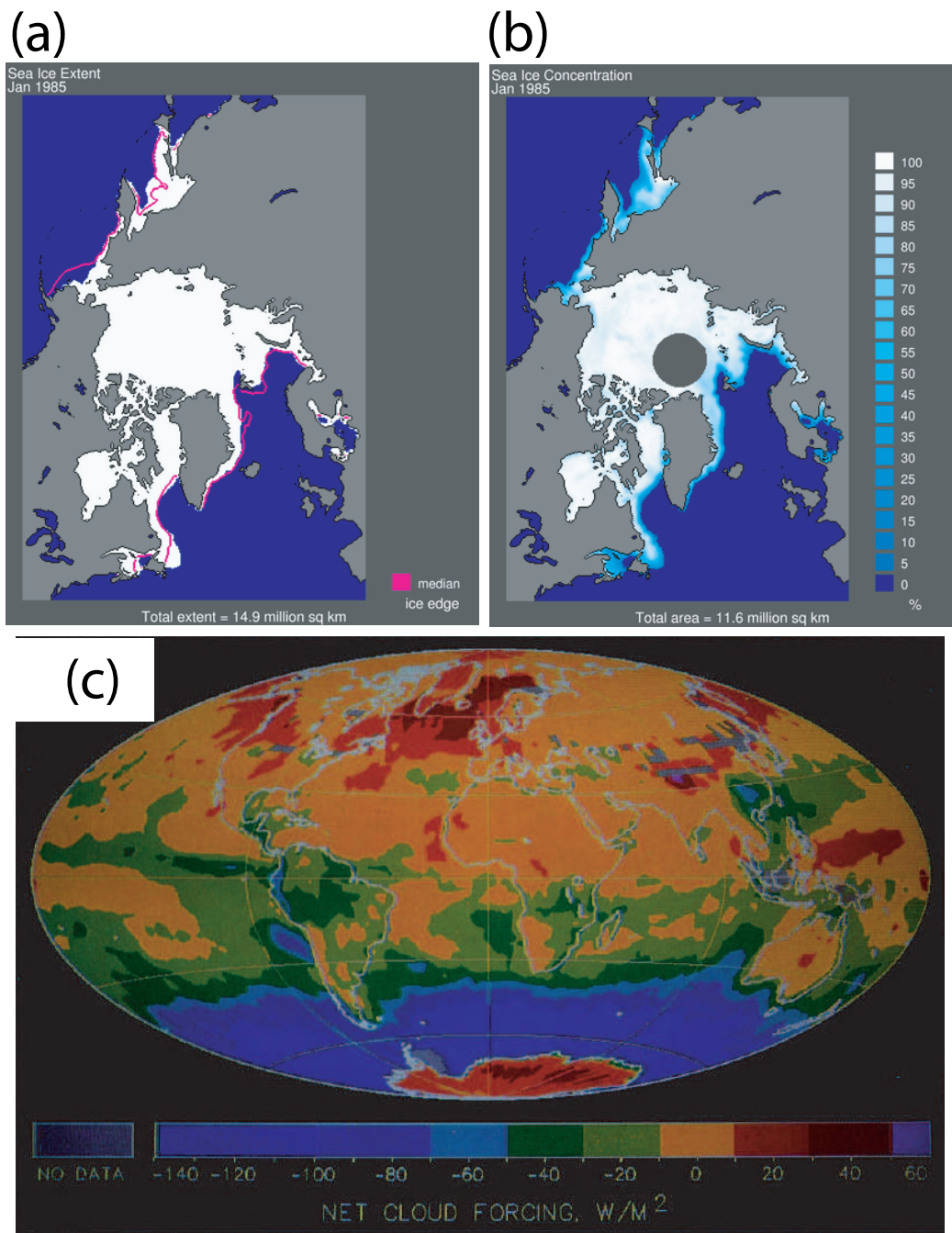


Figure 3.1: Cloud radiative forcing and sea ice data for January 1985. (a) Sea ice extent. (b) Sea ice concentration, *i.e.*, fraction sea covered by ice. (c) Net cloud radiative forcing. The sea ice plots were obtained from the National Snow and Ice Data center (Fetterer et al., 2002, updated 2007). The cloud radiative forcing plot is Plate 5b in Harrison et al. (1990).

tain. The OHT and AHT we apply are constant in time and we show results for a dry AHT applied equally by mass to the atmosphere below 245 mb, so that the applied temperature tendency is the same for each pressure level below 245 mb. We apply no vertical velocity, nor clouds associated with large-scale dynamics. SCAM calculates surface heat fluxes using bulk aerodynamic formulae and surface winds from standard CAM input files.

## 3.2 Convective Clouds and Sea Ice

We find that SCAM has two different types of equilibria at  $79.5^\circ$  latitude over ocean: (1) An equilibrium with perennial or seasonal sea ice, which we will call the ice state and (2) An equilibrium without sea ice, which we will call the ice-free state. At low  $\text{CO}_2$  and low heat transport (HT) only the ice state is stable and at high  $\text{CO}_2$  and high HT only the ice-free state is stable. There is a small parameter regime at the boundary of the ice-free and ice regimes in which both ice-free and ice state are possible at the same external forcing.

Fig. 3.2 displays the seasonal cycle of some important physical quantities for the ice-free and the ice states. For both states we specify  $\text{AHT}=100 \text{ W m}^{-2}$ ,  $\text{OHT}=0$ , (roughly equal to modern values at  $80^\circ\text{N}$ , Trenberth and Stepaniak, 2003) and  $\text{CO}_2=1000 \text{ ppm}$ . We display model output for boundary conditions at which the ice and ice-free states are both stable to emphasize the striking difference between the two states without confounding the difference between states with differences caused by boundary conditions. It is not clear whether using the same AHT for the ice and ice-free states is realistic because the implications of a competition between a reduction in eddy activity due to a decreased meridional

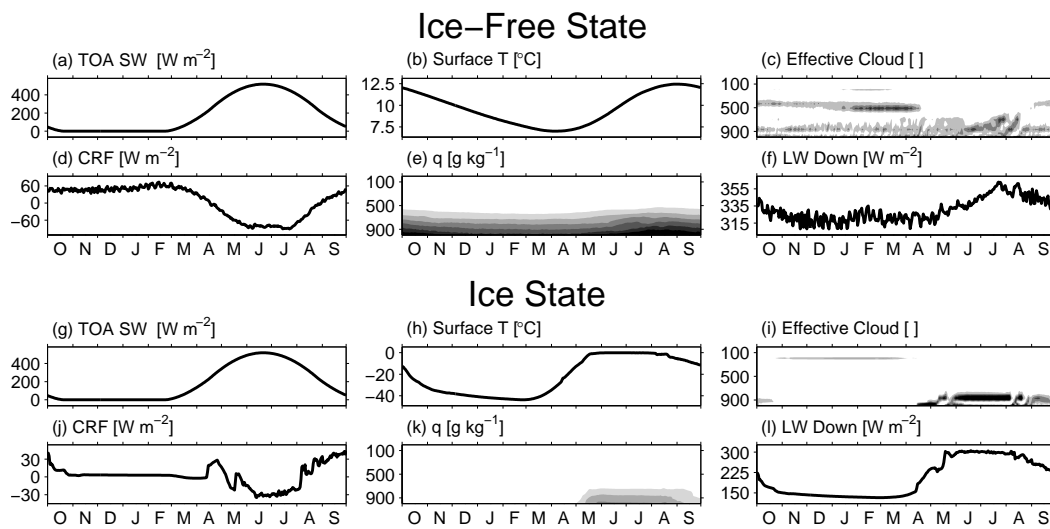


Figure 3.2: Seasonal cycle of important physical quantities in the ice-free (a-f) and ice (g-l) states at  $79.5^{\circ}$ . Each panel displays the average values for the last 15 years of a 50 year model run. The specified convergence of atmospheric heat transport is  $100 \text{ W m}^{-2}$ , the specified convergence of ocean heat transport is zero, and the specified  $\text{CO}_2$  is 1000 ppm. The panels contain (a,g) TOA SW, daily-averaged downward shortwave radiation at the top of the atmosphere, (b,h) Surface T, the surface temperature, (c,i) Effective Cloud, the product of the cloud fraction and the cloud emissivity, with shading intervals of 0.1, (d,j) CRF, the cloud radiative forcing at the surface, (e,k) q, the specific humidity, with shading intervals of  $1 \text{ g kg}^{-1}$ , (f,l) LW Down, downward longwave radiation at the surface.

temperature gradient and increased latent HT due to potentially warmer subtropical temperatures are not fully understood (Pierrehumbert, 2002; Caballero and Langen, 2005). As SCAM is isolated from lower latitudes, we cannot address this issue here.

Although we apply the same external forcing in both cases, the annual-mean temperature is much higher and the amplitude of the seasonal cycle is much lower in the ice-free state. Strikingly, the minimum temperature for the ice-free state is  $7^{\circ}\text{C}$  (Fig. 3.2b) while it is  $-44^{\circ}\text{C}$  for the ice state (Fig. 3.2h). Strong convection occurs in the ice-free state throughout polar night and causes optically thick mid-tropospheric convective clouds (Fig. 3.2c). The surface CRF resulting from these convective clouds averages  $51 \text{ W m}^{-2}$  during polar night (Fig. 3.2d), whereas the surface CRF averages only  $3 \text{ W m}^{-2}$  during polar night in the ice state (Fig. 3.2j). CRF, which is negative during summer and positive during winter, provides a significant dampening of the seasonal cycle in the ice-free state (Fig. 3.2d). The convection that produces mid-tropospheric clouds during the winter in the ice-free state transports  $14 \text{ W m}^{-2}$  of total heat upward from the lowest 100 mb of the atmosphere, which is only a small fraction of the positive radiative forcing the convective clouds produce. Warmth and high surface evaporation allow the ice-free state to stay moist (Fig. 3.2e) through polar night. Moisture and convective clouds vastly increase the winter optical depth and downward longwave radiation in the ice-free state (*c.f.* Figs. 3.2f,l).

The radiative effects of the convective clouds and moisture are essential for the maintenance of the ice-free state. In the ice-free state, the SST falls only  $5.4^{\circ}\text{C}$  from its maximum to its minimum, during which time surface loses an average of  $59 \text{ W m}^{-2}$ . We calculate

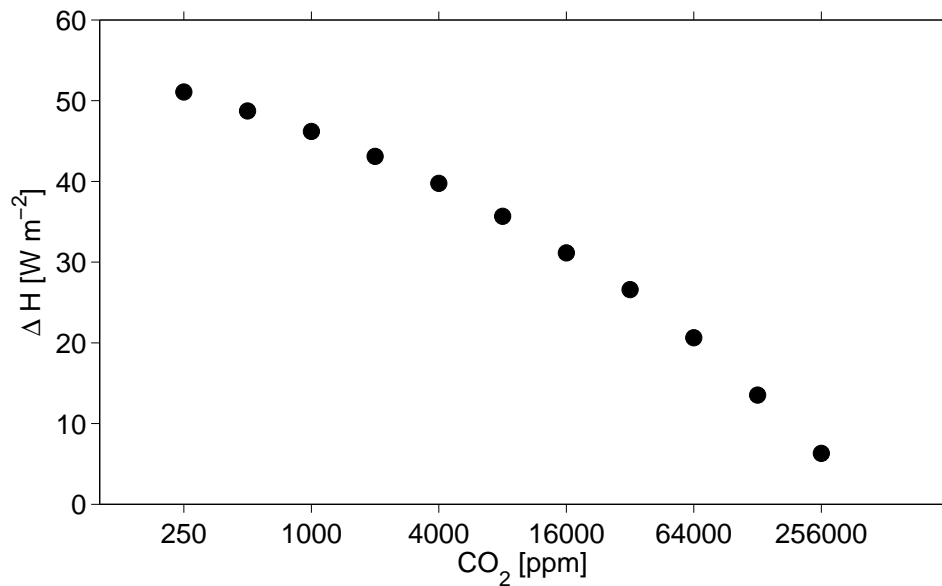


Figure 3.3: The amount of externally imposed heat transport required by the surface to maintain the ice-free state ( $\Delta H$ ) as a function of  $\text{CO}_2$  concentration.  $\Delta H$  is the annually-averaged heat flux from the ocean surface to the atmosphere at equilibrium with  $\text{OHT}=\text{AHT}=0$ , the sea ice parameterization off, and the SST not allowed to drop below the freezing temperature.

that without winter CRF the ice-free state would be unstable and sea ice would develop after only two years and without the winter radiative forcing of water vapor the ice-free state would be destroyed in a single season (not shown).

### 3.3 Sensitivity to Heat Transport

#### 3.3.1 Idealized Heat Transport Constraints

Convective clouds and moisture are a radiative blanket that can keep the ocean warm enough that sea ice does not form during polar night by trapping SW radiation or HT. Since HT, which we must specify, is uncertain during periods of equable climate, it is important

to establish the constraints AHT and OHT place on the mechanism.

One estimate of the HT required to maintain a stable ice-free state is the magnitude of the annual-mean surface heat balance deficit ( $\Delta H$ ) obtained by running the model with  $OHT=AHT=0$ , sea ice artificially repressed, and the SST not permitted to drop below the freezing point of seawater. HT would be necessary to maintain an ice-free state even at very large  $CO_2$  concentrations ( $\Delta H > 0$ , Fig. 3.3). The negative curvature of  $\Delta H$  as a function of  $\log(CO_2)$  is due to the non-linearity of the Clausius-Clapeyron equation. At  $CO_2$  concentrations that might be relevant for equable climates (250-4000 ppm, Pagani et al., 2005; Pearson and Palmer, 2000), the atmosphere and ocean would have to supply  $40\text{-}50\text{ W m}^{-2}$  to the surface to maintain an ice-free state in the Arctic ocean.

$\Delta H$  is the effect of HT into the column on the surface heat balance, rather than the total HT into the column. Because roughly half of the HT into the model's atmosphere is radiated upward to space, OHT should be roughly twice as effective at heating the surface as AHT.

### 3.3.2 Heat Transport Constraints in the Full SCAM

Here we test our simple argument for the amount of heat needed by the surface to maintain the ice-free state by running SCAM with thermodynamic sea ice at various  $CO_2$  concentrations and prescribed OHT and AHT. Fig. 3.4 confirms that the ice-free state is viable roughly when  $OHT + \frac{1}{2}AHT$  exceeds  $\Delta H$  (Fig. 3.3). The current annual-mean AHT is roughly  $100\text{-}110\text{ W m}^{-2}$  at  $80^\circ\text{N}$  (Trenberth and Stepaniak, 2003) and its value during

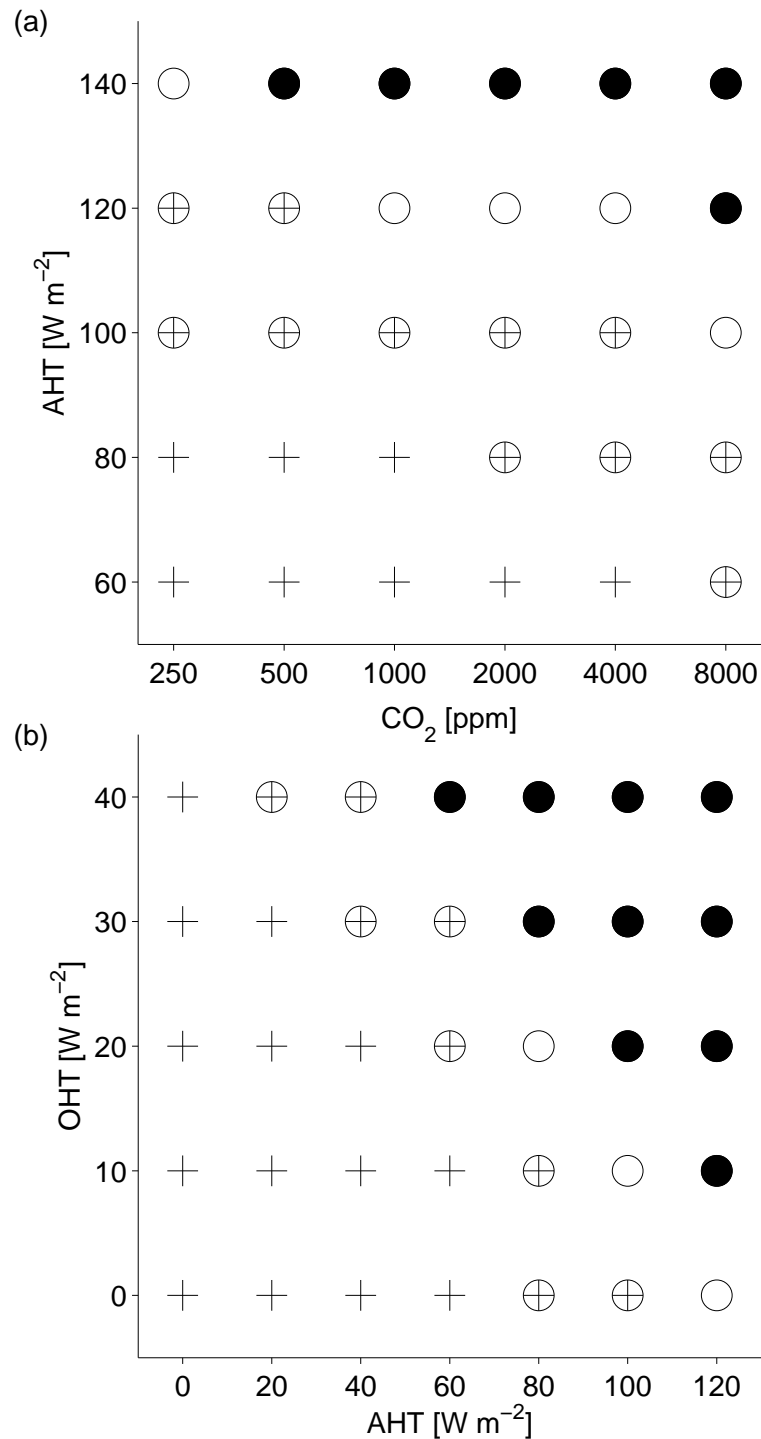


Figure 3.4: Stability of the ice-free and ice states as a function of the specified convergence of atmospheric heat transport (AHT), the specified convergence of ocean heat transport (OHT), and the specified  $\text{CO}_2$ . A “+” indicates that the ice state is stable and a circle indicates that the ice-free state is stable. The presence of both symbols indicates that both states are stable. Filled circles indicate that the ice-free state is stable even with longwave cloud radiative forcing artificially set to zero between September 1 and April 1. OHT=0 for all runs in panel (a) and  $\text{CO}_2=2000$  ppm for all runs in panel (b).

equable climates in unknown (Pierrehumbert, 2002; Caballero and Langen, 2005). An ice-free state is possible in SCAM with OHT=0, AHT=100 W m<sup>-2</sup> at current CO<sub>2</sub> levels and with OHT=0, AHT=80 W m<sup>-2</sup> for CO<sub>2</sub>=2000 ppm and higher. For comparison, many full GCMs predict only a small amount of Arctic winter sea ice when the CO<sub>2</sub> concentration is slowly increased to 700-850 ppm, but not run to equilibrium (Zhang and Walsh, 2006).

Without the radiative forcing of clouds and water vapor during winter, the ice-free state would not be stable at any of the AHT, OHT, and CO<sub>2</sub> combinations displayed in Fig. 3.4. Winter CRF alone has a dramatic effect on the stability of the ice-free state, though clouds contribute only about 15% of the total winter downward LW flux (Fig. 3.2d,f). The convergence of AHT would have to be increased by 40% above its modern value of roughly 100 W m<sup>-2</sup> for the the ice-free state to be stable at any CO<sub>2</sub> below 8000 ppm without winter LW CRF (Fig. 3.2a).

### 3.4 Discussion

The main drawback of SCAM is that it requires AHT as a specified boundary condition. Beware of the following assumptions we have made in our treatment of AHT: (1) Our applied AHT is constant in time, although we obtain similar results when we allow it to vary seasonally. (2) We have not included noise representing stochastic weather in the AHT, which might eliminate the parameter regime in which both the ice and the ice-free equilibria are possible. (3) We have presented results in which the specified AHT was dry, which is reasonable at high latitudes in the current climate (Trenberth and Stepaniak, 2003),

although moist AHT might be important at high latitudes in an equable climate (Pierrehumbert, 2002). However, substituting moist for dry AHT does not appear to significantly alter our results (Fig. 3.5). (4) We distributed the AHT equally by mass in the troposphere, neglecting detailed vertical structure.

We believe that our results are sufficiently general that they should be robust to changes in these assumptions. We also obtain qualitatively similar results with a seasonally varying ocean mixed layer depth, our results are insensitive to an increase or decrease by a factor of four in the surface winds (Fig. 3.6), and the ice state is stable when we include leads in the sea ice model.

We remain unsure as to why the feedback we describe has not been documented in coupled GCM runs, but we offer several speculative ideas here. First, signs of high-latitude convection have been observed in an atmospheric GCM forced with a low surface temperature gradient (Korty and Emanuel, 2007) and Huber and Sloan (1999) find strong winter convection in an atmospheric GCM over the Arctic ocean when they specify the SST to be high enough that there's no sea ice. These papers do not discuss the CRF feedback suggested here, its effect on surface temperatures, and its potential to help maintain an ice-free state. Second, we have suggested here that sea ice may introduce some hysteresis into the system, making the initial conditions used in coupled runs potentially important. Third, sea ice parameterizations may not yield reliable predictions in different climates (Eisenman et al., 2007) and sea ice is crucial to the proposed mechanism. Finally, it is possible that climate drift due to inconsistencies between the ocean and atmosphere models, which had

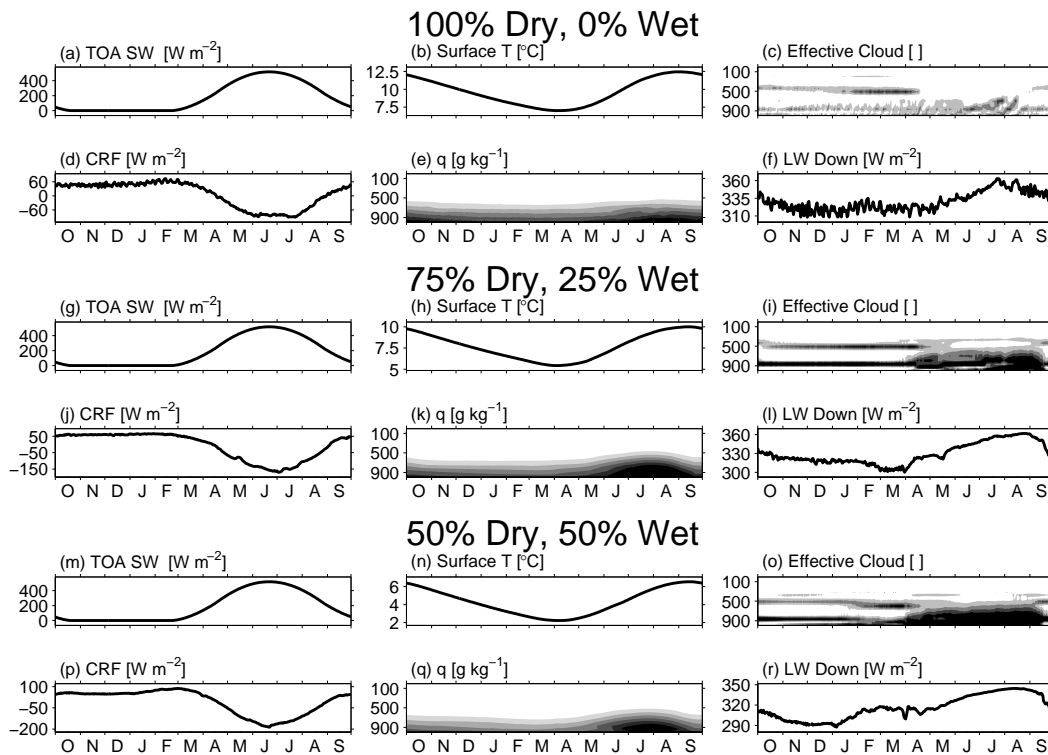


Figure 3.5: Seasonal cycle of important physical quantities in the ice-free state at  $79.5^{\circ}$  with wet and dry atmospheric heat transport accounting for the following percentages of the total: 100% dry, 0% wet (a-f, same as Fig. 1(a-f)); 75% dry, 25% wet (g-l); and 50% dry, 50% wet (m-r). In all cases the total specified atmospheric heat transport is  $100 \text{ W m}^{-2}$ , the specified convergence of ocean heat transport is zero, and the specified  $\text{CO}_2$  concentration is 1000 ppm. Moist heat transport is applied equally by mass below 470 mb. Each panel displays the average values for the last 15 years of a 50 year model run. The panels contain (a,g,m) TOA SW, daily-averaged downward shortwave radiation at the top of the atmosphere, (b,h,n) Surface T, the surface temperature, (c,i,o) Effective Cloud, the product of the cloud fraction and the cloud emissivity, with shading intervals of 0.1, (d,j,p) CRF, the cloud radiative forcing at the surface, (e,k,q) q, the specific humidity, with shading intervals of  $1 \text{ g kg}^{-1}$ , (f,l,r) LW Down, downward longwave radiation at the surface. The ice-free state is stable in all cases; it is stable even when the atmospheric heat transport is 100% wet (not shown). In all cases winter convection is active and important in maintaining the ice-free state. The main effect of increasing the fractional moist heat transport is to increase the cloud amount, particularly during summer, which makes the summer cloud radiative forcing more negative and leads to cooler surface temperatures. The ice-state is also stable at all fractional moist heat transport levels.

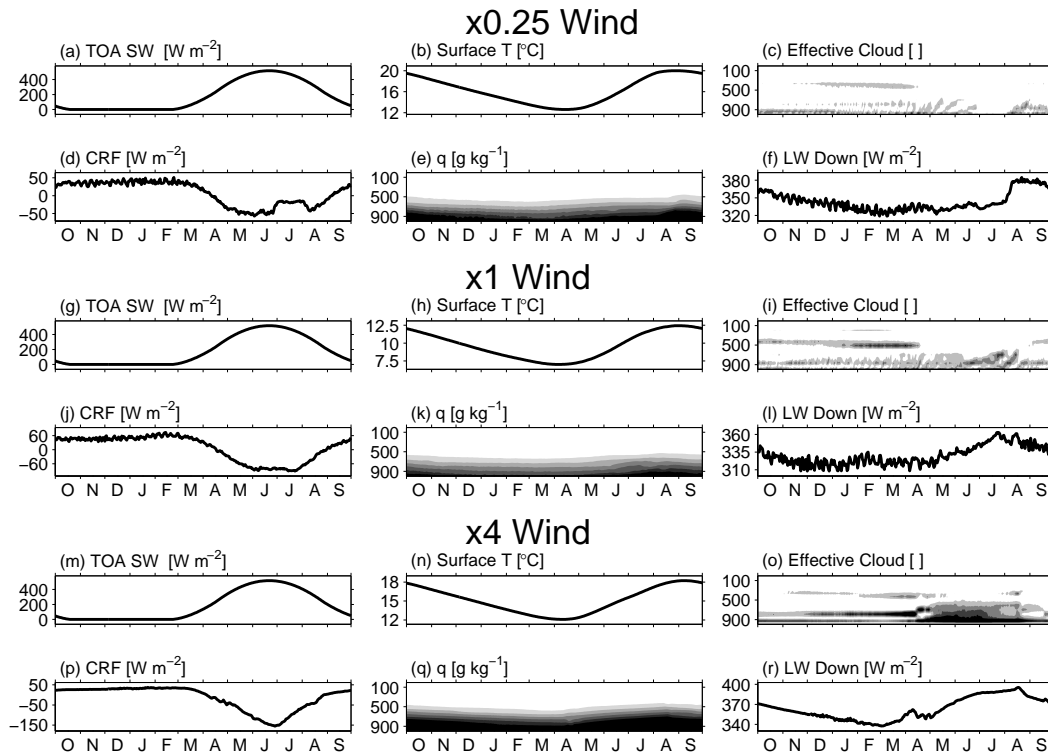


Figure 3.6: Seasonal cycle of important physical quantities in the ice-free state at  $79.5^\circ$  with the specified magnitude of the surface wind velocity 0.25 times the standard value (a-f), at the standard value (g-l, same as Fig. 1(a-f)), and 4 times the standard value. In all cases the total specified atmospheric heat transport is  $100 \text{ W m}^{-2}$ , the specified convergence of ocean heat transport is zero, and the specified  $\text{CO}_2$  concentration is 1000 ppm. Each panel displays the average values for the last 15 years of a 50 year model run. The panels contain (a,g,m) TOA SW, daily-averaged downward shortwave radiation at the top of the atmosphere, (b,h,n) Surface T, the surface temperature, (c,i,o) Effective Cloud, the product of the cloud fraction and the cloud emissivity, with shading intervals of 0.1, (d,j,p) CRF, the cloud radiative forcing at the surface, (e,k,q)  $q$ , the specific humidity, with shading intervals of  $1 \text{ g kg}^{-1}$ , (f,l,r) LW Down, downward longwave radiation at the surface. The ice-free state is stable in all cases and winter convection is active and important in maintaining the ice-free state. We take this insensitivity as evidence that a wind-evaporation feedback (e.g., Emanuel, 1987; Neelin et al., 1987), which cannot be included in a single-column model, would not markedly affect our results. When surface winds are varied between 0.5-2 times their standard value, there is almost no effect on the results (not shown). When surface winds are 4 times standard, winter deep convection and CRF are slightly lower than at lower surface wind values. The ice state is also stable at all surface wind levels shown here.

to be fixed with flux corrections in older models run in present-day configuration, could lead coupled GCMs away from an ice-free Arctic in equable climate runs.

Although we have shown that winter convective clouds and moisture could play an important role in keeping oceans sea ice-free during periods of equable climate, we have not directly confronted the issue of above-freezing winter temperatures at high latitudes in continental interiors (*e.g.*, Greenwood and Wing, 1995). Abbot and Tziperman (2008a) proposed that clouds and moisture due to winter convection over warm and ice-free oceans could be advected over continents, particularly if eddies were fewer and weaker, and lead to warm continental interiors. A full investigation of this idea is beyond the scope of the current work.

### 3.5 Conclusion

Abbot and Tziperman (2008a) argued that the positive radiative forcing associated with the onset of high tropospheric clouds due to deep convection could represent a strong positive feedback on increases in high-latitude surface temperature that might help to explain equable climates. We have investigated this idea using a column model with state-of-the-art atmospheric physics parameterizations, high vertical resolution, a full seasonal cycle, a thermodynamic sea ice model, and a mixed layer ocean. Depending on the CO<sub>2</sub> concentration, OHT, and AHT, we found high-latitude equilibria both with and without sea ice. The ice-free state has a much higher annual-mean temperature and a greatly reduced seasonal cycle. When the system is ice-free, convection occurs throughout the winter and the radia-

tive warming effects of the clouds and water vapor associated with winter convection keep the ocean from freezing. Winter convection both depends on there being no sea ice and is essential for keeping sea ice from forming. We finally investigated various CO<sub>2</sub>, OHT, and AHT values and found that the ice-free state is stable for values that may be reasonable for the Arctic ocean during the late Cretaceous and early Paleogene (OHT=0, CO<sub>2</sub>=250-2000 ppm, AHT=80-100% modern).

# **Chapter 4**

## **Winter Arctic Climate Uncertainty**

### **Under Global Warming due to a Cloud**

#### **Radiative Feedback**

##### **4.1 Introduction**

Sea ice plays a crucial role in Arctic climate. During summer it reflects solar radiation and during winter it insulates the atmosphere from the relatively warm ocean, allowing the atmosphere to drop to extremely low temperatures during polar night. Significant loss of sea ice would put immediate strain on Arctic biota (Smetacek and Nicol, 2005), could accelerate the melting of the Greenland ice sheet (Lemke et al., 2007), and could affect global climate by causing changes in atmospheric and oceanic circulation (Serreze et al.,

2007; McBean et al., 2005).

Clouds make a significant contribution to atmospheric optical depth in the Arctic (Intrieri et al., 2002a,b), which is important for predicting sea ice extent (Francis et al., 2005). Because of the importance of parameterized, subgrid-scale cloud processes (Baker, 1997), changes in cloud radiative forcing (CRF) represent the largest source of uncertainty in climate change predictions (Cess and co authors, 1990; Soden and Held, 2006). Additionally large ensemble sensitivity studies show that perturbations in cloud and convection parameters have the largest effect on current climate simulation (Murphy et al., 2004) and significantly affect the future climate sensitivity distribution (Stainforth et al., 2005).

A novel winter CRF feedback that may strongly affect Arctic winter sea ice and climate sensitivity to increased CO<sub>2</sub> has been proposed recently using simple climate models (Abbot and Tziperman, 2008a,b). This feedback is initiated by CO<sub>2</sub>-induced warming, which leads to some sea ice loss, which allows increased heat and moisture fluxes from the ocean surface. This, in turn, leads to atmospheric convection, and to the development of optically thick convective clouds. These clouds trap outgoing longwave radiation and therefore result in a further warming and sea ice loss in the Arctic. This positive feedback can allow the Arctic to remain ice-free throughout polar night.

In this chapter we show that this proposed winter CRF feedback is active in the state-of-the-art coupled ocean-sea ice-land-atmosphere models that participated in the IPCC fourth assessment report 1%/year CO<sub>2</sub> increase to quadrupling scenario. As a result, the feedback dramatically increases the uncertainty in the predictions of Arctic climate. Specifically, the

winter CRF feedback plays a major role in contributing to the large spread in winter Arctic sea ice concentration that these models forecast for the end of the experiment: two models (NCAR CCSM3.0 and MPI ECHAM5) lose nearly all winter sea ice (Winton, 2006), while some others yield little change at all.

## 4.2 Results

There is a marked difference between the Arctic climate of models that lose winter sea ice and those that retain it. Fig. 4.1 demonstrates this by showing the change in Arctic climate over the experiment for a model that lost most winter sea ice (NCAR CCSM3.0) and a model that showed relatively little change in winter sea ice (GFDL CM2.0). Associated with the Arctic-wide loss of winter sea ice in the NCAR model (Fig. 4.1(a)) is a warming of the surface air temperature by up to 25-30°C (Fig. 4.1(b)). This change in temperature is forced by a strong positive feedback in CRF over the Arctic (Fig. 4.1(c)), which extends throughout regions of the Arctic where there is a large change in sea ice. There is a major increase in the convective precipitation rate throughout the Arctic in the NCAR model (Fig. 4.1(d)), implying that the increase in CRF is associated with the onset of convection and convective clouds. Convection is suppressed during the summer by preferred absorption of shortwave radiation above the boundary layer.

In contrast, the GFDL model shows no change in winter sea ice over the polar region (Fig. 4.1(e)) and only roughly half the surface air temperature warming (Fig. 4.1(f)) as the NCAR model (Fig. 4.1(b)). As the GFDL model retains winter polar sea ice, there is no

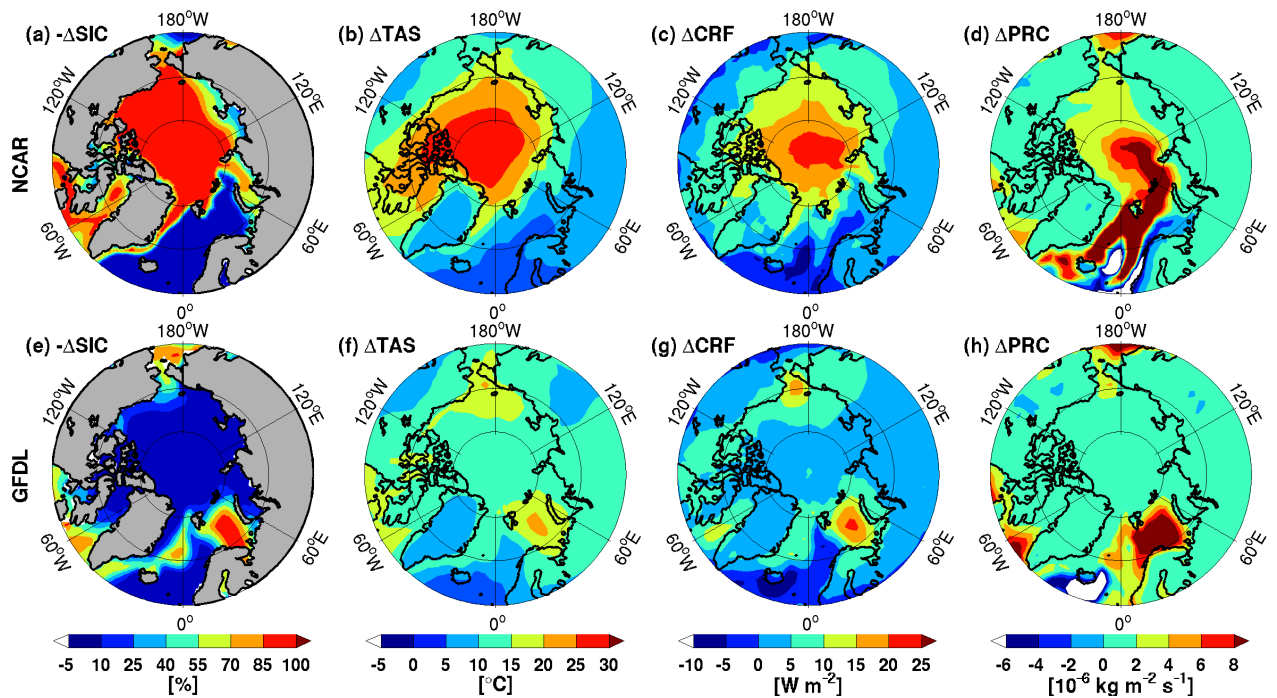


Figure 4.1: Amplified change in winter (DJF) Arctic climate due to the proposed winter CRF feedback over the course of the IPCC 1%/year  $\text{CO}_2$  increase to quadrupling experiment. The models are NCAR CCSM3.0, which loses most Arctic winter sea ice, and GFDL CM2.0, which loses minimal winter Arctic winter sea ice. For each variable, the difference between the mean over the last ten years and the mean over the first ten years is plotted. (a,e)  $-\Delta\text{SIC}$ , the negative of the change in sea ice concentration; (b,f)  $\Delta\text{TAS}$ , the change in surface air temperature; (c,g)  $\Delta\text{CRF}$ , the change in cloud radiative forcing; (d,h)  $\Delta\text{PRC}$ , the change in convective precipitation rate.

CRF feedback (Fig. 4.1(g)) and no change in convective precipitation (Fig. 4.1(h)) in the polar region in this model; however, it does show a large change in winter sea ice between Scandinavia and Svalbard (latitude 70-80°N) and in the Bering Strait (latitude 65-75°N) (Fig. 4.1(e)). In both of these regions the change in surface air temperature is much larger than in surrounding areas (Fig. 4.1(f)), there is a strong positive CRF feedback (Fig. 4.1(g)), and a large change in convective precipitation (Fig. 4.1(h)). So even though the winter CRF feedback is not active over the pole in the GFDL model, it is as effective in the GFDL model as in the NCAR model in the regions where the GFDL model does lose winter sea ice.

To further establish the connection between the proposed CRF feedback, caused by winter convection, and the Arctic warming in the NCAR model, we note a significant increase in the polar region (ocean north of 80°N) winter cloud fraction between 600-900 mb and a decrease below 900 mb (Fig. 4.2(a)). This rearrangement in winter cloud fraction, together with the increase in winter convective precipitation (Fig. 4.1(d)), firmly establish convection as the central process causing the winter CRF feedback in the NCAR model. Alternatively, the GFDL model, which does not lose winter sea ice, shows little change in the winter polar cloud fraction (Fig. 4.2(b)) even though its winter polar surface temperature increases by about 13°C (Fig. 4.1(f)).

A total loss of winter sea ice is associated with an increase in the average CRF of 9.5-14.8 W m<sup>-2</sup> (95% confidence interval) throughout the polar region and sustained over the entire winter (Fig. 4.3(a)). Given that a doubling of CO<sub>2</sub> leads to a radiative forcing of about 4 W m<sup>-2</sup>, the radiative forcing that results from a complete loss of winter sea ice is

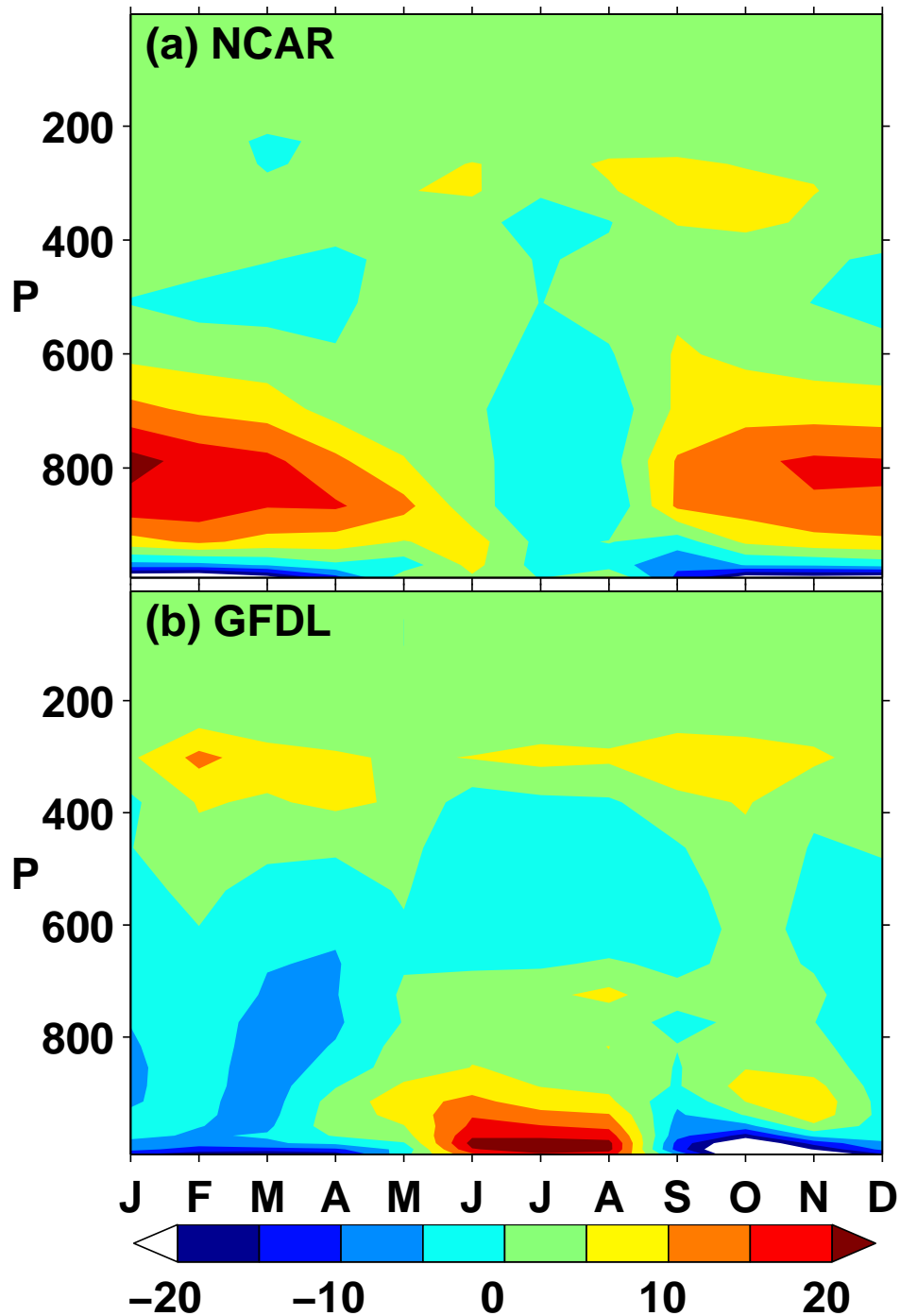


Figure 4.2: Convection-induced change in winter polar cloud fraction associated with winter CRF feedback. Change in polar cloud fraction for the NCAR CCSM3.0 and GFDL CM2.0 models over the course of the 1%/year  $\text{CO}_2$  increase to quadrupling experiment. The difference between the mean cloud fraction over the last ten years and the mean over the first ten years is plotted as a function of month and elevation. Convection-induced changes are evident during the winter in the NCAR model.

equivalent to 2.5-3.5 doublings of CO<sub>2</sub>. The inability of the IPCC models to consistently predict the onset of this strong positive cloud feedback, or lack thereof, means that the winter CRF feedback strongly amplifies the uncertainty in the winter sea ice predictions of the models. Although the CRF feedback is active to different degrees in the IPCC models, it would likely be fully active in most models at high enough CO<sub>2</sub> or even at quadrupled CO<sub>2</sub> if the models were integrated until they were closer to equilibrium. As the feedback relies on subgrid-scale convection and cloud processes that must be parameterized in these models, it is not currently possible to accurately estimate the CO<sub>2</sub> concentration at which the feedback should be fully activated, which is precisely what leads to the increased uncertainty in winter Arctic sea ice forecasts highlighted in this chapter. Still, we next endeavor to understand some of the factors that may control the activation of the winter CRF feedback.

Surprisingly, the change in winter polar sea ice concentration is completely uncorrelated with the equilibrium climate sensitivity (Fig. 4.3(b)), the transient climate sensitivity (Fig. 4.5(a)), and the change in global mean surface air temperature over the 1%/year CO<sub>2</sub> increase to quadrupling experiment (Fig. 4.5(b)). This important results indicates that the conventional measures of sensitivity to global climate change are not useful for predicting the critical climate phenomenon of winter Arctic sea ice loss: more "sensitive" models are no more likely to lose winter Arctic sea ice than less "sensitive" models. This is because global sensitivity measures cannot predict which model will be most affected by the CRF feedback over the Arctic.

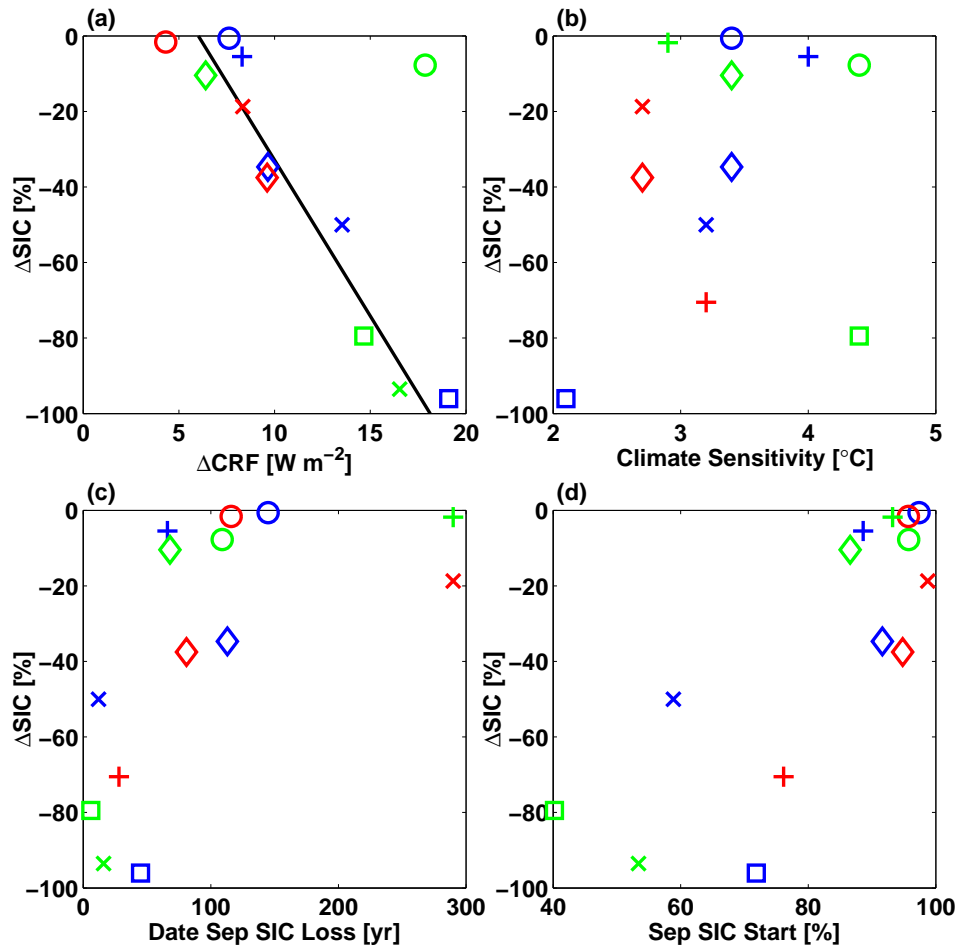


Figure 4.3: Causes of uncertainty in the winter sea ice forecast of models that participated in the 1%/year  $\text{CO}_2$  increase to quadrupling experiment. The change in winter (DJF) polar sea ice concentration ( $\Delta\text{SIC}$ ) is plotted as a function of (a) the change in winter polar cloud radiative forcing ( $\Delta\text{CRF}$ ) (excluding CNRM,  $r^2=0.92$ ), (b) the equilibrium global climate sensitivity ( $r^2=0.006$ ), (c) the year the September polar sea ice first drops below 25%, and (d) the September polar sea ice concentration at the start of the experiment. The polar region is defined by sea gridpoints north of  $80^\circ\text{N}$ . See Fig. 4.4 for model symbol legend. The change in sea ice and CRF is the difference between the mean of these variables over the last ten years of the experiment and the mean over the first ten years. The equilibrium climate sensitivity is the equilibrium change in global mean surface temperature when  $\text{CO}_2$  is doubled. The results plotted in (c) do not depend strongly on the sea ice cutoff of 25% and look similar if instead we plot the last year the September polar sea ice is above this cutoff.

○	CCMA CGCM3.1
○	CNRM CM3
○	GFDL CM2.0
+	GFDL CM2.1
+	GISS
+	INGV ECHAM4
◇	INMCM3.0
◇	IPSL CM4
◇	MIROC3.2 MEDRES
×	MIUB ECHO
×	MPI ECHAM5
×	MRI CGCM2.3.2a
□	NCAR CCSM3.0
□	UKMO HADGEM1

Figure 4.4: Symbols used to denote each IPCC model in Figures 4.3 and 4.5.

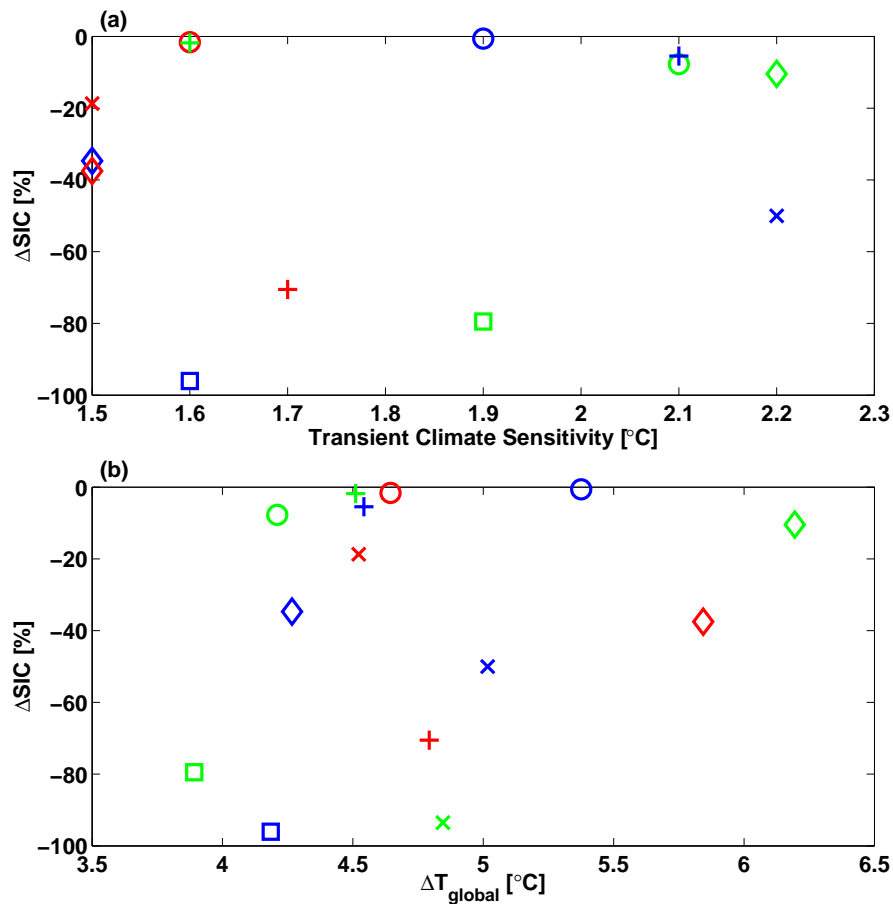


Figure 4.5: Lack of correlation between polar sea ice forecasts and global climate sensitivity. Change in polar sea ice concentration ( $\Delta\text{SIC}$ ) as a function of (a) transient climate sensitivity ( $r^2=0.04$ ) and (b) change in global mean temperature ( $\Delta T_{\text{global}}$ ) for the climate models that participated in the IPCC 1%/year  $\text{CO}_2$  increase to quadrupling experiment ( $r^2=0.07$ ). See Fig. S2 for model symbol legend.  $\Delta\text{SIC}$  and  $\Delta T_{\text{global}}$  are the difference between the mean of these variables over the last ten years of the experiment and the mean over the first ten years. The polar region is defined by sea gridpoints north of  $80^\circ\text{N}$ . The transient climate sensitivity is the change in global mean surface temperature in a  $\text{CO}_2$  doubling experiment at the time of  $\text{CO}_2$  doubling.

The change in winter polar sea ice appears to be linked to the timing of September sea ice loss (Fig. 4.3(c)), which is reasonable given that the proposed winter CRF feedback functions by trapping heat absorbed by the open ocean during the summer. Other factors, such as the summer albedo feedback (Budyko, 1969; North, 1984), can also decrease September sea ice and contribute to the activation of the CRF feedback; however, it is important to note that the proposed feedback is essential to the elimination of winter sea ice in the IPCC models. For example in the NCAR model, without the convective clouds due to this feedback, the polar ocean would lose about 35% more heat to the atmosphere during polar night, causing the polar SST to drop below the freezing point during a single winter. Finally, the change in winter polar sea ice is closely related to the September sea ice concentration at the beginning of the experiment (at pre-industrial CO<sub>2</sub> concentrations). This is important because the models underestimate the observed loss of Arctic summer sea ice when they are run for the last 50 years (Stroeve et al., 2007). We therefore conclude that the actual climate system may be more likely to lose winter sea ice than is implied by the fact that only two out of 14 models predict a complete collapse of winter sea ice.

### **4.3 Discussion and Conclusions**

One shortcoming of this chapter deserves further attention. Although we have shown that the winter CRF feedback increases the uncertainty in sea ice predictions, we have not explicitly compared its relevance to other feedbacks known to be important for Arctic sea ice prediction. One such feedback we would like to compare the winter CRF feedback with is

the ocean heat transport feedback (e.g., Holland et al., 2006), which is the poleward shift in ocean heat transport associated with the receding of the sea ice boundary that is observed in some models. We anticipate that fully disentangling the importance of the various feedback mechanisms will require sensitivity model runs, in which we run an atmospheric GCM with one feedback at a time disabled to determine which feedbacks produce the largest effect on sea ice. We plan to pursue this work in the future.

The proposed winter CRF feedback (Abbot and Tziperman, 2008a,b) may be an important part of the mechanism that maintained the the warm climates of the Cretaceous and early Paleogene periods (Farrell, 1990; Kory et al., 2008; Sloan et al., 1992; Kirk-Davidoff et al., 2002), when the CO<sub>2</sub> concentration may have been as high as a few thousand ppm (Pearson and Palmer, 2000; Pagani et al., 2005) and the Arctic ocean was warm and ice-free (Zachos et al., 2001; Sluijs and coauthors, 2006). The winter CRF feedback would not necessarily saturate when all the winter sea ice were removed in such climates; the CRF could keep increasing with increasing CO<sub>2</sub> and surface temperature as convection forms higher and thicker clouds (Abbot and Tziperman, 2008b). Additionally, once winter sea ice is lost and the winter CRF feedback is fully active, it may provide such extensive warming that it would be difficult for sea ice to regrow. This would mean that if winter sea ice were lost due to global warming, greenhouse gas levels might have to be reduced below the level at which winter sea ice was lost before winter sea ice could return, so that Arctic sea ice could exhibit hysteresis as CO<sub>2</sub> were varied (Abbot and Tziperman, 2008b; Eisenman, 2007).

The increased winter Arctic sea ice uncertainty pointed to here, together with factors

that lead to uncertainty in summer sea ice (Eisenman et al., 2007), suggest that our ability to reliably predict Arctic climate change is still far from satisfactory and that dramatic changes cannot be ruled out.



# **Chapter 5**

## **Controls on the Activation and Strength of a High-Latitude Convective Cloud Feedback**

### **Feedback**

#### **5.1 Introduction**

Cloud feedbacks represent the most important source of uncertainty in the climate system (Cess and co authors, 1990, 1996; Baker, 1997; Murphy et al., 2004; Stainforth et al., 2005; Soden and Held, 2006). This motivates the idea that cloud feedbacks might play an important role in explaining past "equable climates" and makes understanding clouds important for understanding future climate under increased greenhouse gas levels. Equable climates, which prevailed during the late Cretaceous and early Paleogene (~100 to ~35 million years

ago), were characterized by warm high latitudes (e.g., Zachos et al., 2001; Sluijs and coauthors, 2006), particularly during the winter and over continents (e.g., Greenwood and Wing, 1995), and tropical temperatures only somewhat higher than modern (e.g., Pearson et al., 2001; Norris et al., 2002; Roche et al., 2006; Tripathi et al., 2003). Various mechanisms have been proposed to explain either the relatively cool tropical temperatures or relatively warm polar temperatures, including increased ocean heat transport due to ocean mixing by increased hurricane activity (Emanuel, 2002; Korty et al., 2008), the Hadley cell extending nearly to the pole (Farrell, 1990), and high-latitude longwave heating due to thick polar stratospheric clouds (Sloan et al., 1992; Sloan and Pollard, 1998; Peters and Sloan, 2000; Kirk-Davidoff et al., 2002).

Abbot and Tziperman (2008a) proposed a positive feedback on high-latitude temperatures that results from the onset of convective clouds. A related suggestion was also briefly made by Sloan et al. (1999) and Huber and Sloan (1999). In this proposed feedback, an initial warming leads to destabilization of the high-latitude atmosphere to convection, causing convection, which results in convective clouds and increased atmospheric moisture, both of which trap outgoing longwave radiation and lead to further warming.

Over ocean this feedback should occur preferentially during winter (Abbot and Tziperman, 2008b; Abbot et al., 2008b) because during summer marine boundary layer clouds block low-level atmospheric solar absorption so that solar absorption occurs preferentially in the mid-troposphere and stabilizes the lower atmosphere.

The convective cloud feedback as outlined in Abbot and Tziperman (2008b) and Abbot

et al. (2008b) is intimately tied to sea ice, which insulates the ocean and prevents convection when it is present, while the feedback prevents the formation of sea ice when there is none (Abbot and Tziperman, 2008b; Abbot et al., 2008b). Abbot and Tziperman (2008a), however, found that the convective cloud feedback can operate based on atmospheric processes alone. This distinction is important because it underscores the possibility that the convective cloud feedback could lead to further warming even after the complete removal of sea ice and we will return to it in the discussion (section 5.4).

The convective cloud feedback allows for multiple equilibria: one solution which is convecting and is warm and another solution which is not convecting and is cold. The purpose of this paper is to determine what parameters control the lowest (critical) CO<sub>2</sub> value at which the warm state can exist and the temperature difference between the two states. The critical CO<sub>2</sub> is important because it determines whether the convective cloud feedback could have been active during periods of equable climate and whether it could be active in a future climate under global warming. The temperature difference between the two states is important because it represents the strength of the convective cloud feedback.

In section 5.2 we develop a simple two-level atmosphere-surface model that encapsulates the most basic physics that can describe the atmosphere-only convective cloud feedback. We use this model to qualitatively determine the way in which various parameters affect the onset of the feedback and its strength. This analysis should aid interpretation of the convective cloud feedback in more complex models, for example the IPCC coupled GCMs in which the convective cloud feedback has been shown to be active (Abbot et al.,

2008b).

In Section 5.3 we extend this analysis using SCAM, the NCAR single column atmospheric model. SCAM contains the full cloud, convection, and radiation parameterizations of the NCAR community atmosphere model (CAM), but heat transports into it and velocities acting on it must be prescribed. We show that SCAM's behavior is consistent with that of the two-level model and that the lessons from the simpler model can be used to understand the more complete SCAM.

## **5.2 Two-Level Model**

### **5.2.1 Developing the Model**

In this section we construct a simple two-level model of the atmosphere in which we attempt to capture the simplest system in which the convective cloud feedback can function. Based on previous work (Abbot and Tziperman, 2008a,b; Abbot et al., 2008b) we expect the convective cloud feedback to be active at high latitudes (roughly poleward of  $60^\circ$ ) during winter, and we will make assumptions accordingly throughout this section. In this model the top level represents the free troposphere (200-900 mb) (henceforth the atmosphere) and the lower level (henceforth the surface) represents the combined boundary layer (900-1000 mb) and surface, for example, a mixed-layer ocean (top 50 m). In effect we assume that turbulent fluxes tie the surface to the boundary layer so tightly that they

behave as one. Energy balance for this model can be written

$$C_s \frac{dT_s}{dt} = F_s - F_c + \epsilon \sigma T_a^4 - \sigma T_s^4, \quad (5.1)$$

$$C_a \frac{dT_a}{dt} = F_a + F_c + \epsilon \sigma (T_s^4 - 2T_a^4). \quad (5.2)$$

Here  $C_s$  and  $C_a$  are the total heat capacities of the surface and atmospheric columns (standard heat capacity multiplied by total column mass), respectively;  $T_s$  and  $T_a$  are the surface and atmospheric temperatures, respectively;  $F_s$  is the heat flux into the surface and boundary layer from solar radiation and by horizontal heat transport, which can be written  $F_s = F_o + S(1 - \alpha) + F_a^{bl}$  where  $F_o$  is the meridional ocean heat transport convergence,  $S$  is the solar heat flux,  $\alpha$  is the albedo, and  $F_a^{bl}$  is the atmospheric transport convergence into the boundary layer;  $F_a$  is the meridional heat transport convergence into the atmospheric layer;  $F_c$  is the convective heat flux from the boundary layer to the free troposphere;  $\epsilon$  is the emissivity of the free troposphere; and  $\sigma$  is the Stefan-Boltzmann constant.

The convective heat flux,  $F_c$ , and the free tropospheric emissivity,  $\epsilon$ , depend on whether or not there is convection, which in turn depends on the moist stability. We determine moist stability by comparing the surface moist static energy ( $M_s$ )

$$M_s = C_p T_s + L r_s,$$

with the atmospheric saturation moist static energy ( $M_a^*$ )

$$M_a^* = C_p T_a + L r_a^* + g z_a,$$

where  $C_p$  is the specific heat of air at constant pressure,  $L$  is the latent heat of evaporation,  $r_s$  is the surface specific humidity,  $r_a^*$  is the free tropospheric saturation specific humidity,  $g$  is Earth's gravitational constant, and  $z_a$  is the height of the atmospheric layer (we specify the pressure of this layer,  $P_a$ , and calculate  $z_a$  using a scale height of 8 km). We calculate  $r_s$  by assuming a constant boundary layer relative humidity,  $RH$ . If  $M_s < M_a^*$ , the model is stable to moist convection and there is no convection, consequently we set the convective heat flux to zero ( $F_c = 0$ ) and we set the emissivity to a background value ( $\epsilon = \epsilon_0$ ).  $\epsilon_0$  represents the free tropospheric emissivity in the absence of convection, which should be roughly linear in  $\log(\text{CO}_2)$  (Sasamori, 1968). Otherwise we choose  $F_c$  to satisfy the moist stability criticality ( $M_s = M_a^*$ , see below) and set  $\epsilon = \epsilon_0 + \Delta\epsilon$ . Our use of  $F_c$  to satisfy the moist stability criticality represents the basic physics of adjustment to a neutrally buoyant profile in a moist atmosphere. Our assumption that the atmospheric emissivity increases from a background emissivity ( $\epsilon_0$ ) when there is no convection by some offset ( $\Delta\epsilon$ ) upon the onset of convection represents the advent of radiatively thick convective clouds and the increase in high-altitude moisture; this is how the convective cloud feedback manifests itself in this model. Convective clouds could also affect the model albedo and through it  $F_s$ , however, based on previous SCAM and GCM investigations of the seasonality of the convective cloud feedback (Abbot and Tziperman, 2008b; Abbot et al., 2008b), we

will focus on high-latitude winters when the incoming solar radiation,  $S$ , is small or zero, making such an effect irrelevant.

We can solve for the steady-state solutions of the model by setting the time tendencies of (5.1-5.2) to zero. First consider the nonconvecting state, in which  $F_c = 0$  and  $\varepsilon = \varepsilon_0$ . We have

$$0 = F_s + \varepsilon_0 \sigma T_{a1}^4 - \sigma T_{s1}^4, \quad (5.3)$$

$$0 = F_a + \varepsilon_0 \sigma (T_{s1}^4 - 2T_{a1}^4), \quad (5.4)$$

where the subscript 1 signifies that this is the nonconvecting solution. We can solve (5.3-5.4) for the nonconvecting surface and atmospheric temperatures

$$T_{s1} = \left( \frac{2F_s + F_a}{(2 - \varepsilon_0)\sigma} \right)^{\frac{1}{4}} \quad (5.5)$$

$$T_{a1} = \left( \frac{\varepsilon_0 F_s + F_a}{(2 - \varepsilon_0)\varepsilon_0 \sigma} \right)^{\frac{1}{4}} \quad (5.6)$$

This solution is valid so long as  $M_{s1} \leq M_{a1}^*$ .

When the model is convecting, we obtain the equations

$$0 = F_s - F_c + \tilde{\varepsilon} \sigma T_{a2}^4 - \sigma T_{s2}^4, \quad (5.7)$$

$$0 = F_a + F_c + \tilde{\varepsilon} \sigma (T_{s2}^4 - 2T_{a2}^4), \quad (5.8)$$

$$C_p T_{s2} + L r_{s2} = C_p T_{a2} + L r_{a2}^* + g z_a \quad (5.9)$$

where  $\tilde{\epsilon} \equiv \epsilon_0 + \Delta\epsilon$  and the subscript 2 signifies the convecting solution. (5.9) represents the moist convective criticality ( $M_{s2} = M_{a2}^*$ ). (5.7-5.9) can be solved for  $T_{s2}$ ,  $T_{a2}$ , and  $F_c$ . This solution is valid so long as  $F_c > 0$ .

We plot the convecting and nonconvecting solutions of the two-level model as a function of  $\epsilon_0$  in Fig. 5.1. Here we choose  $F_a=100 \text{ W m}^{-2}$ , which is a reasonable high-latitude value (Trenberth and Stepaniak, 2003), and  $F_s=250 \text{ W m}^{-2}$ , which we take, for the most part, to represent heat absorbed and stored by the ocean during the summer and released back into the atmosphere during the winter. The simplicity of the model, with only one layer to represent the atmosphere, requires us to choose an unrealistically high  $F_s=250 \text{ W m}^{-2}$  to achieve above-freezing surface temperatures.  $F_s$  takes much smaller values when we use the more realistic SCAM model (section 5.3). We take  $\Delta\epsilon=0.3$  and  $P_a=600 \text{ mb}$ , representing medium-height convection that produces optically thick clouds.

The nonconvecting solution exists at all values of the clear-sky emissivity ( $\epsilon_0$ ) for these parameter choices (solid black line, Fig. 5.1a). For many other parameter choices, however, the nonconvecting solution does not exist at high  $\epsilon_0$ . The convecting solution exists at high  $\epsilon_0$ , but disappears for  $\epsilon_0$  below some critical  $\epsilon_0$  which we call  $\epsilon_c$ .  $\epsilon_c$  is the two-level model analogue of the logarithm of the critical  $\text{CO}_2$ . Below  $\epsilon_c$ , the two-level model is no longer warm enough to consistently sustain convection (that is, (5.7-5.9) yield  $F_c < 0$ ). Because the free tropospheric emissivity is increased by  $\Delta\epsilon$  due to the appearance of convective clouds and increased moisture in the convecting solution, the convecting solution has a higher surface temperature than the nonconvecting solution at all  $\epsilon_0$ .

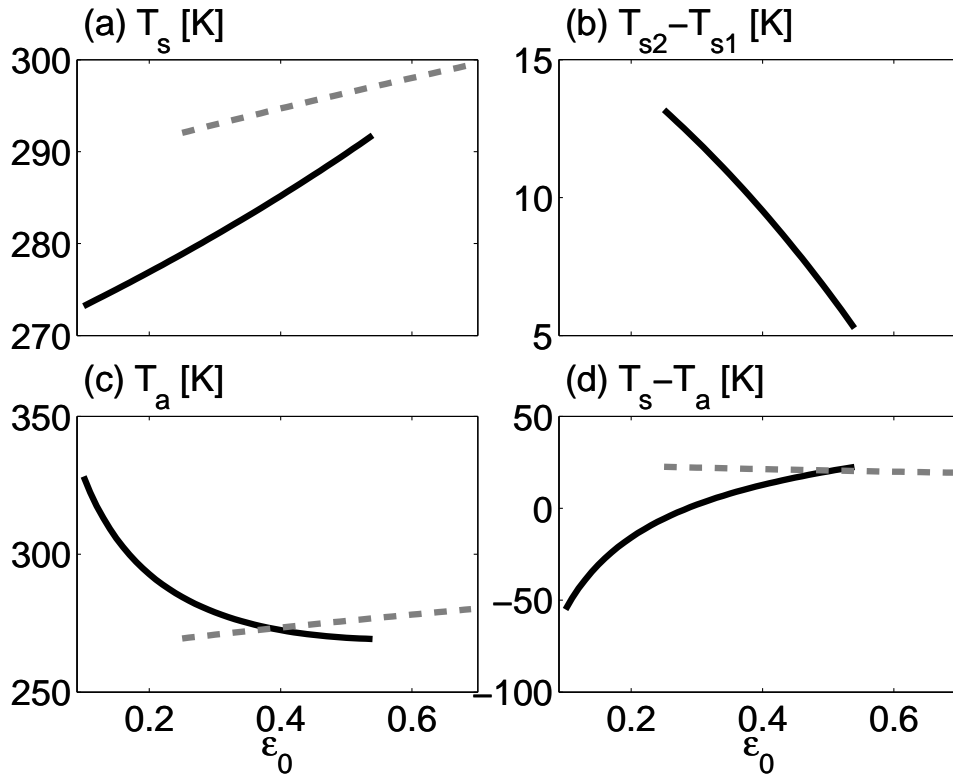


Figure 5.1: Solution to the two-level model as a function of  $\epsilon_0$ , which is a proxy for  $\log(\text{CO}_2)$  concentration. (a) Nonconvecting solution surface temperature ( $T_{s1}$ , black solid line) and convecting solution surface temperature ( $T_{s2}$ , grey dashed line), (b) difference between the surface temperature of the convecting and nonconvecting solutions ( $T_{s2} - T_{s1}$ ), (c) nonconvecting solution atmospheric temperature ( $T_{a1}$ , black solid line) and convecting solution atmospheric temperature ( $T_{a2}$ , grey dashed line), (d) nonconvecting solution lapse rate ( $T_{s1} - T_{a1}$ , black solid line) and convecting solution lapse rate ( $T_{s2} - T_{a2}$ , grey dashed line). Model parameters are:  $F_s=250 \text{ W m}^{-2}$ ,  $F_a=100 \text{ W m}^{-2}$ ,  $\epsilon_0=0.5$ ,  $\Delta\epsilon=0.3$ ,  $P_a=600 \text{ mb}$ , and  $RH=0.85$ .

The vertical temperature profile of the convecting solution follows the moist lapse rate, whereas the lapse rate of the nonconvecting solution is determined radiatively (Fig. 5.1d). This causes the nonconvecting surface temperature to increase much faster with  $\epsilon_0$  than the convecting surface temperature does ( $\frac{dT_{s1}}{d\epsilon_0} > \frac{dT_{s2}}{d\epsilon_0}$ , Fig. 5.1a). Consequently, the maximum difference in surface temperature between the convecting and nonconvecting solutions as a function of  $\epsilon_0$ ,  $(T_{s2} - T_{s1})_{max}$ , occurs at the minimum value of  $\epsilon_0$  at which convection is possible ( $\epsilon_0 = \epsilon_c$ ).

There is a singularity in the nonconvecting atmospheric temperature (5.6) as  $\epsilon_0$  approaches zero if  $F_a$ , the atmospheric heat transport, is nonzero. This leads to a negative lapse rate at low  $\epsilon_0$  (Fig. 5.1(d)), which to some extent could be a realistic representation of a high-latitude winter inversion; however, the extreme increase of  $T_{a1}$  as  $\epsilon_0$  goes to zero is due to the simplicity of the model and is not realistic. In any case, this does not affect the surface temperature (5.5), which is the quantity in which we are primarily interested.

## 5.2.2 Using the Model to Understand the Convective Cloud Feedback

We now focus on how the model parameters affect  $\epsilon_c$ , the lowest  $\epsilon_0$  at which the convecting solution can exist, and  $(T_{s2} - T_{s1})_{max}$ , the maximum difference in surface temperature between the convecting and nonconvecting solutions as a function of  $\epsilon_0$ .  $\epsilon_c$  is important for two reasons. First, since  $\epsilon_0$  can be thought of as roughly representing  $\log(\text{CO}_2)$  in this model,  $\epsilon_c$  is related to the lowest  $\text{CO}_2$  concentration at which the convecting solution can exist, which is critical to whether or not the convecting solution could be real-

ized during an equable climate or future climate with increased greenhouse gases. Second, as  $(T_{s2} - T_{s1})_{max}$  occurs at  $\epsilon_0 = \epsilon_c$  and  $\frac{dT_{s1}}{d\epsilon_0} > \frac{dT_{s2}}{d\epsilon_0}$ , decreasing  $\epsilon_c$  tends to increase  $(T_{s2} - T_{s1})_{max}$ , which is itself important because  $(T_{s2} - T_{s1})_{max}$  represents the strength of the convective cloud feedback. Stated again, the lower the critical  $\text{CO}_2$ , the larger the maximum temperature increase caused by the convective cloud feedback, all other things being equal.

In Figs. 5.2-5.3, we show how  $(T_{s2} - T_{s1})_{max}$  and  $\epsilon_c$  change as we vary  $\Delta\epsilon$ ,  $F_s$ ,  $F_a$ , and  $P_a$ , which are the important independent model parameters.  $\Delta\epsilon$  represents the increase in optical thickness of the atmosphere associated with clouds and water vapor upon the onset of convection. We see  $F_s$  as mostly representing solar heat absorbed by the surface during summer and released into the atmosphere during the winter.  $F_a$  represents the convergence of atmospheric heat transport.  $P_a$  represents the depth of convection. Our main findings in this section are that changing  $\Delta\epsilon$  has a significant effect on  $(T_{s2} - T_{s1})_{max}$  whereas changing the other variables does not, and that  $\epsilon_c$  tends to be more sensitive to changes in all the variables than  $(T_{s2} - T_{s1})_{max}$  does.

Increasing  $\Delta\epsilon$  causes no change in the nonconvecting solution. Increasing  $\Delta\epsilon$  warms the convecting solution, which itself increases  $(T_{s2} - T_{s1})_{max}$ , but it also allows the convecting solution to exist at lower  $\epsilon_0$  (Fig. 5.3a), which, as explained above, further increases  $(T_{s2} - T_{s1})_{max}$  (Fig. 5.2a).

Increasing  $F_s$ , which destabilizes the atmosphere to convection, allows the convecting solution to exist at lower  $\epsilon_0$  (decreases  $\epsilon_c$ , Fig. 5.3b); however,  $(T_{s2} - T_{s1})_{max}$  increases

slightly as  $F_s$  increases (Fig. 5.2b) instead of decreasing as one might expect from the decrease in  $\epsilon_c$ . This is because the surface and atmosphere are more tightly coupled in the convecting solution so more of the heating resulting from increasing  $F_s$  goes into increasing the surface temperature in the nonconvecting solution than in the convecting solution.

Increasing  $F_a$  increases the surface temperature more in the convecting solution than in the nonconvecting solution, which increases  $(T_{s2} - T_{s1})_{max}$  (Fig. 5.2c), because the surface and atmosphere are more tightly coupled in the convecting solution. The warming effect of  $F_a$  tends to destabilize the atmosphere to convection, but this effect is dominated by the direct stabilizing effect of  $F_a$  so that  $\epsilon_c$  increases with  $F_a$  (Fig. 5.3c). This increase in  $\epsilon_c$  as  $F_a$  increases helps to explain why the increase in  $(T_{s2} - T_{s1})_{max}$  with  $F_a$  is so small.

Increasing  $P_a$  has no effect on the nonconvecting solution. It does cause a large decrease in  $\epsilon_c$  (Fig. 5.3d) because it is easier to reach the moist convective criticality if the height of convection is lower (the gravitational term in (5.9) is smaller). Decreasing the height of convection also means that the  $T_{a2}$  is closer to  $T_{s2}$ , so that the atmosphere provides less radiative forcing, and  $(T_{s2} - T_{s1})_{max}$  decreases somewhat as  $P_a$  is increased. This effect is relatively large at any particular value of  $\epsilon_0$ , but the effect on the maximum temperature difference is muted by the fact that  $\epsilon_c$  decreases as well as  $P_a$  is increased.

### 5.3 SCAM

We next analyze SCAM to determine whether the insight provided by the simple analytical model regarding the critical  $\text{CO}_2$  needed for the warm convecting state to exist ( $\epsilon_c$ ) and

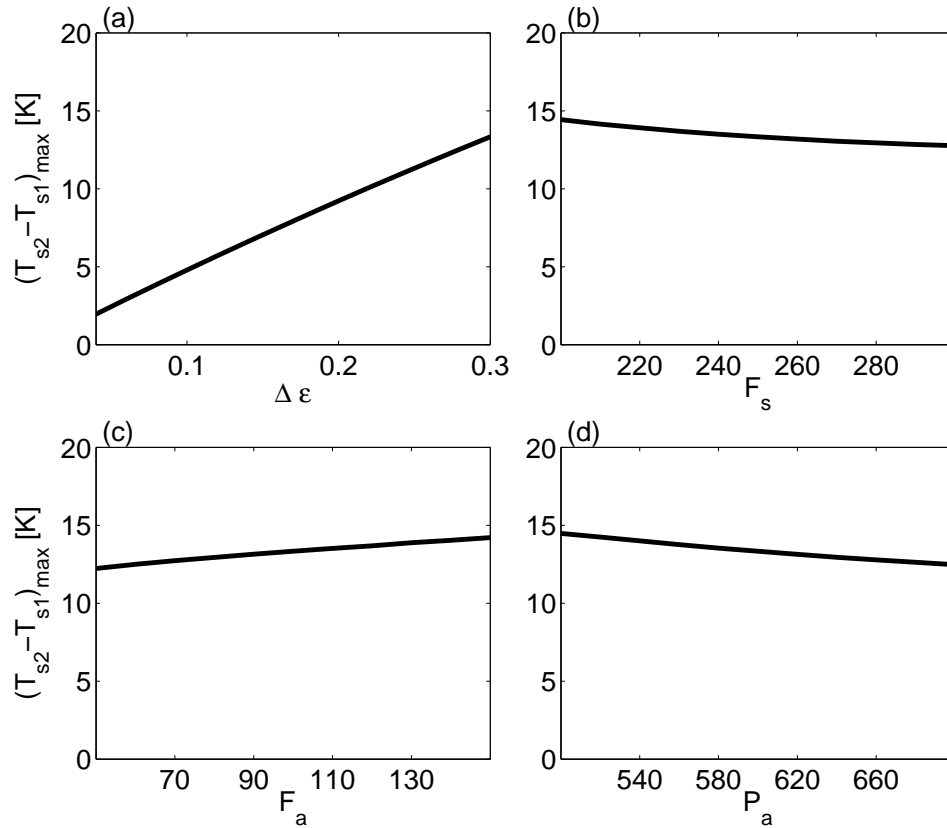


Figure 5.2: Maximum difference in surface temperature between the convecting and nonconvecting solutions as a function of (a)  $\Delta \epsilon$ , the increase in atmospheric emissivity resulting from the onset of convection; (b)  $F_s$ , the heat flux into the surface, we view as mostly representing solar heat absorbed by the surface during summer and released into the atmosphere during the winter; (c)  $F_a$ , the heat flux into the atmosphere; (d)  $P_a$ , pressure of the atmospheric level (depth of convection). Model parameters, except the parameter varied, are as in Fig. 5.1.

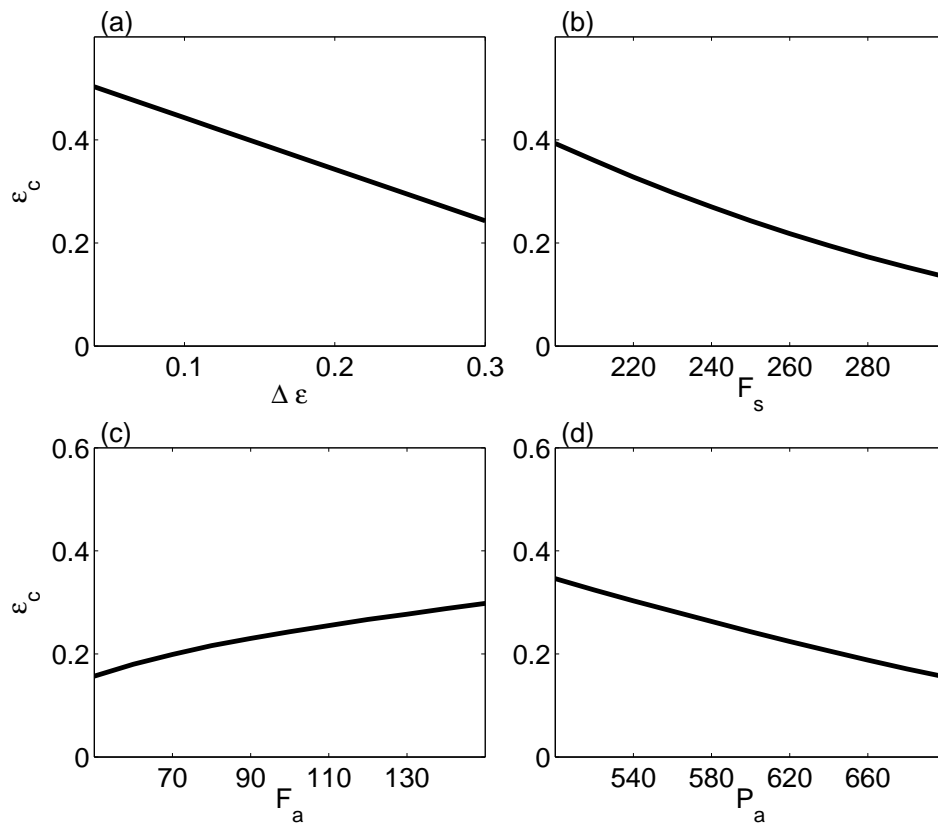


Figure 5.3: As in Fig. 5.2, but for  $\epsilon_c$ , the smallest emissivity at which the convective solution exists.

the maximum strength of the convective cloud feedback  $((T_{s2} - T_{s1})_{max})$  is valid in a more quantitative model. As in section 5.2 we are interested in investigating the convective cloud feedback in SCAM at high latitudes and during winter. Consequently we run SCAM to steady state in simulated polar night (zero solar forcing,  $S=0$ ). The real Arctic ocean is not in steady state during polar night: it radiates heat to space throughout polar night and continually cools. We have, however, already shown that the convective cloud feedback can function in the presence of a seasonal cycle (Abbot and Tziperman, 2008b; Abbot et al., 2008b), and, as our objective here is to understand the feedback in depth, we feel justified in using the steady state assumption, which greatly simplifies our analysis. In addition, in an ice-free Arctic ocean, the surface heat capacity would be very high so that the approximation of considering the steady state solution should be reasonable. In order to obtain an above-freezing equilibrated surface temperature at realistic atmospheric heat transport (AHT) values, we need to specify a nonzero net surface heat flux (NSHF) from the surface to the atmosphere. The NSHF represents a combination of the convergence of ocean heat transport and the winter release of heat that the ocean stored during the summer.

We couple SCAM to a mixed layer ocean of depth 50 m, set the surface wind velocity to a constant  $5 \text{ m s}^{-1}$ , and set the vertical velocity to zero at all vertical levels. We run SCAM with ozone and sea salt aerosol set to their annual mean values at a latitude of  $79.5^\circ\text{N}$  and a longitude of  $143.4^\circ\text{W}$ , which is over the Arctic Ocean. We set all other aerosol concentrations to zero. All boundary conditions that we apply to SCAM are time-invariant. We apply the AHT to the atmosphere as dry transport equally by mass below 200

mb, with the AHT going to zero smoothly as a hyperbolic tangent with a vertical thickness of 50 mb. This means that, other than the smoothing near 200 mb, the applied temperature tendency is the same for each pressure level below 200 mb. In a related study, Abbot and Tziperman (2008b) found that the apportionment of AHT between dry and moist transport did not qualitatively affect their results.

When we run SCAM with zero solar forcing ( $S=0$ ) and large enough AHT and NSHF values, we find multiple equilibria, with a stable warm and convecting state possibly relevant to both future greenhouse warming and past equable climates, over a wide range of  $\text{CO}_2$  values (e.g., Fig. 5.4-5.5). In Fig. 5.4 we show the surface temperature of the warm and cold states with a realistic polar AHT of  $100 \text{ W m}^{-2}$  and different NSHF values, while in Fig. 5.5 we show that both states exist even when we drastically change the distribution of heat transports to  $\text{NSHF}=170 \text{ W m}^{-2}$  and  $\text{AHT}=0 \text{ W m}^{-2}$ . The solution of SCAM (Fig. 5.4-5.5) as a function of  $\log(\text{CO}_2)$  looks similar to that of the two-level model (Fig. 5.1) as a function  $\epsilon_0$ . There is a wide range in  $\log(\text{CO}_2)$  over which both the warm and cold solutions exist and, particularly in Fig. 5.5, the surface temperature of the cold state increases faster with  $\text{CO}_2$  than the surface temperature of the warm state. The cold state sea surface temperature sometimes reaches the freezing point of seawater,  $-1.8^\circ\text{C}$ , (Fig. 5.4) in which case we hold the sea surface temperature at this value. This represents an extra artificial heat flux from the surface into the atmosphere, in addition to the applied NSHF, however, even with this extra heat flux the cold state is still stable. Such cold states would approach the ice-states of Abbot and Tziperman (2008b) if allowed to fully equilibrate in a

model that included sea ice.

The warm equilibrium is significantly warmer than the cold equilibrium when both states exist. For example, with  $\text{CO}_2=2\,000$  ppm,  $\text{AHT}=100\text{ W m}^{-2}$ , and  $\text{NSHF}=70\text{ W m}^{-2}$ , the surface temperature is  $7.0^\circ\text{C}$  in the warm state and  $-1.8^\circ\text{C}$  in the cold state (it is prescribed not to go below the freezing temperature of sea water, as described above). The convective cloud feedback is the major cause of this difference, as the cloud radiative forcing in the warm state ( $45.7\text{ W m}^{-2}$ ) is nearly double that in the cold state ( $25.6\text{ W m}^{-2}$ ). The change in cloud radiative forcing is due to more and thicker high clouds in the warm state (Fig. 5.6c,d). These clouds result from stronger and deeper convection (Fig. 5.6g,h), which leads to increased mid-tropospheric ice condensate (Fig. 5.6f) and increased cloud fraction (Fig. 5.6c).

SCAM calculates the depth of convection, thickness of clouds, and amount of moisture. So in SCAM there are no analogues to  $P_a$  and  $\Delta\epsilon$  from the two-level model for us to vary; however, we can investigate the effect of changing the NSHF (analogue of  $F_s$  in the two-level model) and the AHT (analogue of  $F_a$ , with a complication to be explained) on the convective cloud feedback in SCAM. The lowest  $\text{CO}_2$  at which the warm state exists (critical  $\text{CO}_2$ , analogue of  $\epsilon_c$  in the two-level model), one of the most important variables investigated in this paper, decreases sharply as the NSHF is increased (Table 5.1), which is consistent with the strong decrease of  $\epsilon_c$  as  $F_s$  increases in the two-level model (Fig. 5.3b). For AHT values comparable to modern Arctic values, the critical  $\text{CO}_2$  spans the entire plausible  $\text{CO}_2$  range for the early Paleogene ( $\sim 250\text{--}\sim 4000$  ppm, Pagani et al., 2005; Pearson

and Palmer, 2000) when the NSHF is changed by  $20 \text{ W m}^{-2}$  (Table 5.1). This underscores the importance of the absorption of summer solar radiation for the maintenance of the warm state.

The critical  $\text{CO}_2$  in SCAM also decreases sharply as the AHT is increased, which appears to contradict the increase in  $\epsilon_c$  as  $F_a$  increases in the two-level model (Fig. 5.3c). The main reason for this is that, as the AHT in SCAM is applied equally throughout the troposphere, it is not a direct analogue for  $F_a$  from the two-level model, but should actually be thought of as some combination of  $F_s$  and  $F_a$ . Furthermore, an AHT applied in this way does not directly change the stability, so that its main effect is to warm the model, which decreases the critical  $\text{CO}_2$ . We should note that the formulation of the vertical distribution of AHT in SCAM we have used is not necessarily realistic, as, for example, we have not taken into account reduced near-surface AHT due to surface friction (e.g., Branscome et al., 1989; Stone and Yao, 1990). The main lesson we should learn from these SCAM runs and the two-level model is that the effect of the AHT on the critical  $\text{CO}_2$  depends strongly on the detailed vertical distribution of AHT.

There is no discernible pattern in the change in the maximum surface temperature difference between the warm and cold states as AHT and NSHF are varied (Table 5.2). This is consistent with the relatively small changes in  $(T_{s2} - T_{s1})_{max}$  as  $F_s$  and  $F_a$  are varied in the two-level model (section 5.2.2). Additionally, because of the high sensitivity of the critical  $\text{CO}_2$  to NSHF, we only vary AHT and NSHF over relatively small ranges compared to the ranges over which we varied  $F_s$  and  $F_a$  in the two-level model.

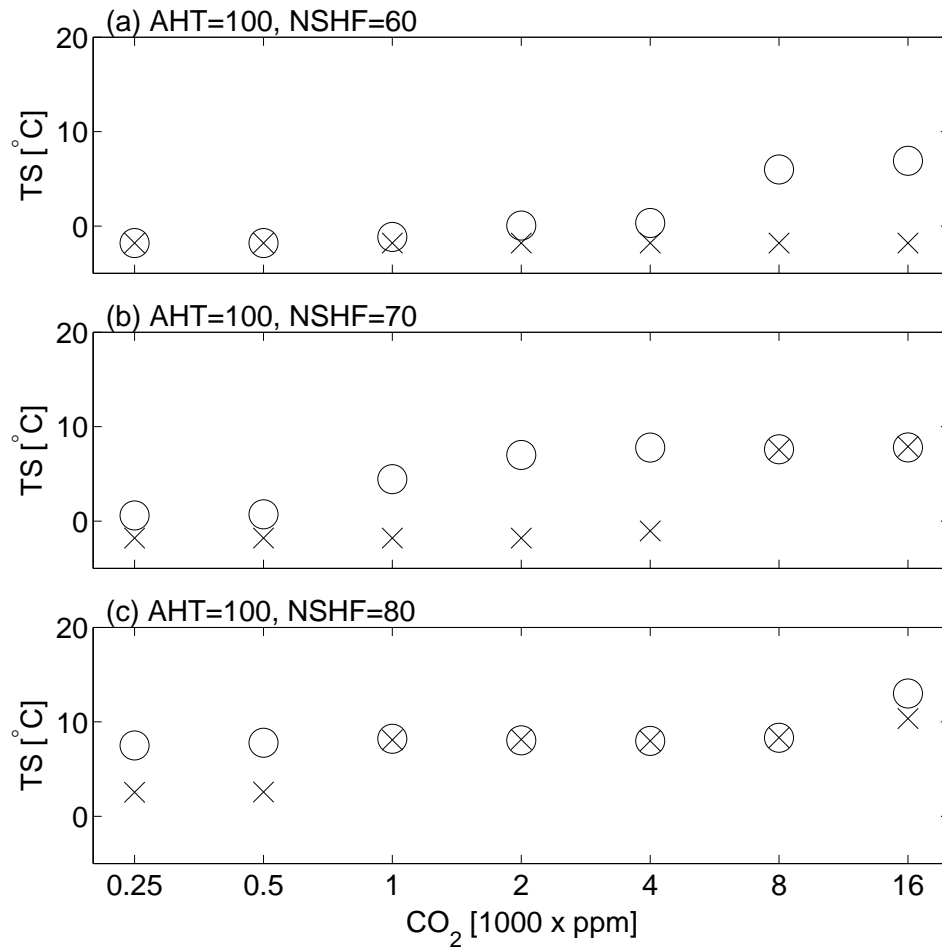


Figure 5.4: Equilibrated surface temperature (TS) of the warm (circles) and cold (crosses) states in SCAM at different  $\text{CO}_2$  levels with zero solar radiation ( $S=0 \text{ W m}^{-2}$ ), an atmospheric heat transport (AHT) of  $100 \text{ W m}^{-2}$ , and a net surface heat flux (NSHF) of (a)  $60 \text{ W m}^{-2}$ , (b)  $70 \text{ W m}^{-2}$ , (c)  $80 \text{ W m}^{-2}$ .

Table 5.1: The critical  $\text{CO}_2$  concentration (ppm), the lowest  $\text{CO}_2$  concentration at which the warm state can exist (the convective cloud feedback can be active), in SCAM as a function of the prescribed atmospheric heat transport (AHT) and net surface heat flux (NSHF). We ran SCAM at every doubling of  $\text{CO}_2$  concentration between 250 ppm and 16 000 ppm, as in Figs. 5.4 and 5.5. The warm state does not exist at any  $\text{CO}_2$  concentration below 16 000 ppm for  $\text{AHT}=90 \text{ W m}^{-2}$  and  $\text{NSHF}=60$  and  $70 \text{ W m}^{-2}$ .

	$\text{NSHF}=60 \text{ W m}^{-2}$	$\text{NSHF}=70 \text{ W m}^{-2}$	$\text{NSHF}=80 \text{ W m}^{-2}$
$\text{AHT}=90 \text{ W m}^{-2}$	-	-	2 000
$\text{AHT}=100 \text{ W m}^{-2}$	8 000	1 000	250
$\text{AHT}=110 \text{ W m}^{-2}$	250	250	250

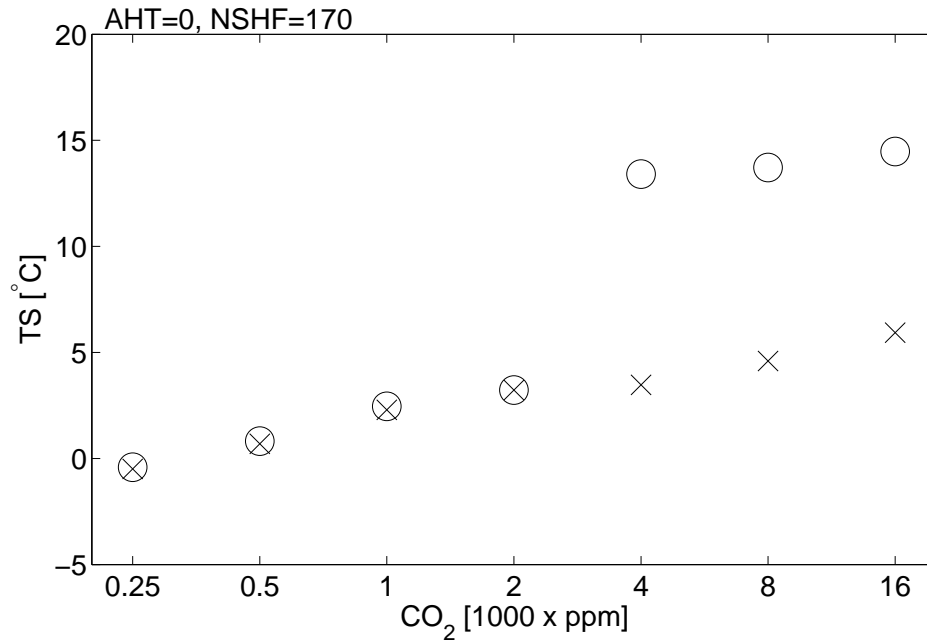


Figure 5.5: Equilibrated surface temperature (TS) of the warm (circles) and cold (crosses) states in SCAM at different CO<sub>2</sub> levels with zero solar radiation ( $S=0 \text{ W m}^{-2}$ ), zero atmospheric heat transport ( $AHT=0 \text{ W m}^{-2}$ ), and a net surface heat flux (NSHF) of  $170 \text{ W m}^{-2}$ .

Table 5.2: The maximum temperature difference ( $^{\circ}\text{C}$ ) between the warm and cold states in SCAM as a function of the prescribed atmospheric heat transport (AHT) and net surface heat flux (NSHF). We ran SCAM at every doubling of CO<sub>2</sub> concentration between 250 ppm and 16 000 ppm, as in Figs. 5.4 and 5.5. The warm state does not exist at any CO<sub>2</sub> concentration below 16 000 ppm for  $AHT=90 \text{ W m}^{-2}$  and  $NSHF=60$  and  $70 \text{ W m}^{-2}$ ;

	$NSHF=50 \text{ W m}^{-2}$	$NSHF=60 \text{ W m}^{-2}$	$NSHF=70 \text{ W m}^{-2}$
$AHT=90 \text{ W m}^{-2}$	-	-	3.5
$AHT=100 \text{ W m}^{-2}$	8.7	8.8	5.2
$AHT=110 \text{ W m}^{-2}$	9.8	10.2	3.5

## 5.4 Discussion

Results from the two-level model (section 5.2) helped us motivate and understand results from SCAM (section 5.3). For example, both models agree that the critical  $\text{CO}_2$  at which the convective cloud feedback activates is sharply dependent on surface heat flux. As far as the surface heat flux in these models can be interpreted as the winter release of heat stored by the ocean during the summer, this suggests that more clouds during summer, which reflect solar radiation and therefore reduce the amount of solar radiation absorbed by the surface, should lead to a higher critical  $\text{CO}_2$ . The use of both models in conjunction with each other also helped us understand that the vertical distribution of the atmospheric heat transport is at least as important as its magnitude for determining the critical  $\text{CO}_2$ . This represents an important limitation on our ability to predict the critical  $\text{CO}_2$  since currently even the magnitude of the atmospheric heat transport during equable climates, resulting from a competition between reduced dry static energy transport, due to reduced meridional temperature gradient, and increased latent energy transport, due to increased subtropical temperature and moisture, is unknown (Pierrehumbert, 2002; Caballero and Langen, 2005).

The two-level model, however, is useful beyond its relation to SCAM. SCAM interactively predicts the depth of convection, thickness of clouds, and amount of moisture, whereas, in the two-level model we are able to vary these at will, through the parameters  $\Delta\epsilon$  and  $P_a$ , to understand their effect on the convective cloud feedback. The main interesting and unexpected results from the two-level model are that increasing the height of convection significantly increases the critical  $\text{CO}_2$  and that increasing the height of con-

vection has very little effect on the maximum surface temperature difference between the cold and warm state, although it does significantly increase the convecting solution surface temperature and, therefore, the surface temperature difference at any particular  $\epsilon_0$  ( $\text{CO}_2$ ).

This type of understanding, gained from the two-level model, could be quite useful for interpretation of general circulation model (GCM) results. For example Abbot et al. (2008b) found that the convective cloud feedback increased the uncertainty in winter sea ice forecasts in the coupled ocean-sea ice-land-atmosphere GCMs that participated in the IPCC fourth assessment report 1%/year  $\text{CO}_2$  increase to quadrupling scenario. The extent to which sea ice was lost and the feedback was active are related to the critical  $\text{CO}_2$  and perhaps insight from the two-level model could help us understand the differences between these models.

Two of the GCMs that participated in the IPCC fourth assessment report 1%/year  $\text{CO}_2$  increase to quadrupling scenario completely lost winter sea ice at the end of the experiment. The Arctic winter sea surface temperature in these models was barely above freezing, and the cloud radiative forcing was about  $30 \text{ W m}^{-2}$  which, though significant, is much smaller than roughly  $50 \text{ W m}^{-2}$  found in SCAM in this paper and by Abbot and Tziperman (2008b) when the surface temperature was  $10\text{-}15^\circ\text{C}$  higher. This difference in cloud radiative forcing was mainly due to the fact that the convection was shallower in the ice-free GCMs (reaching about 800 mb) than in SCAM (reaching 400-500 mb). Abbot et al. (2008b) speculated that the GCMs might have produced deeper convection and a stronger feedback if the  $\text{CO}_2$  were further increased or the run were integrated until it were closer to equilibrium.

This paper raises the possibility that the convective cloud feedback operating in the atmosphere alone could introduce sufficient nonlinearity to allow a hysteresis such that if the GCMs were started from much warmer ice-free conditions, instead of ice-covered conditions, they might have equilibrated with deeper convection and a higher surface temperature like SCAM did.

Renno (1997) and Sobel et al. (2007) have found multiple equilibria in single column atmospheric models that include representations of the hydrological cycle. The Renno (1997) study does not include clouds, so it is quite different from this study. The work of Sobel et al. (2007) is more similar to this study in that they find two separate steady-states, one convecting, and one not convecting; however, by using the weak temperature gradient assumption, they focus on the tropics, and their model uses fixed surface temperatures, rather than prognostic surface temperatures in an energy-conserving model. The convecting and nonconvecting states of Sobel et al. (2007) are not "warm" and "cold," since both are forced at the same surface temperature, rather they are "wet" and "dry."

In the two-level model of section 5.2, we assumed that the atmospheric emissivity increased by a constant offset ( $\Delta\epsilon$ ) upon the onset of convection. One might alternatively suspect that the radiative effect of convective clouds might increase with the strength of convection. This is the case in the warm SCAM states of Fig. 5.4: the cloud radiative forcing increases roughly linearly with the maximum convective mass flux in the mid-troposphere (not shown). When we modify the two-level model so that the emissivity increases linearly with the convective heat flux ( $F_c$ ) instead of all at once when convection starts, we find that

the model still exhibits hysteresis and our main conclusions are unaltered.

The convective cloud feedback could help to keep the Arctic ocean ice-free throughout the winter. This would likely lead to a situation with relatively warm ocean surrounded by relatively cold continent. This could lead to a low pressure system over the ocean and possibly, even though the Coriolis parameter would be large and the Ekman number small, lead to Ekman pumping, inflow at low levels, and vertical ascent. In this paper, we have specified the vertical velocity to be zero at every level (section 5.3), so we have neglected such an effect; however, it seems likely that such upward motion would augment the convective activity over the ocean.

The two-level model we used in this study is intentionally quite simple and SCAM, though it has sophisticated cloud, convection, and radiation schemes, lacks dynamics. In both models we need to specify horizontal heat transports, which define the models' interaction with surrounding areas, and prescribe a net surface heat flux to simulate seasonal heat storage. In some sense the simplicity of these models is a limitation of this study; however, the convective cloud feedback has been shown to be active in state-of-the-art coupled GCMs (Abbot et al., 2008b) and here we have used the two simple models in conjunction to gain a deeper understanding of the feedback.

A major part of the equable climate mystery is warmth during the winter in continental interiors (e.g., Greenwood and Wing, 1995). Implicitly, this paper has focused on polar night over oceans since we have net heat flux from the surface into the atmosphere, which would have to come from either ocean heat transport or the storage of heat during the

summer by the ocean and release during the winter. We are currently investigating the role the convective cloud feedback could play in warming continental interiors.

## 5.5 Conclusions

In this paper we used a simple two-level model of the atmosphere and ocean and NCAR's single column atmospheric model coupled to a mixed layer ocean to analyze the critical CO<sub>2</sub> concentration at which a high-latitude convective cloud feedback can become active and the strength of this high-latitude convective cloud feedback, as measured by its ability to raise the surface temperature. The critical CO<sub>2</sub> is particularly important because it determines whether the convective cloud feedback could have been active during periods of equable climate and in a future climate, because understanding what controls it may aide in understanding why the convective cloud feedback is more active in some GCMs than in others at the same CO<sub>2</sub> concentration, and because it has a large effect on the overall strength of the feedback (section 5.2.2). Our main findings follow.

- If the feedback produces more and thicker convective clouds, it should activate at a lower CO<sub>2</sub> and be stronger.
- If the feedback produces deeper convection, it should activate at a higher CO<sub>2</sub>, be much stronger at any particular CO<sub>2</sub>, and have a somewhat larger maximum strength.
- If the net heat released by the surface during winter, produced either by ocean heat transport or by the release of seasonally-stored heat, increases, the critical CO<sub>2</sub>

should decrease sharply and the strength of the feedback should not change much.

- The effects of atmospheric heat transport are complicated and depend on the detailed vertical structure of this heat transport.

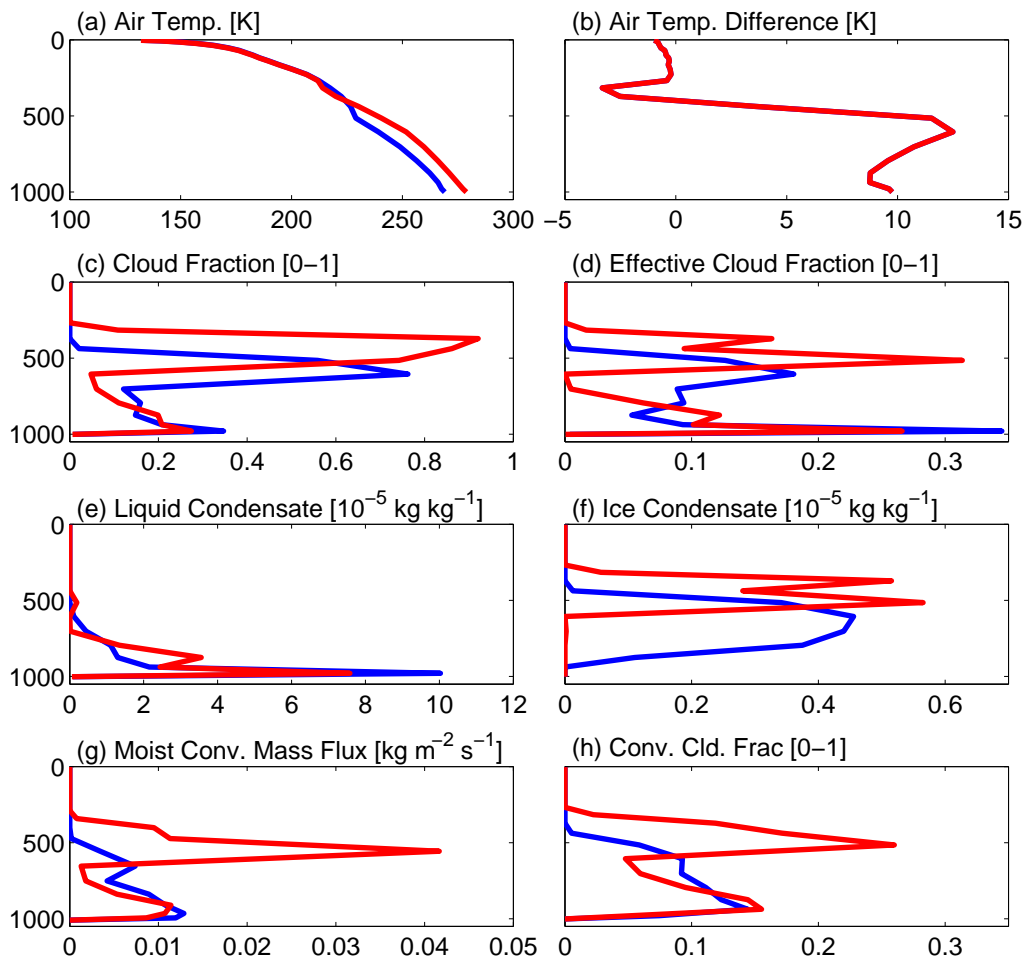


Figure 5.6: Vertical profiles of important SCAM output with zero solar radiation ( $S=0 \text{ W m}^{-2}$ ), an atmospheric heat transport (AHT) of  $100 \text{ W m}^{-2}$ , a net surface heat flux (NSHF) of  $70 \text{ W m}^{-2}$ , and  $\text{CO}_2=2000 \text{ ppm}$  for the warm (red) and cold (blue) states. The effective cloud fraction is the product of the cloud fraction and the cloud emissivity for each layer. The convective cloud fraction is the cloud fraction produced by the convection scheme. The total cloud fraction in a region with convection is often higher than the convective cloud fraction because the model often produces stratiform clouds in these regions as well.



# Chapter 6

## Conclusion

In this thesis we have proposed a high-latitude convective cloud feedback that might help to explain the "equable climates," periods of low equator to pole surface temperature difference and low seasonal cycle in high-latitude surface temperature, that prevailed during the late Cretaceous and early Paleogene ( $\sim 100$  to  $\sim 35$  million years ago). In this proposed feedback, an initial warming, perhaps due to increased greenhouse gas concentration, leads to destabilization of the high-latitude atmosphere to convection, causing convection, which results in convective clouds and increased atmospheric moisture, both of which trap outgoing longwave radiation and lead to further warming. We have also argued that this feedback could potentially play a role in determining future high-latitude climate under increased greenhouse gas concentrations.

In Chapter 2 we constructed a simple, zonally-averaged global climate model forced by annual-mean solar radiation and used this model to investigate the climate under high

CO<sub>2</sub> concentrations. We carefully tried to include the most important physical processes relating to clouds, convection, and their interaction with radiation in this model, albeit in a greatly simplified manner. With this model we argued that the onset of deep convection at high latitudes and an associated increase in cloud radiative forcing, representing a significant positive feedback on climate change, is a plausible outcome of increased CO<sub>2</sub> concentrations.

We pursued this idea in Chapter 3 by investigating the effect of seasonality on this convective cloud feedback using the National Center for Atmospheric Research (NCAR) single column model (SCAM). This model has many advantages over the simple model we used in Chapter 2, including high vertical resolution, state-of-the-art physical parameterizations, and a full seasonal cycle. SCAM's main disadvantage is that, as it is a single column model, vertical and horizontal velocities and horizontal heat transports must be applied to it. We showed using this model that the convective cloud feedback enables the ocean to stay ice-free throughout the year at drastically lower CO<sub>2</sub> concentrations than would otherwise be possible. We also learned an important lesson about the seasonality of the convective cloud feedback: the feedback should be most active during winter, at least over ocean, because summer marine boundary layer clouds block low-level atmospheric solar absorption so that solar absorption occurs preferentially in the mid-troposphere and stabilizes the lower atmosphere during the summer.

Chapter 4 was a direct extension of the ideas presented in the single column model of Chapter 3 using fully-coupled state-of-the-art ocean-atmosphere global climate models.

We used an archive of these models run at four times preindustrial CO<sub>2</sub> concentrations created for the Intergovernmental Panel on Climate Change (IPCC) fourth assessment report to show that the convective cloud feedback is active in some of these models, dramatically affects their Arctic climate, and decreases the models' ability to accurately predict the winter Arctic sea ice cover at these CO<sub>2</sub> concentrations. We plan to extend this work in the future by performing sensitivity runs using a global climate model in which we systematically eliminate the various feedbacks that are important for determining sea ice in the future to determine which of the feedbacks are most important.

In Chapter 5 we returned to SCAM and a simple analytical model to investigate the critical threshold CO<sub>2</sub> concentration at which the convective cloud feedback can become active and the magnitude of the warming caused by the feedback. Given the results of Chapters 4 and 5, we focused on the high-latitude winter in this chapter. Using these models we argued that increases in heat fluxes affecting the surface heat exchange, such as ocean heat transport and solar energy absorbed by the ocean during summer and reemitted to the atmosphere during winter, should strongly decrease the critical CO<sub>2</sub>. We found that the effects of atmospheric heat transport depend on the details of its vertical distribution. We also found that the more radiatively thick the clouds that the convective cloud feedback produces are, the lower the critical CO<sub>2</sub> and the stronger the convective cloud feedback, and that a higher critical CO<sub>2</sub> results from deeper convection.

In the chapters of this thesis we have made what we believe is a fairly strong case for the ability of the convective cloud feedback to produce enhanced warming over the ocean

at high CO<sub>2</sub> concentrations, but we have not addressed its ability to warm the land. This is important because there is strong evidence that the pronounced high-latitude warming and decreased seasonality during equable climates occurred over land as well as over ocean (e.g., Markwick, 1998; Wing and Greenwood, 1993; Greenwood and Wing, 1995). High land temperatures during winter represent a particularly interesting and difficult-to-explain aspect of equable climates because continental land surface has a much lower heat capacity than ocean and because the distance of thousands of kilometers separating some interior regions from the ocean means that increasing ocean temperatures does not necessarily imply that temperatures in continental interiors will increase. For example, in the modern climate average winter surface air temperatures in continental interiors at 60-70°N are -25°C to -40°C, even though sea surface temperatures at these latitudes are 5°C to 10°C (Peixoto and Oort, 1992). There are a number of ways that the convective cloud feedback could potentially affect continental interiors. For example, clouds and moisture formed by winter convection over warm and ice-free oceans could be advected over continents, particularly if baroclinic eddies, which have a drying effect, were fewer and weaker due to decreased baroclinicity resulting from decreased meridional temperature gradient. It is also possible that convection could be sustained in the continental interiors themselves, if they were moist and "swamp-like." Although the role of the convective cloud feedback over land is beyond the scope of this thesis, we are pursuing this subject in our current research.

It is possible that no single mechanism can fully explain equable climate dynamics by itself. It may be that the complete explanation of the paleoclimatic observations during

equable climates may involve the convective cloud feedback in conjunction with one or more of the other potential mechanisms that have previously been proposed to explain equable climates, which we briefly outlined in the Introduction. We will explain how this might work in the next three paragraphs.

The convective cloud feedback mechanism produces clouds that act as a blanket that is able to trap heat at high latitudes throughout the winter, but this heat must somehow be supplied to the high latitudes. Some of this heat could come from solar energy absorbed during summer by the ocean and rereleased during winter, but undoubtedly some would reach the high latitudes by way of atmospheric heat transport as well. Currently most meridional heat transport into the highest latitudes, e.g., across  $60^\circ$ , occurs in the form of dry transport by baroclinic eddies (Trenberth and Stepaniak, 2003). As a reduction in the meridional temperature gradient during equable climates would likely reduce eddy activity and dry heat transport by eddies, an increase in eddy latent heat transport (Norris et al., 2002; Pierrehumbert, 2002) or heat transport by the Hadley cell (Farrell, 1990) might be necessary to supply enough heat for the convective cloud feedback to function.

Although there have been significant upward revisions in estimates of equable climate tropical sea surface temperatures recently (Huber, 2008), it is possible that the increase in greenhouse gasses necessary to activate the convective cloud feedback might produce tropical sea surface temperatures that exceed even these increased estimates. If this were the case, the convective cloud feedback mechanism could work nicely with the tropical sea surface temperature buffering mechanism of Emanuel (2002) and Korty et al. (2008). In

this mechanism increased tropical sea surface temperatures lead to increased hurricane activity, which leads to increased ocean mixing and meridional overturning circulation, which causes an increase in low-latitude ocean heat transport that helps to temper the increase in tropical sea surface temperatures.

Finally, recent observational evidence implies that extratropical convection can penetrate into the stratosphere and significantly moisten it (Hanisco et al., 2007; Dessler and Sherwood, 2004), challenging the traditional idea that all moisture in the stratosphere must enter through the tropopause in the tropics. If these observations prove to be correct, they could represent a possible connection between the convective cloud feedback and the equable climate mechanisms based on polar stratospheric clouds (Sloan et al., 1992; Sloan and Pollard, 1998; Peters and Sloan, 2000; Kirk-Davidoff et al., 2002; Kirk-Davidoff and Lamarque, 2008). Specifically, strong and deep convection caused by the convective cloud feedback could moisten the high-latitude stratosphere, making the formation of polar stratospheric cloud favorable. The cloud radiative forcing produced by these polar stratospheric clouds could significantly augment that produced directly by the tropospheric clouds of the convective cloud feedback.

At the close of this work it seems reasonable to briefly discuss its relevance, while touching further on directions for future research. We believe we have shown that simple physical arguments strongly motivate the existence of the high-latitude convective cloud feedback in Nature. We also believe that if activated, the feedback would provide high-latitude warming that could help to explain equable climates. In our opinion, this reduces

the question of the relevance of the feedback, i.e., whether the feedback was active and strong enough to have a significant impact on climate, both for equable climates and future climate, to a question of magnitude. Stated again, critical questions for future research are at what carbon dioxide level the feedback will activate and how much surface temperature increase the feedback can produce. At least in the context of equable climates the former question may require some modification given that the CO<sub>2</sub> concentration during equable climates is unknown. Perhaps in this context a way to think about this question is at what increase in tropical sea surface temperatures, a variable that is somewhat better constrained, can we expect the convective cloud feedback to activate. This way of thinking is useful insofar as tropical sea surface temperature is mainly controlled by atmospheric CO<sub>2</sub> concentration. In any case, the definitive answer to these critical questions is beyond the scope of this thesis, although we began to approach them by using relatively simple models to try to understand what parameters control the onset and strength of the feedback in Chapter 5.

As the basic physics of the convective cloud feedback mechanism should be present in all sophisticated climate models, it might be hoped that these models could be used to determine the relevance of the feedback. Indeed, the state-of-the-art coupled ocean-atmosphere global climate models used by the IPCC do provide evidence that if the feedback were to activate it would have a dramatic effect on high-latitude climate (Chapter 4); however, at a CO<sub>2</sub> concentration of 1 120 ppm the feedback was only fully active in two out of fourteen of these models, which suggests there is some spread in the activation CO<sub>2</sub> that these mod-

els predict. The onset of the feedback is presumably dependent on the details of the sea ice, convection, and cloud formulations in these models, all of which are extremely uncertain, so in some sense it is not surprising that these models do not agree on the onset CO<sub>2</sub> value. This disagreement calls into question a methodology based solely on models, and in the future we plan to use data from the modern observational record to try to understand the feedback better. These data may help to answer the questions of onset and strength of the feedback themselves, or they may help to better constrain and inform the physics of the models so that they may be more useful when used to extrapolate climate to conditions not observed today.

This points to another way in which this thesis is relevant. By identifying the convective cloud feedback as a potentially important aspect of climate that is not well-understood, we hope we will focus attention on the parameterization in models of sea ice and convective clouds at high latitudes. The latter may deserve particular attention as current convective parameterizations are based mostly on lower-latitude convection and may not be directly applicable at high latitudes. Further development of convective parameterizations may require innovative approaches, such as the Cloud-Resolving Convection Parameterization (CRCP), also called convective "superparameterization," (Grabowski and Smolarkiewicz, 1999) or Diabatic Acceleration and REscaling (DARE) (Zhiming Kuang and Bretherton, 2005). In some sense this future-research-focusing role is the best way to view this thesis. We have proposed a new mechanism that could act as a lever, magnifying high-latitude warming as greenhouse gas levels increase, and shown that this mechanism is plausible

and potentially important. If nothing else, this should direct future research toward understanding this mechanism better.



# Bibliography

- Abbot, D. S., and E. Tziperman, 2008a: A high-latitude convective cloud feedback and equable climates. *Q. J. R. Meteorol. Soc.*, **134**. DOI: 10.1002/qj.211.
- Abbot, D. S., and E. Tziperman, 2008b: Sea ice, high-latitude convection, and equable climates. *Geophys. Res. Lett.*, **35**. L03702, doi:10.1029/2007GL032286.
- Abbot, D. S., and E. Tziperman, 2008c: Controls on the activation and strength of a high-latitude convective cloud feedback. *Journal of the Atmospheric Sciences*. Accepted.
- Abbot, D. S., M. Huber, G. Bousquet, and E. Tziperman, 2008a: Eocene cloud feedback over both land and ocean. In preparation.
- Abbot, D. S., C. C. Walker, and E. Tziperman, 2008b: Winter arctic sea ice uncertainty under global warming due to a cloud radiative feedback. Submitted, available at <http://swell.eps.harvard.edu/~abbot/PAPERS/abbot-tziperman-08c.pdf>.
- Anderson, J. L., et al., 2004: The new GFDL global atmosphere and land model AM2-LM2: Evaluation with prescribed SST simulations. *Journal of Climate*, **17**(24), 4641–4673.
- Arking, A., 1991: The radiative effects of clouds and their impact on climate. *Bulletin of the American Meteorological Society*, **72**(6), 795–813.
- Baker, M. B., 1997: Cloud microphysics and climate. *Science*, **276**(5315), 1072–1078.
- Bony, S., et al., 2006: How well do we understand and evaluate climate change feedback processes? *Journal of Climate*, **19**(15), 3445–3482.
- Branscome, L. E., W. J. Gutowski, and D. A. Stewart, 1989: Effect of surface fluxes on the nonlinear development of baroclinic waves. *Journal of the Atmospheric Sciences*, **46**(4), 460–475.
- Brass, G. W., J. R. Southam, and W. H. Peterson, 1982: Warm saline bottom water in the ancient ocean. *Nature*, **296**, 620–623.
- Budyko, M. I., 1969: The effect of solar radiation variations on the climate of the earth. *Tellus*, **21**, 611–619.

- Bush, A. B. G., and S. G. H. Philander, 1997: The late Cretaceous: Simulation with a coupled atmosphere-ocean general circulation model. *Paleoceanography*, **12**(3), 495–516.
- Caballero, R., and P. L. Langen, 2005: The dynamic range of poleward energy transport in an atmospheric general circulation model. *Geophys. Res. Lett.*, **32**.
- Cess, R. D., 1976: Climate change: Appraisal of atmospheric feedback mechanisms employing zonal climatology. *Journal of the Atmospheric Sciences*, **33**(10), 1831–1843.
- Cess, R. D., and co authors, 1990: Intercomparison and interpretation of cloud-climate feedback processes in 19 atmospheric general circulation models. *J. Geophys. Res.*, **95**, 16,601–16,615.
- Cess, R. D., and co authors, 1996: Cloud feedback in atmospheric general circulation models: an update. *J. Geophys. Res.*, **101**, 12,791–94.
- Colman, R., 2003: A comparison of climate feedbacks in general circulation models. *Climate Dynamics*, **20**(7-8), 865–873.
- Cubasch, U., et al., 2001: Projections of future climate change. *IPCC Third Assessment Report: Climate Change 2001, The Scientific Basis Contribution of Working Group I to the Third Assessment Report of the Intergovernmental Panel on Climate Change (IPCC)*, J. T. Houghton, Y. Ding, D. Griggs, M. Noguer, P. J. van der Linden, and D. Xiaosu, Eds., Cambridge University Press, UK., p. 944.
- Dessler, A. E., and S. C. Sherwood, 2004: Effect of convection on the summertime extratropical lower stratosphere. *J. Geophys. Res.*, **109**.
- Eisenman, I., 2007: Arctic catastrophes in an idealized sea ice model. *2006 Program of Studies: Ice (Geophysical Fluid Dynamics Program)*, Woods Hole Oceanog. Inst. Tech. Rept. 2007-02, pp. 133–161, <http://gfd.who.edu/page.do?pid=12938>.
- Eisenman, I., N. Untersteiner, and J. Wettlaufer, 2007: On the reliability of simulated Arctic sea ice in global climate models. *Geophysical Research Letters*, **34**.
- Emanuel, K., 2002: A simple model of multiple climate regimes. *J. Geophys. Res.*, **107**(0).
- Emanuel, K. A., 1987: An air-sea interaction-model of intraseasonal oscillations in the tropics. *Journal of the Atmospheric Sciences*, **44**(16), 2324–2340.
- Emanuel, K. A., 1994: *Atmospheric convection*. Oxford University press.
- Farrell, B. F., 1990: Equable climate dynamics. *Journal of the Atmospheric Sciences*, **47**(24), 2986–2995.

- Fetterer, F., K. Knowles, W. Meier, and M. Savoie, 2002, updated 2007: Sea ice index, Boulder, CO: National Snow and Ice Data Center. Digital media. Available at [http://nsidc.org/cgi-bin/wist/wist.pl?wcf=seaice\\_index&submit=Go%21](http://nsidc.org/cgi-bin/wist/wist.pl?wcf=seaice_index&submit=Go%21).
- Francis, J. A., E. Hunter, J. R. Key, and X. J. Wang, 2005: Clues to variability in Arctic minimum sea ice extent. *Geophysical Research Letters*, **32**(21).
- Grabowski, W. W., and P. K. Smolarkiewicz, 1999: Crcp: a cloud resolving convection parameterization for modeling the tropical convecting atmosphere. *Physica D: Nonlinear Phenomena*, **133**. Doi:10.1016/S0167-2789(99)00104-9.
- Greenwood, D. R., and S. L. Wing, 1995: Eocene continental climates and latitudinal temperature gradients. *Geology*, **23**(11), 1044–1048.
- Hack, J. J., J. E. Truesdale, J. A. Pedretti, and J. C. Petch, 2004: *SCAM Users Guide*, <http://www.cesm.ucar.edu/models/atm-cam/docs/scam/>.
- Hanisco, T. F., et al., 2007: Observations of deep convective influence on stratospheric water vapor and its isotopic composition. *Geophys. Res. Lett.*, **34**. L04814.
- Harrison, E. F., P. Minnis, B. R. Barkstrom, V. Ramanathan, R. D. Cess, and G. G. Gibson, 1990: Seasonal variation of cloud radiative forcing derived from the earth radiation budget experiment. *J. Geophys. Res.*, **95**(D11), 18,687–18,703.
- Hartmann, D. L., M. E. Ockert-Bell, and M. L. Michelsen, 1992: The effect of cloud type on Earth's energy balance: Global analysis. *J. Climate*, **5**, 1281–1304.
- Held, I. M., 2000: The general circulation of the atmosphere. *Proc. Program in Geophysical Fluid Dynamics*, Woods Hole Oceanographic Institution, Woods Hole, MA, available at [gfd.who.edu/proceedings/2000/PDFvol2000.html](http://gfd.who.edu/proceedings/2000/PDFvol2000.html).
- Held, I. M., 2005: The gap between simulation and understanding in climate modeling. *Bull. Amer. Meteor. Soc.*, **86**(11), 1609–1614.
- Held, I. M., and A. Y. Hou, 1980: Non-linear axially-symmetric circulations in a nearly inviscid atmosphere. *Journal of the Atmospheric Sciences*, **37**(3), 515–533.
- Held, I. M., and M. J. Suarez, 1978: A two-level primitive equation atmospheric model designed for climatic sensitivity experiments. *Journal of the Atmospheric Sciences*, **35**, 206–229.
- Holland, M. M., C. M. Bitz, and B. Tremblay, 2006: Future abrupt reductions in the summer Arctic sea ice. *Geophysical Research Letters*, **33**(23).
- Holton, J. R., 1992: *An Introduction to Dynamic Meteorology*. 3rd ed., Academic Press.

- Hotinski, R. M., and J. R. Toggweiler, 2003: Impact of a Tethyan circumglobal passage on ocean heat transport and "equable" climates. *Paleoceanography*, **18**(1).
- Huber, M., 2008: A hotter greenhouse? *Science*, **321**(5887), 353–354.
- Huber, M., and L. C. Sloan, 1999: Warm climate transitions: A general circulation modeling study of the Late Paleocene Thermal Maximum (~56 ma). *J. Geophys. Res.*, **104**, 16,633–16,655.
- Huber, M., and L. C. Sloan, 2001: Heat transport, deep waters, and thermal gradients: Coupled simulation of an Eocene greenhouse climate. *Geophysical Research Letters*, **28**(18), 3481–3484.
- Intrieri, J. M., C. W. Fairall, M. D. Shupe, P. O. G. Persson, E. L. Andreas, P. S. Guest, and R. E. Moritz, 2002a: An annual cycle of Arctic surface cloud forcing at SHEBA. *Journal of Geophysical Research-oceans*, **107**(C10).
- Intrieri, J. M., M. D. Shupe, T. Uttal, and B. J. Mccarty, 2002b: An annual cycle of Arctic cloud characteristics observed by radar and lidar at SHEBA. *Journal of Geophysical Research-oceans*, **107**(C10).
- Kirk-Davidoff, D. B., and J.-F. Lamarque, 2008: Maintenance of polar stratospheric clouds in a moist stratosphere. *Climate of the Past*, **4**, 69–78.
- Kirk-Davidoff, D. B., D. P. Schrag, and J. G. Anderson, 2002: On the feedback of stratospheric clouds on polar climate. *Geophysical Research Letters*, **29**(11).
- Klein, S. A., and D. Hartmann, 1993a: The seasonal cycle of low stratiform clouds. *J. Climate*, **6**, 1587–1606.
- Klein, S. A., and D. L. Hartmann, 1993b: The seasonal cycle of low stratiform clouds. *Journal of Climate*, **6**(8), 1587–1606.
- Korty, R. L., and K. A. Emanuel, 2007: The dynamic response of the winter stratosphere to an equable climate surface temperature gradient. *J. Climate*, **20**(21).
- Korty, R. L., and T. Schneider, 2007: A climatology of the tropospheric thermal stratification using saturation potential vorticity. *J. Climate*, **20**.
- Korty, R. L., K. A. Emanuel, and J. R. Scott, 2008: Tropical cyclone mixing during equable climates: could enhanced ocean mixing weaken meridional temperature gradients? *J. Climate*, **21**, 638654, doi:10.1175/2007JCLI1659.1.
- Kyle, H. L., R. H. Hucek, and B. J. Vallette, 1991: *Atlas of Earth's Radiation Budget as measured by Nimbus-7: May 1979-May 1980*, [http://ntrs.nasa.gov/archive/nasa/casi.ntrs.nasa.gov/19910015406\\_1991015406.pdf](http://ntrs.nasa.gov/archive/nasa/casi.ntrs.nasa.gov/19910015406_1991015406.pdf), pp. 133.

- Lemke, P., et al., 2007: Observations: Changes in snow, ice and frozen ground. *Climate Change 2007: The Physical Science Basis. Contribution of Working Group I to the Fourth Assessment Report of the Intergovernmental Panel on Climate Change*, S. Solomon, D. Qin, M. Manning, Z. Chen, M. Marquis, K. Averyt, M. Tignor, and H. Miller, Eds., Cambridge University Press, UK.
- Lian, M. S., and R. D. Cess, 1977: Energy-balance climate models: Reappraisal of ice-albedo feedback. *Journal of the Atmospheric Sciences*, **34**(7), 1058–1062.
- Lindzen, R. S., and B. Farrell, 1980: The role of polar regions in global climate, and a new parameterization of global heat transport. *Mon. Weath. Rev.*, **108**, 2064–2079.
- Lunkeit, F., M. Bottinger, K. Fraedrich, H. Jansen, E. Kirk, A. Kleidon, and U. Luksch, 2005: *Planet Simulator Reference Manual*, [http://www.mi.uni-hamburg.de/fileadmin/files/forschung/theomet/planet\\_simulator/downloads/ Most14.tar.gz](http://www.mi.uni-hamburg.de/fileadmin/files/forschung/theomet/planet_simulator/downloads/Most14.tar.gz), pp. 74.
- Markwick, P. J., 1998: Fossil crocodilians as indicators of late Cretaceous and Cenozoic climates: implications for using palaeontological data in reconstructing palaeoclimate. *Palaeogeography Palaeoclimatology Palaeoecology*, **137**(3-4), 205–271.
- McBean, G., et al., 2005: Arctic climate: Past and present. *Arctic Climate Impact Assessment*, C. Symon, L. Arris, and B. Heal, Eds., Cambridge University Press, UK.
- Moran, K., and coauthors, 2006: The Cenozoic palaeoenvironment of the Arctic Ocean. *Nature*, **441**, 601–605.
- Murphy, J. M., D. M. H. Sexton, D. N. Barnett, G. S. Jones, M. J. Webb, and M. Collins, 2004: Quantification of modelling uncertainties in a large ensemble of climate change simulations. *Nature*, **430**(7001), 768–772.
- Nakamura, M., P. H. Stone, and J. Marotzke, 1994: Destabilization of the thermohaline circulation by atmospheric eddy transport. *J. Climate*, **7**, 1870–1882.
- Neelin, J. D., I. M. Held, and K. H. Cook, 1987: Evaporation-wind feedback and low-frequency variability in the tropical atmosphere. *Journal of the Atmospheric Sciences*, **44**(16), 2341–2348.
- Norris, R. D., K. L. Bice, E. A. Magno, and P. A. Wilson, 2002: Jiggling the tropical thermostat in the Cretaceous hothouse. *Geology*, **30**(4), 299–302.
- North, G. R., 1975: Theory of energy-balance climate models. *Journal of the Atmospheric Sciences*, **32**(11), 2033–2043.
- North, G. R., 1984: The Small Ice Cap Instability in Diffusive Climate Models. *Journal of the Atmospheric Sciences*, **41**, 3390–3395.

- North, G. R., R. F. Cahalan, and J. A. Coakley, Jr., 1981: Energy balance climate models. *Rev. Geophys. Space. Phys.*, **19**, 91–121.
- Ohring, G., and S. Adler, 1978: Some experiments with a zonally averaged climate model. *Journal of the Atmospheric Sciences*, **35**(2), 186–205.
- Otto-Bliesner, B. L., and G. R. Upchurch, 1997: Vegetation-induced warming of high-latitude regions during the late Cretaceous period. *Nature*, **387**, 804–807.
- Pagani, M., J. C. Zachos, K. H. Freeman, B. Tipple, and S. Bohaty, 2005: Marked decline in atmospheric carbon dioxide concentrations during the Paleogene. *Science*, **309**, 600–603.
- Pearson, P. N., and M. R. Palmer, 2000: Atmospheric carbon dioxide concentrations over the past 60 million years. *Nature*, **406**, 695–699.
- Pearson, P. N., P. W. Ditchfield, J. Singano, K. G. Harcourt-brown, C. J. Nicholas, R. K. Olsson, N. J. Shackleton, and M. A. Hall, 2001: Warm tropical sea surface temperatures in the Late Cretaceous and Eocene epochs. *Nature*, **413**(6855), 481–487.
- Peixoto, J. P., and A. H. Oort, 1992: *Physics of Climate*. American Institute of Physics.
- Peters, R. B., and L. C. Sloan, 2000: High concentrations of greenhouse gases and polar stratospheric clouds: A possible solution to high-latitude faunal migration at the latest Paleocene thermal maximum. *Geology*, **28**(11), 979–982.
- Phillips, N. A., 1956: The general circulation of the atmosphere: A numerical experiment. *Quarterly Journal of the Royal Meteorological Society*, **82**(352), 123–164.
- Pierrehumbert, R. T., 2002: The hydrologic cycle in deep-time climate problems. *Nature*, **419**(6903), 191–198.
- Ramanathan, V., R. D. Cess, E. F. Harrison, P. Minnis, B. R. Barkstrom, E. Ahmad, and D. Hartmann, 1989: Cloud-radiative forcing and climate: results from the earth radiation budget experiment. *Science*, **243**(4887), 57–63.
- Rasch, P. J., and J. E. Kristjánsson, 1998: A comparison of the CCM3 model climate using diagnosed and predicted condensate parameterizations. *J. Climate*, **11**, 1587–1614.
- Raymond, D. J., 1995: Regulation of moist convection over the west Pacific warm pool. *Journal of the Atmospheric Sciences*, **52**(22), 3945–3959.
- Renno, N. O., 1997: Multiple equilibria in radiative-convective atmospheres. *Tellus Series a-dynamic Meteorology and Oceanography*, **49**(4), 423–438.
- Roche, D. M., Y. Donnadieu, E. Puceat, and D. Paillard, 2006: Effect of changes in delta-O-18 content of the surface ocean on estimated sea surface temperatures in past warm climate. *Paleoceanography*, **21**(2).

- Sasamori, T., 1968: The radiative cooling calculation for application to general circulation experiments. *J. Appl. Meteor.*, **7**, 721–729.
- Schneider, T., and C. C. Walker, 2006: Self-organization of atmospheric macroturbulence into critical states of weak nonlinear eddy-eddy interactions. *Journal of the Atmospheric Sciences*, **63**, 1569–1586.
- Schouten, S., E. C. Hopmans, E. Schefub, and J. S. S. Damste, 2002: Distributional variations in marine crenarchaeotal membrane lipids: a new tool for reconstructing ancient sea water temperatures? *Earth and Planetary Science Letters*, **204**, 265–274.
- Sellers, W. D., 1969: A global climate model based on the energy balance of the earth-atmosphere system. *J. Appl. Meteor.*, **8**, 392–400.
- Serreze, M. C., M. M. Holland, and J. Stroeve, 2007: Perspectives on the Arctic's shrinking sea-ice cover. *Science*, **315**(5818), 1533–1536.
- Shell, K. M., and R. C. J. Somerville, 2005: A generalized energy balance climate model with parameterized dynamics and diabatic heating. *Journal of Climate*, **18**(11), 1753–1772.
- Shellito, C. J., L. C. Sloan, and M. Huber, 2003: Climate model sensitivity to atmospheric CO<sub>2</sub> levels in the Early-Middle Paleogene. *Palaeogeography Palaeoclimatology Palaeoecology*, **193**(1), 113–123.
- Slingo, A., and J. Slingo, 1991: Response of the national center for atmospheric research community climate model to improvements in the representation of clouds. *J. Geophys. Res.*, **96**, 15,341–15,357.
- Slingo, J. M., 1987: The development and verification of a cloud prediction scheme for the ECMWF model. *Q. J. R. Meteorol. Soc.*, **113**, 899–927.
- Sloan, L. C., and D. Pollard, 1998: Polar stratospheric clouds: A high latitude warming mechanism in an ancient greenhouse world. *Geophysical Research Letters*, **25**(18), 3517–3520.
- Sloan, L. C., and D. K. Rea, 1995: Atmospheric carbon dioxide and early Eocene climate: A general circulation modeling sensitivity study. *Palaeogeog. Paleoclimatol. Paleoecol.*, **119**, 275–292.
- Sloan, L. C., J. C. G. Walker, T. C. Moore, D. K. Rea, and J. C. Zachos, 1992: Possible methane-induced polar warming in the early Eocene. *Nature*, **357**(6376), 320–322.
- Sloan, L. C., M. Huber, and A. Ewing, 1999: Polar stratospheric cloud forcing in a greenhouse world: A climate modeling sensitivity study. *Reconstructing Ocean History: A Window into the Future*, F. Abrantes and A. Mix, Eds., Kluwer Academic / Plenum Publishers, pp. 273–293.

- Sluijs, A., and coauthors, 2006: Subtropical Arctic ocean temperatures and Palaeocene/Eocene thermal maximum. *Nature*, **441**, 610–613.
- Smetacek, V., and S. Nicol, 2005: Polar ocean ecosystems in a changing world. *Nature*, **437**(7057), 362–368.
- Sobel, A. H., G. Bellon, and J. Bacmeister, 2007: Multiple equilibria in a single-column model of the tropical atmosphere. *Geophysical Research Letters*, **34**(22).
- Soden, B. J., and I. M. Held, 2006: An assessment of climate feedbacks in coupled ocean-atmosphere models. *J. Climate*, **19**(14), 3354–3360.
- Sokolov, A. P., and P. H. Stone, 1998: A flexible climate model for use in integrated assessments. *Climate Dynamics*, **14**(4), 291–303.
- Stainforth, D. A., et al., 2005: Uncertainty in predictions of the climate response to rising levels of greenhouse gases. *Nature*, **433**(7024), 403–406.
- Stone, P. H., 1972: A simplified radiative-dynamical model for the static stability of rotating atmosphere. *Journal of the Atmospheric Sciences*, **29**, 405–418.
- Stone, P. H., and M. S. Yao, 1987: Development of a two-dimensional zonally averaged statistical-dynamical model. Part II: the role of eddy momentum fluxes in the general-circulation and their parameterization. *Journal of the Atmospheric Sciences*, **44**(24), 3769–3786.
- Stone, P. H., and M.-S. Yao, 1990: Development of a two-dimensional zonally averaged statistical-dynamical model. Part III: The parameterization of the eddy fluxes of heat and moisture. *J. Climate*, **3**, 726–740.
- Stroeve, J., M. M. Holland, W. Meier, T. Scambos, and M. Serreze, 2007: Arctic sea ice decline: Faster than forecast. *Geophysical Research Letters*, **34**(9).
- Tiedtke, M., 1993: Representation of clouds in large-scale models. *Monthly Weather Review*, **121**(11), 3040–3061.
- Trenberth, K. E., and J. M. Caron, 2001: Estimates of meridional atmosphere and ocean heat transports. *J. Climate*, **14**, 3433–3443.
- Trenberth, K. E., and D. P. Stepaniak, 2003: Covariability of components of poleward atmospheric energy transports on seasonal and interannual timescales. *J. Climate*, **16**, 3691–3705.
- Tripathi, A. K., M. L. Delaney, J. C. Zachos, L. D. Anderson, D. C. Kelly, and H. Elderfield, 2003: Tropical sea-surface temperature reconstruction for the early Paleogene using Mg/Ca ratios of planktonic foraminifera. *Paleoceanography*, **18**(4), 1–13.

- Upchurch, G. R., B. L. Otto-bliesner, and C. Scotese, 1998: Vegetation-atmosphere interactions and their role in global warming during the latest cretaceous. *Philosophical Transactions of the Royal Society of London Series B-biological Sciences*, **353**(1365), 97–111.
- Weaver, C., and V. Ramanathan, 1995: Deductions from a simple climate model: Factors governing surface temperature and atmospheric thermal structure. *J. Geophys. Res.*, **100**, 11,585–11,591.
- Wing, S. L., and D. R. Greenwood, 1993: Fossils and fossil climate: The case for equable continental interiors in the Eocene. *Philosophical Transactions of the Royal Society of London Series B-biological Sciences*, **341**(1297), 243–252.
- Winton, M., 2006: Does the Arctic sea ice have a tipping point? *Geophysical Research Letters*, **33**(23).
- Xu, K. M., and S. K. Krueger, 1991: Evaluation of cloudiness parameterizations using a cumulus ensemble model. *Monthly Weather Review*, **119**(2), 342–367.
- Yao, M. S., and P. H. Stone, 1987: Development of a two-dimensional zonally averaged statistical dynamic-model . Part I. The parameterization of moist convection and its role in the general-circulation. *Journal of the Atmospheric Sciences*, **44**(1), 65–82.
- Zachos, J., M. Pagani, L. Sloan, E. Thomas, and K. Billups, 2001: Trends, rhythms, and aberrations in global climate 65 Ma to present. *Science*, **292**(5517), 686–693.
- Zachos, J. C., L. D. Stott, and K. C. Lohmann, 1994: Evolution of early Cenozoic marine temperatures. *Paleoceanography*, **9**(2), 353–387.
- Zhang, X. D., and J. E. Walsh, 2006: Toward a seasonally ice-covered Arctic Ocean: Scenarios from the IPCC AR4 model simulations. *Journal of Climate*, **19**(9), 1730–1747.
- Zhiming Kuang, P. N. B., and C. S. Bretherton, 2005: A new approach for 3D cloud-resolving simulations of large-scale atmospheric circulation. *Geophysical Research Letters*, **32**. L02809, doi:10.1029/2004GL021024.